LBL-9796

Lawrence Berkeley Laboratory
UNIVERSITY OF CALIFORNIA
Materials & Molecular
Research Division

MULTIPHOTON PROCESSES IN ISOLATED ATOMS AND MOLECULES

Aasmund Sveinung Sudbo
(Ph. D. thesis)

November 1979

Prepared for the U.S. Department of Energy under Contract W-7405-ENG-48

Multiphoton Processes in Isolated Atoms and Molecules

Aasmund Sveinung Sudbo

ABSTRACT

In the first part of this thesis the theory of coherent excitation of a multilevel quantum mechanical system is developed. Damping of the system is taken into account by the use of a density matrix formalism. General properties of the wave function and/or the density matrix are discussed. The physical implications for the behavior of the system are described, together with possible applications of the formalism, including the infrared multiphoton excitation of molecules, and optical pumping in alkali atoms.

The second part of the thesis is a presentation of experimental results on the infrared multiphoton dissociation of molecules, followed by a discussion of the general features of this process. The experimental results were obtained using a crossed laser and molecular beam method, and the emphasis is on determining the properties of the dissociating molecule and the dissociation products. The dissociation process is shown to be described very well by the standard statistical theory (RRKM theory) of unimolecular reactions, a brief presentation of which is also included.

PREFACE

The work leading to this thesis has been unusually varied and inspiring: meeting the challenges of making all the various components of an experiment work together at the same time, enjoying the beauty of a theory gradually making more and more sense, bringing together concepts and experimental techniques from chemistry and physics, and having the feeling of learning something about nature that also others are interested in learning about.

In the completion of this work I am in profound debt to my advisers, Prof. Yuen-Ron Shen and Prof. Yuan-Tseh Lee. Ron has been deeply involved and interested in my work, always ready to share his wealth of knowledge with me. By over and over again showing how well things really can be done, he has taught me the importance of being well organized in learning physics, and of being clear, concise, and careful when trying to teach the world about my learnings. Yuan, with his invaluable experience and knowledge about experimental work, and physics and chemistry in general, has been ready at any time to discuss problems I might have, always with helpful suggestions and a friendliness I have only very rarely encountered before.

The experimental work reported on here is the result mainly of the joint efforts of Peter A. Schulz and me working in the laboratory, and he should be credited just as much for the experimental results as I. I am very grateful for the collaboration with Peter and the good friendship that grew out of it. The resulting exchange of ideas and the sharing of work-load have been invaluable, not only in obtaining the experimental results, but all through the work with this thesis.

I would like to thank all students and postdoctoral fellows in Y. R. Shen's and Y. T. Lee's research groups, for their friendship and helpful advice. In particular, I would like to thank Doug J. Krajnovich and Ed R. Grant, without the assistance of whom some of our results could not have been obtained, and Ann Weightman, for being an unusually patient and helpful secretary. I would also like to thank Rita Jones for the patience, care and esthetic perfection with which she has typed this manuscript.

This work was supported by the Division of Advanced Systems Materials Production, Office of Advanced Isotope Separation, U. S. Department of Energy, under contract No. W-7405-ENG-48. I gratefully acknowledge a fellowship from the Norwegian Research Council for Science and the Humanities.

TABLE OF CONTENTS

INTRODUCTION

During the last five years, in quite a number of laboratories around the world, efforts have been concentrated on understanding the process of multiphoton dissociation: The process whereby a molecule absorbs several tens of photons from a moderately strong infrared laser field and eventually gets dissociated. In our laboratory we have devoted much effort to a thorough experimental characterization of the process. Our experimental results are the subject of chapter 2 of this work.

In describing the process theoretically, one may divide it into two parts, according to the amount of excitation in the molecule. The laser excitation of a molecule over its discrete levels can be treated using the theory of interaction of a multilevel quantum mechanical system with a strong oscillating external field. Chapter 1 of this work is devoted to an extensive development of this general theory. A model calculation on the effect of optical pumping in a free atom subject to decay of excited states is included as an illustration of the theory. Scientists at Los Alamos have applied the same theory to detailed model calculations on the initial multiphoton excitation of the molecule SF_6 over the discrete levels. This is briefly discussed in chapter 1.

At higher excitation energies the density of states of the molecule becomes much larger, and the states form a quasi-continuum. Multiphoton excitation in this region actually involves multiple steps of single photon resonant transitions. The above calculation

is no longer applicable. A phenomenological theory can, however, be developed. Such calculations applied to the multiphoton excitation and dissociation of SF_6 are extensively discussed elsewhere /1/.

Thus this thesis consists of two rather independent parts: First, a chapter on the general theory of a multilevel quantum mechanical system interacting resonantly with an oscillating external field, and second, a chapter centered on the experimental results on infrared multiphoton dissociation of molecules.

Reference:

1. P. A. Schulz: Ph. D. thesis, Dept. of Physics, University of California, Berkeley 1979.

CHAPTER 1 THEORY FOR COHERENT EXCITATION OF A QUANTUM MECHANICAL SYSTEM

1.1 Introduction

In this chapter a method will be developed for describing mathematically the interaction between a strong electromagnetic field and a realistic quantum system like an atom or a molecule. This problem has held the continued attention of physicists ever since the birth of quantum mechanics, and ways of attacking the problem have been discovered and rediscovered by people working in various different areas of physics. We shall concentrate on aspects most relevant to optical (infrared or visible) fields coherently exciting free atoms and molecules. However, bits and pieces and extensions of the formalism to be presented have been used in microwave spectroscopy, nuclear magnetic resonance, electron paramagnetic resonance and related phenomena. An idea of the current viewpoints and centers of interest in coherent excitations can be found in the excellent collection of papers in Ref. 1.1.

The purpose of this chapter is not so much to develop a new formalism as to unite a variety of ideas from various sources into a reasonable simple formalism suited for calculations. The development is guided by the realization that with the availability of digital computers and reliable software for solving numerical probelms in linear algebra /1.2,3/, reduction of a problem to an eigenvalue problem or a system of linear equations (of numerically tractable size or with a structure permitting fast computation of solutions) is just as complete a solution as that with a complicated analytically closed form. Analytical forms are preferable only if they have a structure simple enough to make important qualitative features apparent, like, e.g., the energy denominators in

the expressions in nonlinear optics /1.4/. However, we shall see in this chapter that important qualitative information can also be derived from the formulation of the eigenvalue problem.

Our goal is to calculate observable quantities like populations in specific quantum states, spectrum of scattered light, attenuation/gain and polarization change of probing or exciting fields, given other experimentally measurable quantities like energy levels and oscillator strengths. Keeping in mind that a computer will be used in the calculations, we must limit ourselves to quantum systems with a finite number of discrete levels. We will not attempt to describe ionization or dissociation induced by the field.

We will start from a simple general description, and then extend it to various more realistic cases. For ease of presentation, we will disregard all but the electric dipole interaction between the electromagnetic field and the quantum system. The physical probelms we will discuss are: infrared multiphoton excitation of polyatomic molecules (which is treated further in Chapter 2) and optical pumping of atoms into a polarized state.

1.2 Formalism

There are basically two different approaches to the problem. One involves a completely quantum-mechanical treatment of the coupled system of a quantized electromagetic field (from here on called e.m. field) and a quantum mechanical system (from here on called q.m. system) of interest. This is the so-called "dressed atom" approach /1.5/. However, if the radiation field is sufficiently strong, a semiclassical approach is possible. The limiting equivalence of the two approaches has been dis-

cussed in detail in a classical paper by Mollow /1.6/, and we shall use the semiclassical approach henceforth.

If spontaneous emission and all other dephasing and depopulating terms are negligible, the equation of motion takes the Schrödinger form

$$i\dot{\psi} = H(t)\psi \qquad 1.1$$

where ψ is the time dependent wave function of the q.m. system in a prescribed external e.m. field described by the hamiltonian $\hbar H(t)$. This is often sufficient to describe microwave or infrared excitation, but in the visible or ultraviolet, spontaneous emission cannot be neglected. If this is the case, or if other decay or dephasing mechanisms are nonnegligible, a density matrix formulation is needed. Thus the equation of motion is of the Liouville-type

$$i\dot{\rho} = \mathscr{L}(t)\rho \qquad 1.2$$

where the Liouvillian $\hbar\mathscr{L}$ is an operator defined on the space of density matrices, as opposed to the hamiltonian, which is defined on the space of wavefunctions. This has the undesirable consequence that for q.m. system with N levels, the equation of motion involves N^2 linearly independent components. However, formally, Eq. 1.2 is the same as Eq. 1.1, except that in the presence of dephasing and population decay, $\mathscr{L}$ is not hermitean. As discussed thoroughly in a review article by Omont /1.7/, much the same symmetry properties that ψ posesses, are taken over by ρ. Consider, as an illustration, a $j = j_1$ to $j = j_1 + 1$ transition in an atom. In the absence of external fields, H and $\mathscr{L}$ are both sperically

symmetric, and ψ will transform as the irreducible representations $D_j \oplus D_{j+1}$ under rotation. In the absence of decay, ρ is just the direct product of ψ with its complex conjugate, and will transform as $(D_j \oplus D_{j+1}) \otimes (D_j \oplus D_{j+1}) = 2D_0 \oplus 4(D_1 \oplus D_2 \oplus \ldots \oplus D_{2j}) \oplus 3D_{2j+1} \oplus D_{2j+2}$. If the decay terms in $\mathscr{L}$ are spherically symmetric, they will only couple elements of ρ belonging to the D_j's with the same j, and then ρ can be decomposed into a multipole series. Furthermore, an external field, in the dipole approximation only couples the 2^j- multipoles to 2^j- and $2^{j\pm1}$- multipoles (since the dipole operator is a tensor operator of rank 1, transforming under rotation as D_1). For the same reason, only components of multipoles with azimuthal quantum numbers m differing by less than 2 are coupled by the external field. This is very helpful if the field is weak enought that relaxation dominates over excitation so that perturbation theory can be applied. However, it is less useful in the strong field limit, since then there is not even an approximate spherical symmetry to the total hamiltonian, and the multipole expansion of ρ ceases to be a good approximation. However, one advantage of using the multipole representation of the density matrix still prevails even in this case. Since the dipole operator transforms under totation as D_1, $\mathscr{L}$ in Eq. 1.2 transforms as $D_0 \oplus D_1$, and thus in the matrix representation of $\mathscr{L}$, only elements of the density matrix connecting components with quantum numbers j and m differing by less than 2 are nonzero. Thus the matrix representation of $\mathscr{L}$ can be chosen to have a band structure, a feature which may facilitate numerical diagonalization of $\mathscr{L}$ /1.2/. Here, we shall however use the standard representation of the density matrix. I.e., the wavefunction $\psi = \Sigma_\ell \phi_\ell |\ell\rangle$ instead of the density matrix is chosen to be decomposed into multipoles, and we write $\rho = \Sigma_{k\ell} \rho_{k\ell} |k\rangle\langle\ell|$.

Because $\rho_{k\rho} = \rho^*_{\ell k}$, the Liouville Eq. 1.2 can be rewritten as an equation in real quantities only, as follows. We define a new set of N^2 density matrix elements ρ_k in terms of the matrix elements $\rho_{\ell m}$:

$$\begin{aligned}\rho_k &= \rho_{kk} \text{ for } k = 1,2, \ldots ,N \quad (k \in N_1) \\ &= (\rho_{\ell m} + \rho_{m\ell})/2 \text{ for } k = N+1, N+2, \ldots , N(N+1)/2 \quad (k \in N_2) \\ &= (\rho_{\ell m} - \rho_{m\ell})/2i \text{ for } k = N(N+1)/2, \ldots , N^2 \quad (k \in N_3)\end{aligned} \tag{1.3}$$

We order ℓ and m so that $\ell > m$. When $k \in N_2$, $k = (\ell - 1)(\ell - 2)/2 + m + N$, and when $k \in N_3$, $k = (\ell - 1)(\ell - 2)/2 + m + N(N + 1)/2$. All ρ_k thus defined are real, since $\rho_{\ell m} = \rho^*_{m\ell}$. (In the multipole expansion of the density matrix a similar pairing of components can be made /1.7/ by combining components with equal but opposite values of the azimuthal quantum number m.) Now, let us (by defining $\Gamma = i\mathcal{L}$) write Eq. 1.2 as

$$\dot{\rho}_{\ell m} = - \Sigma_{\ell' m'} \Gamma_{\ell m \ell' m'} \rho_{\ell' m'} \tag{1.4}$$

Using the definition 1.3 for ρ_k, and with $\Gamma_{kk'}$ being defined from $\Gamma_{\ell m \ell' m'}$ in Table 1.1a, we can rewrite Eq. 1.4 as

$$\dot{\rho}_k = - \Sigma_{k'} \Gamma_{kk'} \rho_{k'} \tag{1.5}$$

with ρ_k and $\Gamma_{kk'}$ all being real. Here, $\Gamma_{kk'}$ is defined (with the same relation between k, ℓ, and m as in Eq. 1.3) in Table 1.1a. If we now compare Eqs. 1.5 and 1.1, the latter having matrix form

$$\dot{\phi}_k = - iH_{kk'}\phi_{k'} \qquad 1.6$$

we see a formal similarity. The differences are that whereas $H_{kk'}$ is hermitian and of dimensionality N, $_{kk'}$ is real, but not necessarily symmetric or antisymmetric, and of dimensionality N^2.

Mollow has deduced the form of $\mathscr{L}_{\ell m \ell' m'}$ with spontaneous emission taken into account, in the case of well separated transition frequencies (Ref. 1.6, Eqs. 10.8 and 10.10). By going through Mollow's derivation, we find that even with some near or exact degeneracies, $\mathscr{L}_{\ell m \ell' m'}$ still retains the form

$$\mathscr{L}_{\ell m \ell' m'} = H_{\ell \ell'}\delta_{mm'} - H_{m'm}\delta_{\ell \ell'} - i\gamma_{\ell m \ell' m'} \qquad 1.7$$

where $\gamma_{\ell m \ell' m'}$ is a real decay matrix. Such a form of $\mathscr{L}_{\ell m \ell' m'}$ is not restricted to decay by spontaneous emission; other examples are given in Refs. 1.7 and 1.8. In the case of spontaneous emission, the matrix $\gamma_{\ell m \ell' m'}$ has the form given in Table 1.2. In the table, $\vec{\mu}_{k\ell}$ is the dipole moment of the transition $k \to \ell$ and $A_{k\ell}$ is the Einstein A-coefficient for the transition:

$$A_{k\ell} = \begin{cases} 0 \text{ if state } k \text{ has energy } \hbar\omega_k \text{ below that of state } \ell \\ 4\,\alpha\,\omega_{k\ell}^3 |\vec{\mu}_{k\ell}|^2/(3c^2e^2) \text{ otherwise} \end{cases} \qquad 1.8$$

α is the fine structure constant, $\omega_{k\ell} = \omega_k - \omega_\ell$, and c and e have their usual meaning. We also have the total Einstein coefficient for the decay from the state k: $A_k = \Sigma_\ell A_{k\ell}$.

Now, let us consider the simplest case, that of an isolated q.m. system in a perfectly monochromatic e.m. field. The details are given in Appendix A. Let us start with Eq. 1.6, and then gradually go to the more general cases represented by Eq. 1.4 and 1.5.

From Appendix A we obtain the solution of Eq. 1.6:

$$\phi_k(t) = \Sigma_{a\ell}\, \phi_\ell^{a*}\phi_\ell(0)\phi_k^a \exp[-\, i(\Omega^a + n_k\omega)t] \qquad 1.9a$$

where Ω^a are the so-called quasienergies of the system. Ω^a and ϕ_k^a satisfy the eigenvalue equation (cf. Eq. A.5)

$$\Omega^a\phi_k^a = \Sigma_\ell H'_{k\ell}\phi_\ell^a. \qquad 1.9b$$

The superscript a labels the N eigenvalues Ω^a, when each eigenvector has N components ϕ_k^a, k = 1, 2, ... N. If the hamiltonian of the system is $H_{k\ell} = \hbar\omega_k\delta_{k\ell} + \hbar V_{k\ell}\exp(-\, i\omega t) + \hbar V_{\ell k}^*\exp(i\omega t)$, the operator $H'_{k\ell}$ is defined as

$$H'_{k\ell} = \Delta_k\delta_{k\ell} + V'_{k\ell} \qquad 1.9c$$

with

$$\Delta_k = \omega_k - n_k\omega \;;\; |\Delta_k| \ll \omega \qquad 1.9d$$

$$V'_{k\ell} = \begin{cases} V_{k\ell} & \text{if } n_k - n_\ell = 1 \\ V_{\ell k}^* & \text{if } n_k - n_\ell = -1 \\ 0 & \text{otherwise} \end{cases} \qquad 1.9e$$

For each k, n_k is chosen as that integer that minimizes $|\Delta_k|$. Since $H'_{k\ell}$ is hermitian, the Ω^a are all real frequencies.

Let us point out a few properties of $\phi_k(t)$. In the absence of an external field, $\phi_k(t) \propto \exp(-i\omega_k t)$ and thus oscillates at the frequency ω_k. From Eq. 1.9 we see that if we consider an N-level system, each $\phi_k(t)$ has up to N components oscillating at frequencies $\Omega^a + n_k\omega$ with a = 1, 2, ... N. This is the AC Stark splitting effect on level k. Thus in the limit of weak external field, for each level k there must exist at least one Ω^a such that $\Omega^a + n_k\omega \approx \omega_k$, and the corresponding ϕ_k^a must be much larger than all the other ϕ_k^a, b≠a. In the absence of the field, $\phi_k^a = \delta_{ak}$ and $\Omega^k = \Delta_k = \omega_k - n_k\omega$.

In the extremely strong field limit where all the detunings Δ_k are negligible compared with $V_{k\ell}$, the Ω^a are completely determined by the dipole matrix elements $\mu_{k\ell}$ between the various levels, and are directly proportional to the external field strength E, as can be seen from Eq. 1.9c, since $V_{k\ell} \propto \mu_{k\ell}E$. Thus in a system where N levels are strongly coupled by an oscillating field, each level is split up into N components, and the splitting is proportional to the field strength.

Since the only parameters entering in Eq. 1.9 are energy level positions and dipole transition moments, the application of Eq. 1.9 to calculations on a specfic atom or molecule is a question of spectroscopic knowledge. Given sufficiently detailed spectroscopic data, Eq. 1.9 can be used to calculate the effect of a field of monochromatic radiation with piecewise (in time) constant amplitude, e.g. a square pulse, on the q.m. system.

Since in the infrared, spontaneous emission processes are quite slow and can be neglected compared to the excitations induced by a strong in-

frared laser field, this approach has been used with reasonable success, to calculate the frequency and laser energy fluence dependence of the energy absorbed in collisionless IR multiphoton excitation of SF_6. Following a detailed assignment /1.9/ of a high resolution diode laser absorption spectrum /1.10/ of SF_6 in regions pumped by the CO_2 laser, model calculations have been performed on the molecule /1.11-13/. For laser pulse intensities and durations of the same order of magnitude as those used in experiments on multiphoton excitation and dissociation, the resulting average excitation energy in the SF_6 molecule was calculated as a function of laser frequency. In the model for the SF_6 molecule, the lowest 3-4 vibrational states of the triply degenerate ν_3 mode were included. together with rotational level structure, anharmonicities and Coriolis coupling. This gives a model hamiltonian for SF_6 which was used in Eq. 1.6 to calculate $\phi_k(t)$ of Eq. 1.9, with an average excitation energy $\langle E \rangle = \Sigma_k \mathcal{E}_k |\phi_k(t_p)|^2$, where t_p is the pulse duration. It is interesting to see that experimentally /1.14-15/, the frequency dependence of the multiphoton dissociation yield in SF_6 is closely related to the excitation in the lowlying discrete levels treated in this model. The lack of sharp resonances, the relatively broad frequency dependence, and the red-shift of the multiphoton excitation spectrum relative to the single photon absorption spectrum, are properties found in multiphoton excitation both theoretically and experimentally. Multiphoton dissociation is the subject of Chapter 2 of this work, and we will leave further discussion to that chapter.

The case of the idealized hamiltonian (without decay and dephasing effects) of Eq. 1.1 has, as already pointed out, the attractive feature that the dimensionality of the associated eigenvalue problem is equal to

the number N of levels involved in the problem, as compared with the N^2 dimensionality of the corresponding more general case (Eq. 1.2). Thus, several hundred levels can routinely be treated by standard computer programs /1.3/, and many more, if use can be made of the symmetries of the hamiltonian of the problem. Thus its solution can be used as a zeroth order approximation in a perturbation scheme in solving Eq. 1.4, where the $\gamma_{\ell m \ell' m'}$ of Eq. 1.7 are small compared to $H_{\ell\ell'}\delta_{mm'} - H_{mm'}\delta_{\ell\ell'}$, i.e., when the separation between the corresponding quasienergies Ω^a is large compared to the decay constants $\gamma_{\ell m \ell' m'}$.

In the absence of decay, Eq. 1.1 and 1.6 are completely equivalent to Eq. 1.2 and 1.4, and if $\phi_\ell^a(t)$ is a solution of Eq. 1.6, then

$$\rho_{-1}\rho_{\ell m}^{ab}(t) = \phi_\ell^a(t)\phi_m^b(t)^* \qquad 1.10$$

is a solution of Eq. 1.4. Now, in the presence of decay, we must use the results in Appendix A.2a. We have a zeroth order solution Eq. 1.10 to the problem $i\dot{\rho}_{\ell m} = \Sigma_{\ell' m'}\mathscr{L}_{\ell m \ell' m'}\rho_{\ell' m'}$ and a perturbation operator $\ell_{\ell m \ell' m'} = -i\gamma_{\ell m \ell' m'}$. In analogy with Eq. A.12 we write the complete solution as

$$\rho_{\ell m}(t) = \Sigma_{ab}\alpha^{ab}(t)\phi_\ell^a\phi_m^b\exp[-i(n_\ell - n_m)\omega t] \qquad 1.11$$

where now $\phi_\ell^a(t) = \phi_\ell^a\exp[-i(\Omega^a + n_\ell\omega)t]$ are solutions of Eq. 1.6. By substitution in Eq. 1.4 with damping, we get (cf. Eq. A.13)

$$i\dot{\alpha}^{ab} = (\Omega^a - \Omega^b)\alpha^{ab} - i\Sigma_{a'b'}\gamma^{aba'b'}\alpha a'b' \qquad 1.12a$$

where

$$\gamma^{aba'b'} = \Sigma'_{\ell m \ell' m'} \phi_\ell^{a*} \phi_m^{b} \phi_{\ell'}^{a'} \phi_{m'}^{b'*} \gamma_{\ell m \ell' m'}. \qquad 1.12b$$

According to Appendix A.2a, we should include in the sum on the right hand side of Eq. 1.12b only terms such that $n_\ell - n_m - n_{\ell'} + n_{m'} = 0$. As in Eq. 1.9, $n_k\omega$ is the integer multiple of the field frequency ω that is closest to the system eigenfrequency ω_k. If $\gamma_{\ell m \ell' m'}$ originates in spontaneous emission, we see in Table 1.2 that unless $n_\ell - n_m - n_{\ell'} + n_{m'} = 0$, we will have $\gamma_{\ell m \ell' m'} = 0$.

Following the approximation in Appendix A.2a, the only terms to be included in the right hand side of Eq. 1.12a should be those $\alpha^{a'b'}$ that oscillate at frequencies close to α^{ab}, i.e., we discard all $\gamma^{aba'b'}$ with

$$|\Omega^a - \Omega^b - \Omega^{a'} + \Omega^{b'}| \gg \gamma^{aba'b'}. \qquad 1.13$$

The simplest case is that of well separated quasienergies Ω^a, when the only a, b, a' and b' for which 1.13 does not hold are

$$a = a' \text{ and } b = b' \qquad 1.14a$$

$$\text{or} \quad a = b \text{ and } a' = b'. \qquad 1.14b$$

In this case the lowest order approximation to Eq. 1.12 is

$$i\dot{\alpha}^{ab} = (\Omega^a - \Omega^b - i\gamma^{abab})\alpha^{ab}, \quad a \neq b \qquad 1.15a$$

$$\dot{\alpha}^{aa} = -\Sigma_{a'} \gamma^{aaa'a'} \alpha^{a'a'}. \qquad 1.15b$$

Thus the N^2-dimensional problem of Eq. 1.4 has been reduced to an N-dimensional problem, Eq. 1.15b.

This is the simplest case. If the set of quasienergies have accidental near degeneracies or nearly equally spaced values, then a, b, a' and b' with $a \neq b \neq a' \neq b'$ can be found such that Eq. 1.13 does not hold. One example is the case where a system is excited close to resonance (see, e.g., the twolevel system of Appendix B). Then, the quasienergies come in pairs of equal but opposite values $\Omega^{a^+} \approx -\Omega^{a^-}$, implying $\Omega^{a^+} - \Omega^{b^+} \approx \Omega^{b^-} - \Omega^{a^-}$. Thus, instead of Eq. 1.15a, we get

$$i\begin{pmatrix} \dot{\alpha}^{a^+b^+} \\ \dot{\alpha}^{b^-a^-} \end{pmatrix} = \Omega \begin{pmatrix} \alpha^{a^+b^+} \\ \alpha^{b^-a^-} \end{pmatrix} \qquad 1.15c$$

where the 2×2 matrix Ω is

$$\Omega = \begin{pmatrix} \Omega^{a^+} - \Omega^{b^+} - i\gamma^{a^+b^+a^+b^+} & -i\gamma^{a^+b^+b^-a^-} \\ -i\gamma^{b^-a^-a^+b^+} & \Omega^{b^-} - \Omega^{a^-} - i\gamma^{b^-a^-b^-a^-} \end{pmatrix} \qquad 1.15d$$

This is an illustration of a more general principle: Eq.1.12a can often be decomposed into subsets of equations of lower dimensionality (than N^2). Each set then involves α^{ab}'s which all have about the same $\Omega^a - \Omega^b$ (in the sense of Eq. 1.13), in analogy with standard first order degenerate Rayleigh-Schrödinger perturbation theory.

Going back to the assumption that we do not have near degeneracies or nearly equally spaced levels in the quasienergies Ω^a (which are determined by dipole oscillator strengths, external field strengths, and external field frequency), we can use Eq. 1.15 as an approximation for Eq. 1.12 where the $\gamma^{aba'b'}$'s are assumed to be small compared to the $(\Omega^a - \Omega^b)$'s. Then, the following results are obtained:

(1) Eq. 1.15b can be reduced to an eigenvalue equation by the substitution

$$\alpha^{aa}(t) = a^{aa;c}\exp(-\gamma^{c}t) \qquad 1.15e$$

where $a^{aa;c}$ and γ^{c}, c = 1, 2 ... N, are the N different solutions of the eigenvalue problem

$$\gamma^{c}a^{aa;c} = \Sigma_{a'}\gamma^{aaa'a'}a^{a'a';c}. \qquad 1.15f$$

(2) Equation 1.15a has solutions of the form

$$\alpha^{ab}(t) = a^{ab}\exp(-i\Omega^{ab}t) \qquad 1.15g$$

where

$$\Omega^{ab} = \Omega^{a} - \Omega^{b} - i\gamma^{abab}. \qquad 1.15h$$

(3) Let us also define

$$b^{ac} = a^{c}a^{aa;c} \qquad 1.15i$$

where a^{c} together with a^{ab} are constants to be determined from the initial values of $\rho_{\ell m}(t)$.

(4) By substituting Eqs. 1.15e, g, and i in Eq. 1.11, we get

$$\rho_{\ell m}(t) = \Sigma_{a\neq b}a^{ab}\phi_{\ell}^{a}\phi_{m}^{b*}\exp\left\{-i[\Omega^{ab} + (n_{\ell} - n_{m})\omega]t\right\} +$$

$$+ \Sigma_{ac} b^{ac} \phi_{\ell}^{a} \phi_{m}^{a*} \exp\left\{- [\gamma^{c} + i(n_{\ell} - n_{m})\omega]\right\} t \ . \qquad 1.16a$$

With $\rho_{\ell m}(0)$ given, a^{ab} and $b^{ac} = a^{c} a^{aa;c}$ satisfy

$$a^{ab} = \Sigma_{\ell m} \phi_{\ell}^{a*} \phi_{m}^{b} \rho_{\ell m}(0) \qquad 1.16b$$

$$\Sigma_{c} a^{c} a^{aa;c} = \Sigma_{\ell m} \phi_{\ell}^{a*} \phi_{m}^{a} \rho_{\ell m}(0) . \qquad 1.16c$$

The contents of Eq. 1.16 are as follows: In the absence of damping, each element $\rho_{\ell m}(t)$ of the density matrix has up to N^2 components, oscillating at frequencies $\Omega^{a} - \Omega^{b} + (n_{\ell} - n_{m})\omega$, with a = 1, 2 ... N, b = 1, 2 ... N. There are N components all oscillating at the same integer multiple $(n_{\ell} - n_{m})\omega$ of the field frequency, corresponding to a = b above.

In the presence of damping, the components oscillating at a frequency $\Omega^{a} - \Omega^{b} + (n_{\ell} - n_{m})\omega$, where $\Omega^{a} \neq \Omega^{b}$, will remain the same, except that they decay with a rate γ^{abab}. The N components oscillating at the same frequency $(n_{\ell} - n_{m})\omega$ will all mix and give rise to N new components decaying independently, at rates γ^{c}. If, and only if, some of the Ω^{a} are nearly degenerate, will there be more than N components mixing. If in a density matrix element $\rho_{\ell m}(t)$ there are several components oscillating close to the same frequency, they may be mixed by the perturbation introduced by the damping, just like the N components oscillating at $(n_{\ell} - n_{m})\omega$.

Let us, for completeness, also write down the eigenvalue equations in the case that the damping rates are of the same order of magnitude as the quasienergies Ω^{a}. Then the full N^2-dimensional Eq. 1.4 or 1.5 has to be used. The eigenvalue equation is (cf. Eq. A.5)

$$\Omega^a \rho^a_{\ell m} = \Sigma_{\ell' m'} \mathscr{L}_{\ell m \ell' m'} \rho^a_{\ell' m'} \qquad 1.17a$$

which can also be writeen as (cf. Eq. 1.5) (defining $\gamma^a = i\Omega^a$)

$$\gamma^a \rho^a_k = \Sigma_{k'} \Gamma'_{kk'} \rho_{k'} \qquad 1.17b$$

and where

$$\mathscr{L}'_{\ell m \ell' m'} = (\Delta_\ell - \Delta_m)\delta_{\ell\ell'}\delta_{mm'} + (V'_{\ell\ell'}\delta_{mm'} - V'_{m'm}\delta_{\ell\ell'}) - i\gamma_{\ell m \ell' m'}. \qquad 1.17c$$

Δ_ℓ and $V'_{\ell\ell'}$ have the same meaning as in Eq. 1.9, and the relation between $\Gamma'_{kk'}$ and $i\mathscr{L}_{\ell m \ell' m'}$ is like between $\Gamma_{kk'}$ and $\Gamma_{\ell m \ell' m'}$ in Table 1.1a. It is given explicitly in Table 1.1b. If this full N^2-dimensional treatment is necessary, the number N of levels that can be included in the practical calculation will be severely limited.

Apart from the expansion of the density matrix into spherical multipoles discussed previously, which is only possible in the absence of external fields, no systematic analysis of equations of the general form 1.17 seems to exist. There is no systematic way to exploit the structure of the matrix $\Gamma'_{kk'}$ of Table 1.1b so as to decompose it into submatrices of lower dimensionality. However, judging from systematic distribution of the relatively few nonzero elements of $\Gamma'_{kk'}$ (see Table 1.1b), this would seem to be possible.

1.3 General Properties of the Density Matrix $\rho_{\ell m}(t)$

So far, we have developed a formalism for finding the time-dependent

density matrix for a system of N levels coupled resonantly by an external field. The problem reduces to an eigenvalue problem (Eq. 1.9b, Eq. 1.15d, Eq. 1.17b). Thus the solution of Eq. 1.4 can be written in the form

$$\rho^a_{\ell m}(t) = \rho^a_{\ell m}\exp\left\{-\left[\gamma^a + i(n_\ell - n_m)\omega\right]t\right\}. \qquad 1.18a$$

For each pair ℓ, m, $\rho^a_{\ell m}(t)$ has N^2 components, oscillating at the frequencies $\mathrm{Im}(\gamma^a) + (n_\ell - n_m)\omega$, a = 1, 2, ... N^2. Each component decays away with time constant $\mathrm{Re}(\gamma^a)$. Since in Eq.1.17b, the matrix Γ'_{kk}, is real, if γ^a is an eigenvalue corresponding to the eigenvector $\rho^a_{\ell m}$, γ^{a*} is an eigenvalue corresponding to the eigenvector $\rho^{a*}_{m\ell}$; i.e., the γ^a always occur in complex conjugate pairs, giving rise to physically acceptable solutions ($\rho_{\ell m}(t) = \rho^*_{m\ell}(t)$) of the form

$$\rho_{\ell m}(t) = \alpha\rho^a_{\ell m}\exp\left\{-\left[\gamma^a + i(n_\ell - n_m)\omega\right]t\right\} +$$

$$+ \alpha^*\rho^{a*}_{m\ell}\exp\left\{-\left[\gamma^{a*} + i(n_m - n_\ell)\omega\right]t\right\}. \qquad 1.18b$$

Now, consider the trace of ρ, $\mathrm{Tr}\rho = \Sigma_\ell \rho_{\ell\ell}(t) = 1$. Using Eq. 1.18a and differentiating with respect to t, we get

$$0 = \frac{d}{dt}\,\mathrm{Tr}\rho^a = -\gamma^a\exp(-\gamma^a t)\Sigma_\ell\rho^a_{\ell\ell} \qquad 1.19a$$

or

$$\gamma^a\Sigma_\ell\rho^a_{\ell\ell} = \gamma^a\mathrm{Tr}\rho^a(0) = 0. \qquad 1.19b$$

Thus either γ^a or $\mathrm{Tr}[\rho^a(0)]$ should be zero.

Physically, as we shall see later in examples (the simplest being the twolevel problem of Appendix B), all γ^a, except γ^0, should have a positive real part signifying damping. On the other hand, γ^0 corresponds to the steady state solution

$$\rho_{\ell m}(t \to \infty) = \rho^0_{\ell m} \exp[-i(n_\ell - n_m)\omega t]. \qquad 1.20$$

This solution is the only one with a nonzero trace, as shown above. Thus the typical system has a steady state response to the external field which oscillates at multiples $(n_\ell - n_m)\omega$ of the field frequency, and all other components $\rho^a_{\ell m}$, $a \neq 0$ decay away.

The most important component $\rho^a(t)$ of the density matrix, next to the steady state solution $\rho^0(t)$, is the one with the smallest real part $\mathrm{Re}(\gamma^a)$. This component is the one that determines how long it takes for $\rho(t)$ to reach steady state, and it also shows which of the density matrix elements $\rho_{k\ell}(t)$ that take that long to reach steady state.

In the twolevel system treated in Appendix B, regardless of detuning from resonance and external field strength the values of non-zero $\mathrm{Re}(\gamma^a)$ all have the same order of magnitude. This is, as we shall see, not true in general. The real as well as the imaginary part of γ^a may vary strongly with external field frequency, strength, and polarization state.

1.4 Physical Implications of the Form of the Density Matrix

So far, the only thing we have accomplished, is to show what the form of the density matrix is for a q.m. system driven close to reson-

ance by a steadily oscillating e.m. field, and how this solution for the density matrix can be calculated using a computer. Let us now discuss the physical implication of the solution for the q.m. system.

1.4a Fluorescence Spectrum

The spectrum of the radiation reemitted from the q.m. system can in part be determined by analysis of the set of eigenvalues Ω^a (Eq. 1.17a or 1.15f). Since the semiclassical fluorescence radiation field is proportional to the oscillating dipole moment $\Sigma_{\ell m}\vec{\mu}_{\ell m}\rho_{m\ell}(t)$, it will have up to N^2 frequency components (corresponding to the various $\mathrm{Re}(\Omega^a)$, centered at $\mathrm{Re}(\Omega^a) + (n_m - n_\ell)\omega$ for each integer $(n_m - n_\ell)$. Each line has a Lorenzian line shape with half width given by $\mathrm{Im}(\Omega^a)$.

However, as pointed out earlier, at times long compared to the various $[\mathrm{Im}(\Omega^a)]^{-1}$, typically all components of the density matrix except one (oscillating at integer multiples of the field frequency and thus giving rise to elastically scattered radiation) will have died away. Analysis of the fluorescence spectrum using the quantized description of the e.m. field however shows (see, e.g., Ref. 1.5 or 1.6) that the fluorescence at the frequencies $\mathrm{Re}(\Omega^a)+(n_m-n_\ell)\omega$ will <u>not</u> die away in the long time limit. Qualitatively this can be understood by realizing that two-photon fluorescence, which cannot be completely described in a simple semiclassical frame, may be important. Somewhat loosely, we may say that emission of a pair of photons with frequencies ω_+ and ω_-, where $\omega_+ + \omega_- = 2\omega$, may be resonantly enhanced in the driven q.m. system. This happens when ω_+ or ω_- is within a distance $\approx \mathrm{Im}(\Omega^a)$ from any of the system oscillation frequencies $\mathrm{Re}(\Omega^a)+\omega$. But for a formally correct deduction of the steady state fluorescence spectrum, one has to consider the equation of motion

for the quantized e.m. field, as in Refs. 1.5 and 1.6.

1.4b Absorption Spectrum

The absorption by the strongly driven system of a weak probe field is characterized by the same resonance frequencies as the ones observed in the resonance fluorescence spectrum, $\mathrm{Re}(\Omega^a) + (n_\ell \quad n_m)\omega$. The absorption spectrum can be calculated semiclassically, by first calculating the perturbation on the density matrix induced by the probe field. This is done in appendix A.2c. If we look at Eq. A.18c, we see that there are Lorenzian resonances of half widths $\mathrm{Im}(\Omega^a)$ in $\rho(t)$ for probe frequencies ω' equal to some of the integer multiples of the external field frequency ω, added to any of the $\mathrm{Re}(\Omega^a)$. Depending on the relative phases of the corresponding oscillating polarization and the probe field, the probe field may experience absorption or amplification. Absorption is a wellknown phenomenon, and recently also amplification has been demonstrated experimentally for such a system /1.16/.

1.4c Limitations of the Formalism

The formalism developed uses the rotating wave approximation, i.e., it is assumed that a limited number of levels in the q.m. system we are studying have eigenfrequencies ω_k near some integer multiple $n_k\omega$ of the e.m. field frequency ω. The off-resonant elements $\rho_{k\ell}(t)$ (where $\omega_k - \omega_\ell$ is not close to an integer multiple of the field frequency) of the density matrix are neglected. Also, introducing the same order of magnitude errors as by neglecting the off-resonant terms, we neglect the components $\rho^a_{k\ell;n}$ (see Eq. A.3) with frequencies $n\omega$ that are not close to $\omega_k - \omega_\ell$.

According to the discussion in Appendix A.2d, the corresponding errors we make are of order of $\mathscr{L}_{\ell m \ell' m'}/\omega$ in the $\rho^a_{k\ell}$, and $|\mathscr{L}_{\ell m \ell' m'}|^2/\omega$ in the Ω^a. The latter corrections $\Delta\Omega^a$ include the so-called field induced level shifts, which thus are neglected in the rotating wave approximation. The form of Eq. A.4 shows that for these shifts to be calculated consistently, not only off-resonant energy levels in the system must be taken into consideration, but also all the terms $\rho^a_{k\ell;n}$ with different values of n.

From appendix A.2d we conclude that there are two cases when the solution $\rho^a_{\ell m}(t)$ of Eq. 1.18a may not be a good approximation to the true density matrix of the system. One is if the external field is too strong, so that the operator $\mathscr{L}_{\ell m \ell' m'}$ has off-diagonal elements that are comparable in magnitude to the detuning from resonance of the eigenfrequencies of the states we are neglecting. The other case is if some of the eigenvectors $\rho^a_{\ell m}$ that we find from Eq. 1.17 are close to being parallell. As discussed in appendix A.2d, if the eigenvectors $\rho^a_{\ell m}$ are nearly parallell, they are much more sensitive to perturbations (like states neglected in the calculation) than if they are orthogonal (i.e., $\Sigma_{\ell m} \rho^a_{\ell m}\rho^b_{m\ell} = 0$ if $a \neq b$, as is the case in the absence of damping, for instance). Thus our formalism is essentially an approximation for weak external fields and weak damping.

The time scale on which this approximation is good, is limited by two factors. One is connected with the fact that as discussed above, the Ω^a have errors $\Delta\Omega^a$. Thus for times $t > \tau$, where $\tau\Delta\Omega^a \simeq 1$, these errors may begin to have serious effects on $\rho_{\ell m}(t) = \Sigma_a\, a^a \rho^a_{\ell m} \times$ $\times\exp\{-i[\Omega^a + (n_\ell - n_m)\omega]t\}$. This is only important if $\Delta\Omega^a$ is comparable in magnitude to $\mathrm{Im}(\Omega^a)$, so that the components $\rho^a_{\ell m}$ do not decay

away before the errors $\Delta\Omega^a$ become important. The other factor is connected with ionization and dissociation continua, which are completely neglected in our treatment. For sufficiently intense external fields, multiphoton ionization and dissociation processes may be all but negligible /1.1/. If, however, the ionization and/or dissociation rates in the system we are considering are small compared to the typical magnitude of the various Ω^a's, then the ionization and/or dissociation processes may be considered weak perturbations that may be ignored for times short compared to the ionization/dissociation life time.

1.5 Optical Pumping in a Free Atom

As an example of how the theory developed can be used, let us consider a simplified model of a free alkali atom excited on the D_2 resonance line by a CW "single frequency" laser. In the model we will disregard the hyperfine structure of the energy levels. Except in the case of a strong laser field, this is a poor approximation, since the hyperfine splitting of the electronic ground state is substantial. The model, however, demonstrates many of the most important qualitative features of such a system. Thus we are considering the $^2S_{1/2}$-$^2P_{3/2}$ transition in a free atom. The $^2P_{3/2}$ states decay by spontaneous emission. This is a system of a total of 6 states, giving rise to a 36-element density matrix. Thus the system is small enough to be treated using Eq. 1.17. The matrix elements $\mu^{0,\pm1}_{jm;j'm'}$ of the electric dipole operator of the system can be calculated with the help of Clebsch-Gordan coefficients, and are given in Table 1.3. If the

laser field is written as $\vec{\mathcal{E}}(t) = \vec{E}\exp(i\omega t) + \vec{E}^{*}\exp(-i\omega t)$, and $\vec{E} = E^{+}(\hat{x} + i\hat{y}) + E^{0}\hat{z} + E^{-}(-\hat{x} + i\hat{y})$, then in Eq. 1.17c the interaction matrix element $V'_{jm,j'm'}$ is

$$V'_{jm;j'm'} = \hbar^{-1}\Sigma_{k=0,\pm1}(-1)^{k}E^{k}\mu^{-k}_{jm;j'm'} \ . \qquad 1.21$$

The space axes and the time origin can always be chosen so that the E^{k} are real. From Table 1.3 the Einstein coefficients of the various transitions can easily be calculated, together with the other decay constants of Eq. 1.17c (see Table 1.2). The matrix $A_{jm;j'm'}$ of Einstein coefficients is given in Table 1.4. Starting from the dipole matrix element of the $^{2}S_{1/2}(m = 1/2)$ to the $^{2}P_{3/2}(m = 3/2)$ transition

$$\mu_{o} \equiv \mu^{-}_{3/2,3/2;1/2,1/2} \qquad 1.22a$$

as a basic unit, a natural unit for the Einstein coefficients is

$$A_{o} = A_{3/2,3/2;1/2,1/2} = 4\alpha\mu_{o}^{2}\omega^{3}/(3e^{2}c^{2}) \qquad 1.22b$$

where ω is the angular frequency of the transition, α is the fine structure constant, and c and e have their usual meaning. The corresponding natural unit of electric field is

$$E_{o} = \hbar A_{o}/\mu_{o}. \qquad 1.22c$$

For fields $E \ll E_{o}$, the excitation rates, roughly given by $\mu_{o}E/\hbar$, are small compared to the decay rates given by the Einstein coefficients,

whereas for $E \gg E_o$, the excitation is strong compared to the damping system, and we are in the saturation regime. For alkali atoms, typical dipole matrix elements for transitions around 600 nm wavelength are of the order of $3ea_o$ (where a_o is the Bohr radius). Thus $E_o \simeq 4\alpha\hbar a_o\omega^3/(ec^2) \simeq$ 105 V/m corresponding to a laser intensity of $I_o = \frac{1}{2}c\varepsilon_o(2E_o)^2 = 58$ W/m^2 = 5.8 mW/cm^2. This very moderate laser intensity marks the transition, as discussed above, from the weak field regime to the saturation regime.

The system was analyzed using Eq. 1.17b, incorporated into a computer program. The program consists of constructing the damping matrix Γ_{kk} (Table 1.1b), and diagonalizing this matrix, using standard available computer software /1.3/. Given initial values for the density matrix elements, the initial density matrix is expanded in terms of the eigenvectors ρ_k^a, and the density matrix at later times is calculated. The program was tested on models consisting of several two-level systems (for which exact solutions are known, see Appendix B), and further checked against requirements like: one and only one eigenvalue γ^o of Γ_{kk}, should be zero, real part of all nonzero eigenvalues γ^a should be positive, circularly polarized light should polarize the system completely, a linearly polarized field should be equivalent to a superposition of two oppositely rotating circularly polarized fields, RCP and LCP light should be equivalent, and the response of the system should be symmetric with respect to detuning from resonance of the laser field.

In Table 1.5, we have an example of results from a calculation with $E^+ = E^o = 0$, $E^- = E_o$, excitation on resonance, and population initially incoherently distributed with equal probability in the $m = \pm \frac{1}{2}$ substates of the ground $^2S_{\frac{1}{2}}$ level. As we can see, the real part of the nonzero decay constants all fall between $0.3A_o$ and A_o. This is related to the

fact that the Einstein coefficients of the system are in this range. In the strong field limit, the imaginary parts of the decay constants γ^a (i.e., the oscillation frequencies of the density matrix) should be differences between the various quasienergies Ω^a (see Eq. 1.15h). We see that this is approximately true, even though the field is not particularly strong. These oscillation frequencies are of the same order of magnitude as the various $V'_{jm;j'm'}$ (see Eq. 1.21), and thus related to the transition moments $\mu^-_{jm;j'm'}$. Calculations with various strengths of the electric field E^- show that for small fields all the decay constants are real, whereas when $E^- \gtrsim E_o/3$ (for definition of E_o, see Eq. 1.22) some of the decay constants become complex. This implies that for strong fields we have oscill ·ions in the populations of the various levels. The amplitudes of these oscillations for the case described above, excitation on resonance with $E^- = E_o$, are included in Table 1.5d. In this case the oscillations damp out in of the order of one period of oscillation. However, our calculations show that as E^- increases, the decay rates $\mathrm{Re}(\gamma^a)$ do not change very much, whereas the nonzero oscillation frequencies $\mathrm{Im}(\gamma^a)$ increase approximately in proportio .th E^-. Thus for strong fields, many oscillations of substantial amplitude (see Table 1.5d) may occur in the population of the various m-sublevels of, e.g., the $^2S_{\frac{1}{2}}$-level, before the oscillations damp out. Similar population oscillations occur in the two-level system (see Appendix B).

With a perfectly polarized field, after a time long compared to $1/\mathrm{Re}(\gamma^1)$, all the population will end up in the $^2P_{3/2}(m = -3/2)$ and the $^2S_{\frac{1}{2}}(m = -\frac{1}{2})$ states of the atom, and the system reduces to a two-level system. If the laser field then is turned off, all the population will eventually end up in the $^2S_{\frac{1}{2}}(m = -\frac{1}{2})$ state, as the $^2P_{3/2}(m = -3/2)$

state decays.

Figure 1.1 shows how an admixture of oppositely polarized light alters this. We still choose $E^{-2} + E^{+2} = E_o^2$, and the graph shows the fraction of population that eventually will end up in the $^2S_{\frac{1}{2}}(m = -\frac{1}{2})$ state, as a function of E^-/E^+. Like above, we imagine the laser being turned on for a time long compared to $1/\mathrm{Re}(\gamma^1)$, and ask what the situation is like long after the laser is turned off. As we can see, for $(E^-/E^+) < 1$, we have to a good approximation that the $^2S_{\frac{1}{2}}(m = -\frac{1}{2})$ population is $0.4\ (E^-/E^+)^2$. I.e., the depolarization of the final population is directly proportional to the relative intensities of the two polarizations in the laser field.

Figure 1.2 shows how the polarization of the laser light influences the time needed to reach the steady-state. The graph shows the smallest decay constant $\mathrm{Re}(\gamma^1)$ as a function of polarization ratio E^-/E^+. We see that the response to circularly polarized light ($E^-/E^+ = 0$) relaxes twice as fast as the response to linearly polarized light ($E^-/E^+ = 1$).

Figure 1.3 shows in more detail how the polarization of the light influences the system response. The dashed curve is the magnitude of the smallest decay constant $\mathrm{Re}(\gamma^1)$ for circularly polarized light relative to the decay constant for linearly polarized light, as a function of laser field amplitude. The laser frequency is tuned to resonance. For weak fields, the polarization does not matter, whereas for fields of intensity $I \gtrsim I_o$, the system relaxes twice as fast towards the steady-state response if the field is circularly polarized rather than linearly polarized.

The solid curve of Fig. 1.3 is the magnitude of the steady-state electric dipole polarization induced in the atom by circularly polarized

light. The solid curve of Fig. 1.3 is the magnitude of the steady-state electric dipole polarization induced in the atom by circularly polarized light relative to the polarization for linearly polarized light. The laser frequency is tuned to resonance, and the induced polarization is 90° out of phase with the laser field, like for a two-level system excited on resonance. For weak fields the polarizability of the system is 1.5 times greater for circularly polarized light than for linearly polarized light. This is because $|\mu_{3/2,3/2;1/2,1/2}|^2 = (3/2)|\mu_{3/2,1/2;1/2,1/2}|^2$. For more intense fields, $I \gtrsim I_o$, the difference in polarizability disappears.

Figures 1.4 and 1.5 show how fast the system population is polarized by circularly polarized light. The smallest decay constant $\mathrm{Re}(\gamma^1)$ is plotted as a function of laser frequency detuning Δ from resonance, and of laser field amplitude E^-. For small field amplitudes and/or large detuning, $\mathrm{Re}(\gamma^1)$ is proportional to the field amplitude squared, i.e., to the laser intensity, whereas for strong fields close to resonance ($I \gtrsim I_o$ and $|\Delta| \lesssim \mu_o E^-/\hbar$), the decay rate has a saturated value of $A_o/3$. For large detuning ($|\Delta| \gtrsim \max(A_o/3, \mu_o E^-/\hbar)$) the decay rate $\mathrm{Re}\ (\gamma^1) \propto \Delta^{-2}$.

Calculations were also run with various combinations of strong fields of different polarization, including the case with all three polarizations nonzero. (This is only possible using two crossed laser beams to excite the atom.) When the laser frequency was on resonance, the decay rates were always in the range between $0.1A_o$ and A_o. Only the eigenvectors ρ_k^a were strongly affected by changes in the polarization of light.

The following conclusions, drawn from the sample calculations on

the model system above, should be of fairly general applicability to systems of this kind.

A system excited by a square pulse from a "single frequency" laser will during the pulse relax toward a steady-state response. This response is quite sensitive to the polarization of the laser light. The rate at which the system relaxes towards the steady state during the laser pulse, however, is only moderately affected by changes in the polarization.

For strong laser fields tuned to resonance with the levels excited, the relaxation rate is limited by the inherent decay rates of the system. For weak fields, or fields tuned away from resonance, the rate is proportional to the laser intensity. This is the same type of functional dependence on external field strength and detuning from resonance as we find in the steady-state energy absorption from a laser field by a two-level system (see Appendix B), or by the atom treated above.

After the pulse is over, the atom is left in a certain final state, independent of pulse duration if the pulse is long enough. The final state will be different from the long pulse limit only if the product of the pulse duration and the smallest decay rate during the pulse is of the order of one or smaller. For weak or off-resonant laser fields, this product is proportional to the laser pulse energy fluence, that thus becomes an important parameter. As discussed in Chapter 2, the pulse energy fluence is also an important parameter in the infrared multiphoton excitation of molecules.

The above general features are not very different from what one would get by treating the system with plain rate equations, disregarding the coherence of the excitation. However, just like in the case of

a two-level system, coherence shows up in the oscillation of population between the states of the system, when the driving field is sufficiently strong. The system we have treated is still small enough that these oscillations only have a few frequency components (see Table 1.5d). Then the net overall oscillations can be quite substantial. However, this is not necessarily the case for systems with more levels. Then the oscillations will have more frequency components, which might very well add up to produce very small net oscillations. Quack /1.19/ has carried out numerical and theoretical calculations showing how this can come about, even in the absence of inherent damping of the system.

1.6 Other Possible Applications

The formalism developed above has several applications. We already mentioned the infrared multiphoton excitation, and we have seen an example of optical pumping in an alkali atom. The latter case can be treated in greater detail if the laser field is strong enough to make the approximation of Eq. 1.14 valid, i.e. well into the saturation regime for the pumped transition. Then the corresponding equation of motion (1.15) can be easily solved for a system of up to a few hundred levels. Such a system might, e.g., be an alkali atom with hyperfine structure in both lower and upper states. For a square pulse of laser radiation, the final polarization of the atoms, the population distribution over hyperfine states, the time it takes for the atoms to reach their final population distributions, etc., can all be calculated for various laser intensities, laser pulse durations and polarization states of the laser radiation.

In Appendix C is shown how the formalism developed in Section 1.2

can be extended to cases where the amplitude, frequency and/or phase of the exciting field varies in time. There are quite a few experimental situations that might be of interest to treat with this formalism. It should be pointed out that the e.m. field is assumed to be completely coherent. Thus fields with random fluctu in phase and/or amplitude are not included. For the latter type of field, considerable effort has been devoted to treating twolevel system models lately (see, e.g., /1.17/ and /1.18/). The approach used in Appendix B and all of this chapter does not attempt to cover this type of excitation. The types of laser sources our approach deals with are lasers with well characterized pulses, like transform-limited single pulses or trains of modelocked pulses, and phase-, frequency-, and/or amplitude-modulated "single frequency" lasers. The approach of describing the field in terms of time-dependent phase, amplitude and frequency is only feasible in a system with quite few levels. This is particularly true (just like in the case with a perfectly steady monochromatic field) if the damping in the system is important, such that the density matrix and not the state vector has to be used in the full treatment.

On the other hand, we should emphasize that we have a formalism which is valid for fields of rapidly varying intensity and frequency, of arbitrary strength, as long as the interaction matrix elements between field and q.m. system are small, i.e., as long as the detuning from resonance of the energy levels neglected in the treatment of the system are large compared to the interaction matrix elements.

References

1.1 "Multiphoton Processes," edited by J. H. Eberly and P. Lambropoulos (Wiley, New York, 1978).

1.2 G. Dahlquist and Aa. Bjørck, "Numerical Methods" (Prentice Hall, Englewood Cliffs, N. J., 1974).

1.3 B. T. Smith, "Matrix Eigensystem Routines-EISPACK Guide" (Springer, New York, 1974); J. J. Dongarra, C. E. Moler, J. R. Bunch, and J. W. Stewart, "A Guide to LINPACK" (SIAM, Philadelphia, 1979).

1.4 N. Bloembergen, "Nonlinear Optics" (W. A. Benjamin, N.Y., 1964).

1.5 The "dressed atom" concept is discussed, e.g., by C. Cohen-Tannoudji and S. Reynaud, in Ref. 1.1, p. 103-118.

1.6 B. R. Mollow, Phys. Rev. A12, 1919 (1975).

1.7 A. Omont, Prog. Quant. Electr. 5, 69 (1977).

1.8 A. Abragam, "The Principles of Nuclear Magnetism," Chapter VII (Clarendon Press, Oxford, 1961).

1.9 C. D. Cantrell and H. W. Galbraith, J. Molec. Spectrosc. 58, 165 (1975).

1.10 J. P. Aldridge, H. Filip, H. Flicker, R. F. Holland, R. S. McDowell, N. G. Nereson, and K. Fox, J. Molec. Spectrosc. 58, 158 (1975).

1.11 J. R. Ackerhalt and H. W. Galbraith, J. Chem Phys. 69, 1200 (1978); Opt. Lett. 3, 109 (1978).

1.12 C. D. Cantrell and K. Fox, Opt. Lett. 2, 151 (1978).

1.13 H. W. Galbraith and J. R. Ackerhalt, Opt. Lett. 3, 152 (1978).

1.14 R. V. Ambartzumian, Yu. A. Gorokhov, V. S. Letokhov, G. N. Makarov, and A. A. Puretzky, JEPT Lett. 23, 22 (1976); Sov. Phys. JETP 44, 231 (1976).

1.15 P. A. Schulz, A. S. Sudbø, E. R. Grant, D. J. Krajnovich, Y. R.

Shen, and Y. T. Lee, J. Chem. Phys. (to be published).

1.16 S. Ezekiel and F. Y. Wu, Ref. 1.1, p. 119.

1.17 L. Mandel and H. J. Kimble, Ref. 1.1, p. 145.

1.18 A. T. Georges, P. Lambropoulos, and P. Zoller, Phys. Rev. Lett. 42, 1609 (1979).

1.19 M. Quack, J. Chem. Phys. 69, 1282 (1978).

Table 1.1a

Conversion of Eq. 1.2 into an equation involving only real quantities. Definition of the matrix $\Gamma_{kk'}$ (Eqs. 1.3 and 1.5).

$k' \in$ / $k \in$	N_1	N_2	N_3
N_1	$\mathrm{Re}(\Gamma_{kkk'k'})$	$2\mathrm{Re}(\Gamma_{kk\ell'm'})$	$-2\mathrm{Im}(\Gamma_{kk\ell'm'})$
N_2	$\mathrm{Re}(\Gamma_{\ell mk'k'})$	$\mathrm{Re}(\Gamma_{\ell m\ell'm'} + \Gamma_{\ell mm'\ell'})$	$-\mathrm{Im}(\Gamma_{\ell m\ell'm'} - \Gamma_{\ell mm'\ell'})$
N_3	$\mathrm{Im}(\Gamma_{\ell mk'k'})$	$\mathrm{Im}(\Gamma_{\ell m\ell'm'} - \Gamma_{\ell mm'\ell'})$	$\mathrm{Re}(\Gamma_{\ell m\ell'm'} - \Gamma_{\ell mm'\ell'})$

Table 1.1b

The damping matrix $\Gamma'_{kk'}$ of Eq. 1.17b, expressed in terms of the decay terms $\gamma_{\ell m \ell' m'}$ (Eq. 1.7) and the matrix elements $V'_{\ell\ell'}$ of the hamiltonian (Eq. 1.9). As in Eq. 1.9a, $\Delta_k = \omega_k - n_k\omega$.

$k \in$ \ $k' \in$	N_1	N_2	N_3
N_1	$\gamma_{kkk'k'}$	$2\gamma_{kk\ell'm'}$	$2V'_{m'\ell'}(\delta_{k\ell'} - \delta_{km'})$
N_2	$\gamma_{\ell mk'k'}$	$\gamma_{\ell m\ell'm'} + \gamma_{\ell mm'\ell'}$	$-(\Delta_\ell - \Delta_m)(\delta_{\ell\ell'}\delta_{mm'} + \delta_{\ell m'}\delta_{m\ell'}) -$ $- V'_{\ell\ell'}\delta_{mm'} + V'_{m'm}\delta_{\ell\ell'} +$ $+ V'_{\ell m'}\delta_{m\ell'} - V'_{\ell' m}\delta_{\ell m'}$
N_3	$V'_{\ell m}(\delta_{mk'} - \delta_{\ell k'})$	$(\Delta_\ell - \Delta_m)(\delta_{\ell\ell'}\delta_{mm'} - \delta_{\ell m'}\delta_{m\ell'})$ $+ V'_{\ell\ell'}\delta_{mm'} - V'_{m'm}\delta_{\ell\ell'} -$ $- V'_{\ell m'}\delta_{m\ell'} + V'_{\ell' m}\delta_{\ell m'}$	$\gamma_{\ell m\ell'm'} - \gamma_{\ell mm'\ell'}$

Table 1.2

Values of the decay matrix $\gamma_{\ell m \ell' m'}$ in the case of spontaneous emission.

Condition	$\gamma_{\ell m \ell' m'}$
$\ell = m = \ell' = m'$	A_ℓ
$\ell = m \neq \ell' = m'$	$-A_{\ell'\ell}$
$\ell \neq m$, $\ell' = \ell$, $m' = m$	$(A_\ell + A_m)/2$
all other	zero, unless $\omega_\ell - \omega_m - \omega_{\ell'} + \omega_{m'}$ is small enough to be comparable in magnitude to some of the A_ℓ, in which case we get $\frac{1}{2}\left(\frac{A_{\ell'\ell}}{\lvert\vec{\mu}_{\ell'\ell}\rvert^2} + \frac{A_{m'm}}{\lvert\vec{\mu}_{m'm}\rvert^2}\right)\vec{\mu}_{m'm} \cdot \vec{\mu}^*_{\ell'\ell}$

Table 1.3

Matrix elements $\mu^{k}_{jm;j'm'}$ of the electric dipole operator, in units of $\mu_o \equiv \mu^{-}_{3/2,3/2;1/2,1/2}$.

$k = 1$

		j' = 3/2, m' = 3/2	3/2, 1/2	3/2, -1/2	3/2, -3/2	1/2, 1/2	1/2, -1/2
j = 3/2, m = 3/2		0	0	0	0	0	0
j = 3/2, m = 1/2		0	0	0	0	0	0
j = 3/2, m = -1/2		0	0	0	0	$\sqrt{1/3}$	0
j = 3/2, m = -3/2		0	0	0	0	0	1
j = 1/2, m = 1/2		-1	0	0	0	0	0
j = 1/2, m = -1/2		0	$-\sqrt{1/3}$	0	0	0	0

$k = 0$

j = 3/2, m = 3/2		0	0	0	0	0	0
j = 3/2, m = 1/2		0	0	0	0	0	$\sqrt{2/3}$
j = 3/2, m = -1/2		0	0	0	0	$\sqrt{2/3}$	0
j = 3/2, m = -3/2		0	0	0	0	0	0
j = 1/2, m = 1/2		0	0	$\sqrt{2/3}$	0	0	0
j = 1/2, m = -1/2		0	$\sqrt{2/3}$	0	0	0	0

$k = -1$

j = 3/2, m = 3/2		0	0	0	0	1	0
j = 3/2, m = 1/2		0	0	0	0	0	$\sqrt{1/3}$
j = 3/2, m = -1/2		0	0	0	0	0	0
j = 3/2, m = -3/2		0	0	0	0	0	0
j = 1/2, m = 1/2		0	0	$-\sqrt{1/3}$	0	0	0
j = 1/2, m = -1/2		0	0	0	-1	0	0

Table 1.4

Einstein coefficients $A_{jm;j'm'}$, in units of $A_o = A_{3/2,3/2;1/2,1/2}$.

		j'	3/2				1/2	
		m'	3/2	1/2	-1/2	-3/2	1/2	-3/2
j	m							
3/2	3/2		0	0	0	0	1	0
	1/2		0	0	0	0	2/3	1/3
	-1/2		0	0	0	0	1/3	2/3
	-3/2		0	0	0	0	0	1
1/2	1/2		0	0	0	0	0	0
	-1/2		0	0	0	0	0	0

Table 1.5a

Quasienergies Ω^a (in units of A_o, see Eq. 1.22) and corresponding eigenvectors ϕ^a_{jm} for a $^2S_{1/2}$-$^2P_{3/2}$-transition excited by circularly polarized light of intensity $I = I_o$ (see Eq. 1.22).

a			1	2	3	4	5	6
Ω^a			-1	$-\sqrt{1/3}$	0	0	$\sqrt{1/3}$	1
	j	m						
ϕ^a_{jm}	3/2	3/2	0	0	0	1	0	0
		1/2	0	0	1	0	0	0
		-1/2	0	$\sqrt{1/2}$	0	0	$\sqrt{1/2}$	0
		-3/2	$\sqrt{1/2}$	0	0	0	0	$\sqrt{1/2}$
	1/2	1/2	0	$\sqrt{1/2}$	0	0	$-\sqrt{1/2}$	0
		-1/2	$\sqrt{1/2}$	0	0	0	0	$-\sqrt{1/2}$

Table 1.5b

Decay constants $Re(\gamma^a)$ and oscillation frequencies $Im(\gamma^a)$ (in units of A_o) for the system of Table 1.5a. The fourth coloumn of the table tells which of the eigenvectors ρ_k^a that give a nonzero contribution to the expansion of the density matrix in terms of the eigenvectors.

a	$Re(\gamma^a)$	$Im(\gamma^a)$	contribution to density matrix
0	0.0	0.0	nonzero
1	0.3020	0.0	nonzero
2	0.3436	0.4085	0
3	0.3436	0.4085	0
4	0.3436	-.4085	0
5	0.3436	-.4085	0
6	0.5	0.0	0
7	0.5	0.0	0
8	0.5990	1.0549	nonzero
9	0.5990	-1.0549	nonzero
10	0.6564	1.5161	0
11	0.6564	1.5161	0
12	0.6564	-1.5161	0
13	0.6564	-1.5161	0
14	0.75	0.5204	0
15	0.75	0.5204	0
16	0.75	0.5204	0
17	0.75	0.5204	0
18	0.75	-.5204	0
19	0.75	-.5204	0
20	0.75	-.5204	0
21	0.75	-.5204	0
22	0.75	0.9683	0
23	0.75	0.9683	0
24	0.75	0.9683	0
25	0.75	0.9683	0
26	0.75	-.9683	0
27	0.75	-.9683	0
28	0.75	-.9683	0
29	0.75	-.9683	0
30	0.75	1.9843	nonzero
31	0.75	-1.9843	nonzero
32	1.0	0.0	0
33	1.0	0.0	0
34	1.0	0.0	0
35	1.0	0.0	0

Table 1.5c

Steady state density matrix $\rho^{o}_{jm;j'm'}$, for the system of Table 1.5a. Elements with $j \neq j'$ have an additional term $\exp(\pm i\omega t)$, where ω is the laser frequency.

		j'	3/2				1/2	
		m'	3/2	1/2	-1/2	-3/2	1/2	-1/2
j	m							
3/2	3/2		0	0	0	0	0	0
	1/2		0	0	0	0	0	0
	-1/2		0	0	0	0	0	0
	-3/2		0	0	0	4/9	0	2i/9
1/2	1/2		0	0	0	0	0	0
	-1/2		0	0	0	-2i/9	0	5/9

Table 1.5d

Population in the various levels for each of the eigenvectors ρ_k^a for the system of Table 1.5a. The atom is initially unpolarized and in the $^2S_{1/2}$ level, and only eigenvectors with nonzero contributions to the population are listed. For $a \neq 0$ the population may oscillate, in which case the complex amplitude of the oscillation is listed. Also for $a \neq 0$, the total population $Tr(\rho^a)$ is zero, so that negative as well as positive populations are present even for eigenvectors that are not associated with population oscillations (i.e., γ^a is real).

a \ j		3/2				1/2	
a \ m		3/2	1/2	-1/2	-3/2	1/2	-1/2
0		0.0	0.0	0.0	0.4444	0.0	0.5555
1		0.0	0.0	0.2776	-.2961	0.3351	-.3166
8+9	Re	0.0	0.0	-.2776	0.0868	0.1649	0.0259
	Im	0.0	0.0	0.0781	-.0636	0.1896	-.0429
30+31	Re	0.0	0.0	0.0	-.2351	0.0	0.2351
	Im	0.0	0.0	0.0	0.0713	0.0	-.0713

Figure Captions

Fig. 1.1 Fraction of population in the $^2S_{1/2}(m = 1/2)$ state, after a long laser pulse of field amplitude $2E_o$ (see Eq. 1.22), tuned to resonance, as a function of LCP relative to RCP field amplitudes, E^-/E^+.

Fig. 1.2 Smallest nonzero decay constant $Re(\gamma^1)$, in a laser field of amplitude $2E_o$ (see Eq. 1.22), tuned to resonance, as a function of LCP relative to RCP field amplitudes, E^-/E^+.

Fig. 1.3 - - - - - Ratio between the smallest nonzero decay constants $Re(\gamma^1)$, for circularly and linearly polarized light, as a function of laser field amplitude (in units of E_o, see Eq. 1.22). ———— Ratio between the induced steady state electric polarizations for circularly and linearly polarized light on resonance, as a function of laser field amplitude (in units of E_o, see Eq. 1.22).

Fig. 1.4 Smallest nonzero decay constant $Re(\gamma^1)$ (in units of A_o, see Eq. 1.22) for circularly polarized light on resonance, as a function of laser field amplitude (in units of E_o, see Eq. 1.22).

Fig. 1.5 Smallest nonzero decay constant $Re(\gamma^1)$ (in units of A_o, see Eq. 1.22), for circularly polarized light, and for three different field amplitudes E^+ (in units of E_o, see Eq. 1.22), as a function of detuning Δ (in units of A_o) from resonance.

Figure 1.1

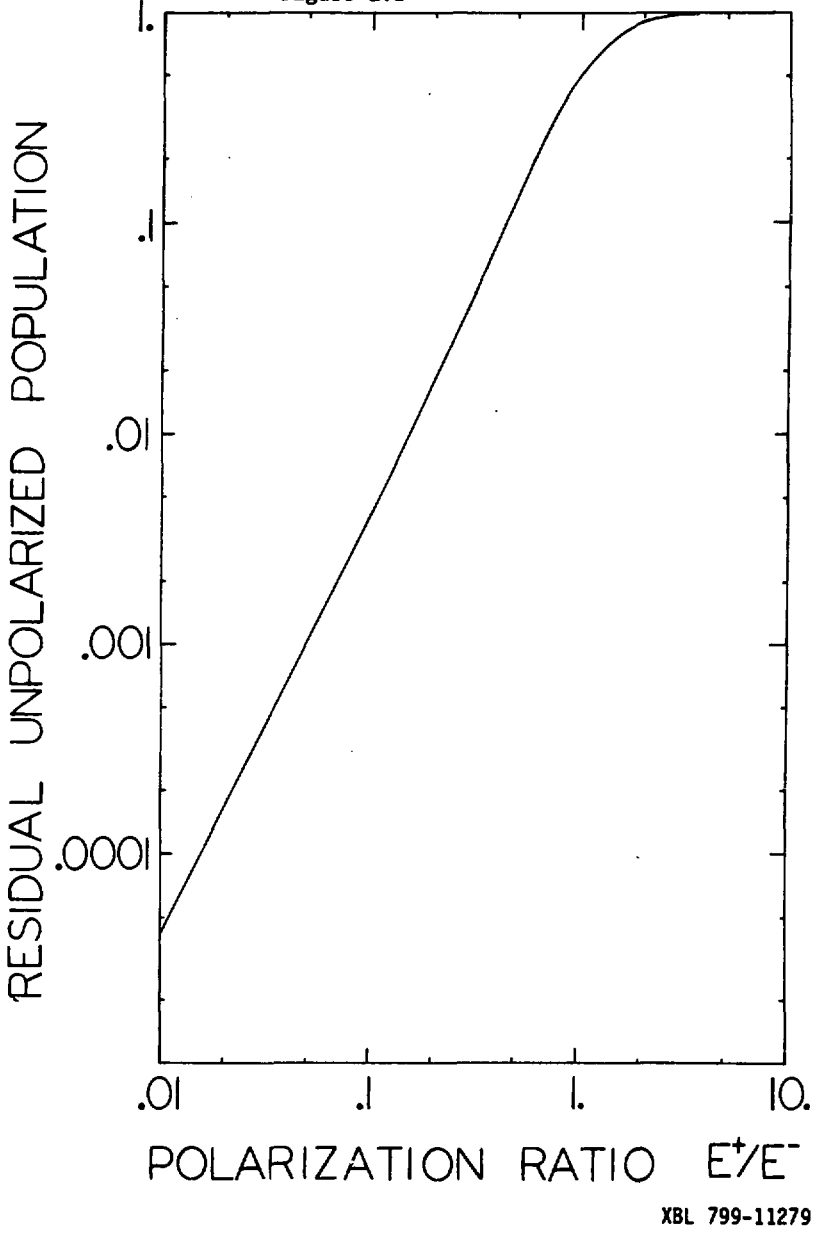

XBL 799-11279

Figure 1.2

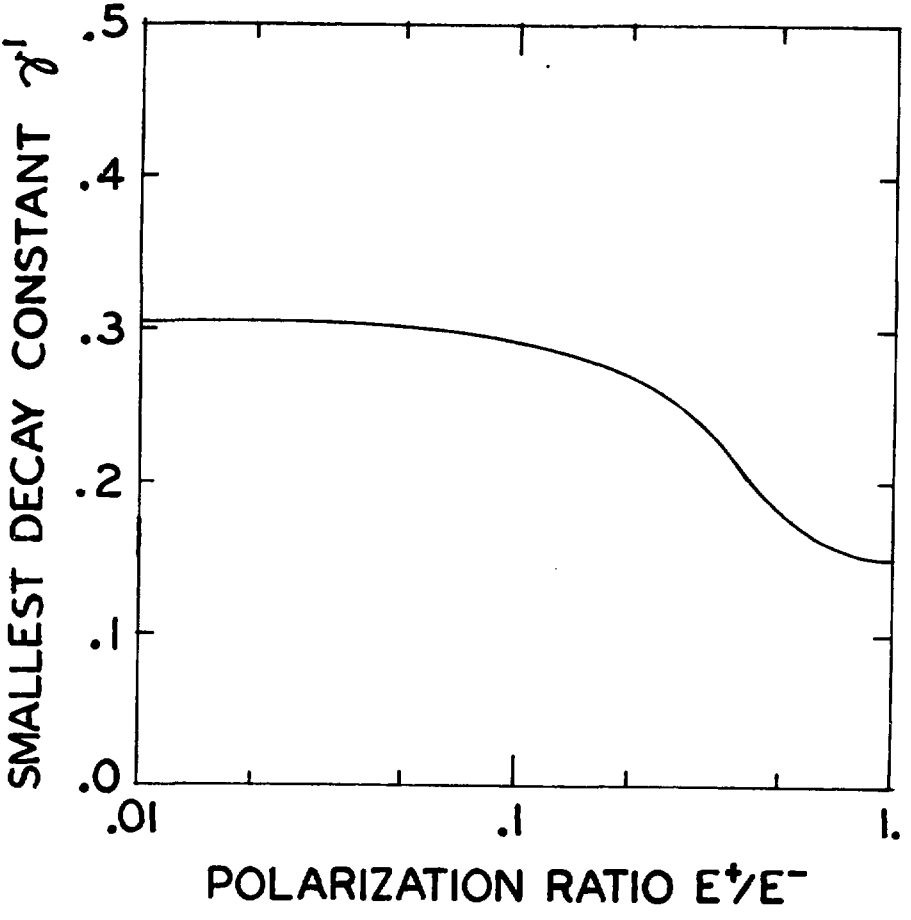

XBL 799-11275

Figure 1.3

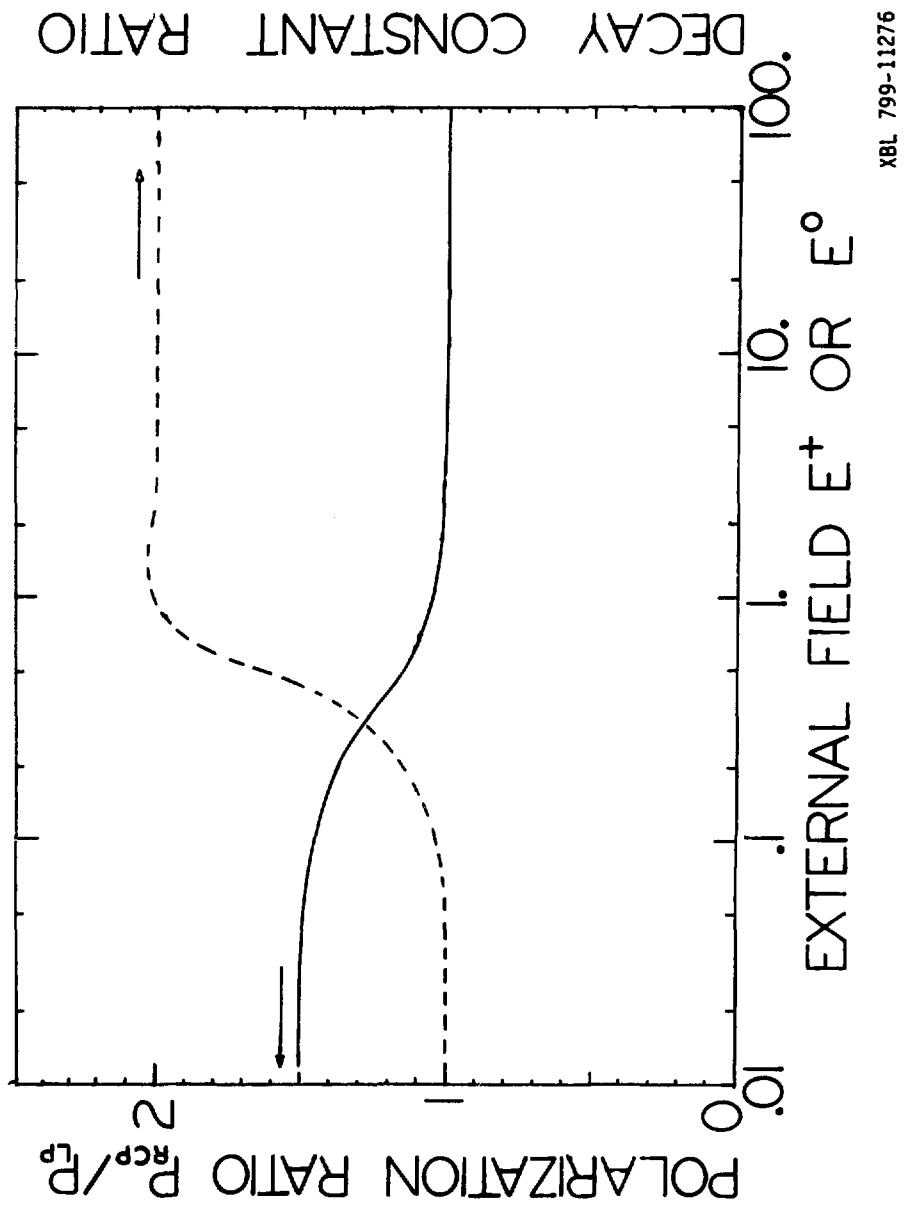
DECAY CONSTANT RATIO
100.
10.
1.
.1
.01
EXTERNAL FIELD E+ OR E°
POLARIZATION RATIO RCP/RLP
2
1
0
XBL 799-11276

Figure 1.4

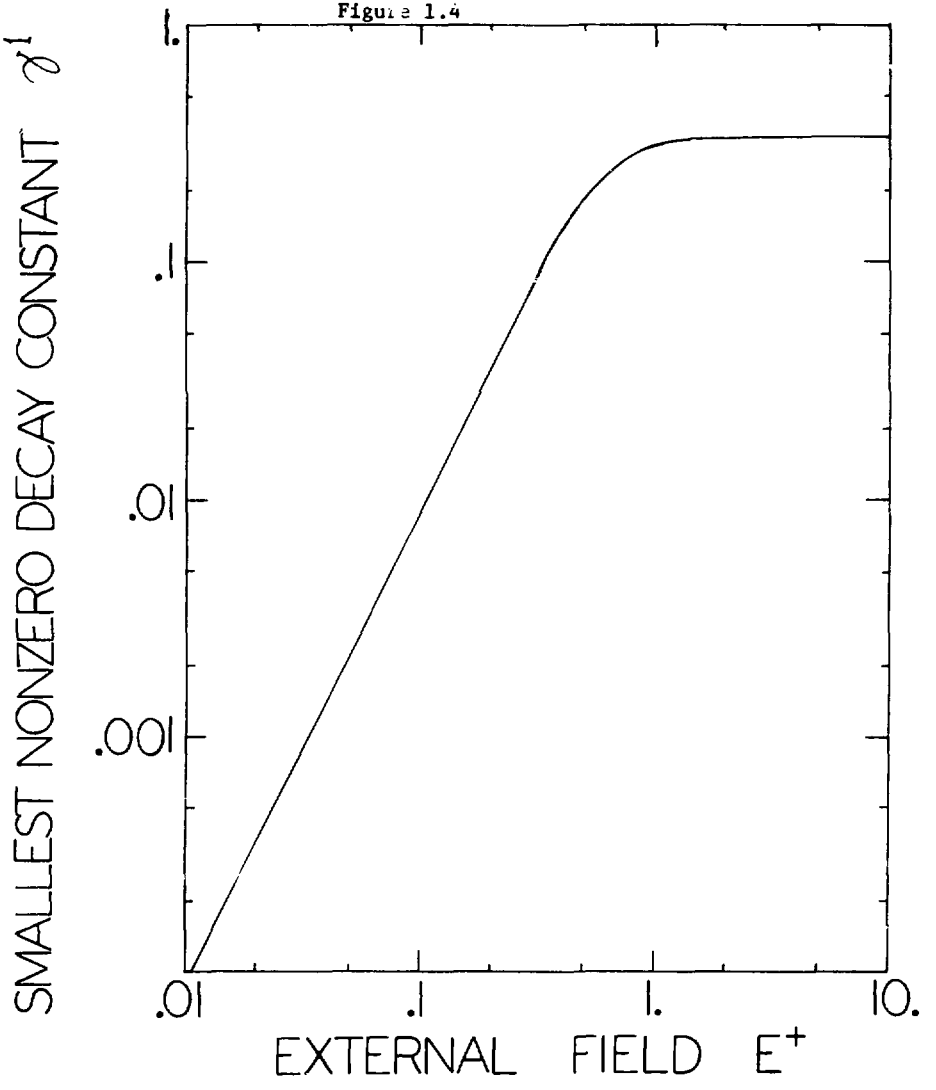

XBL 799-11277

Figure 1.5

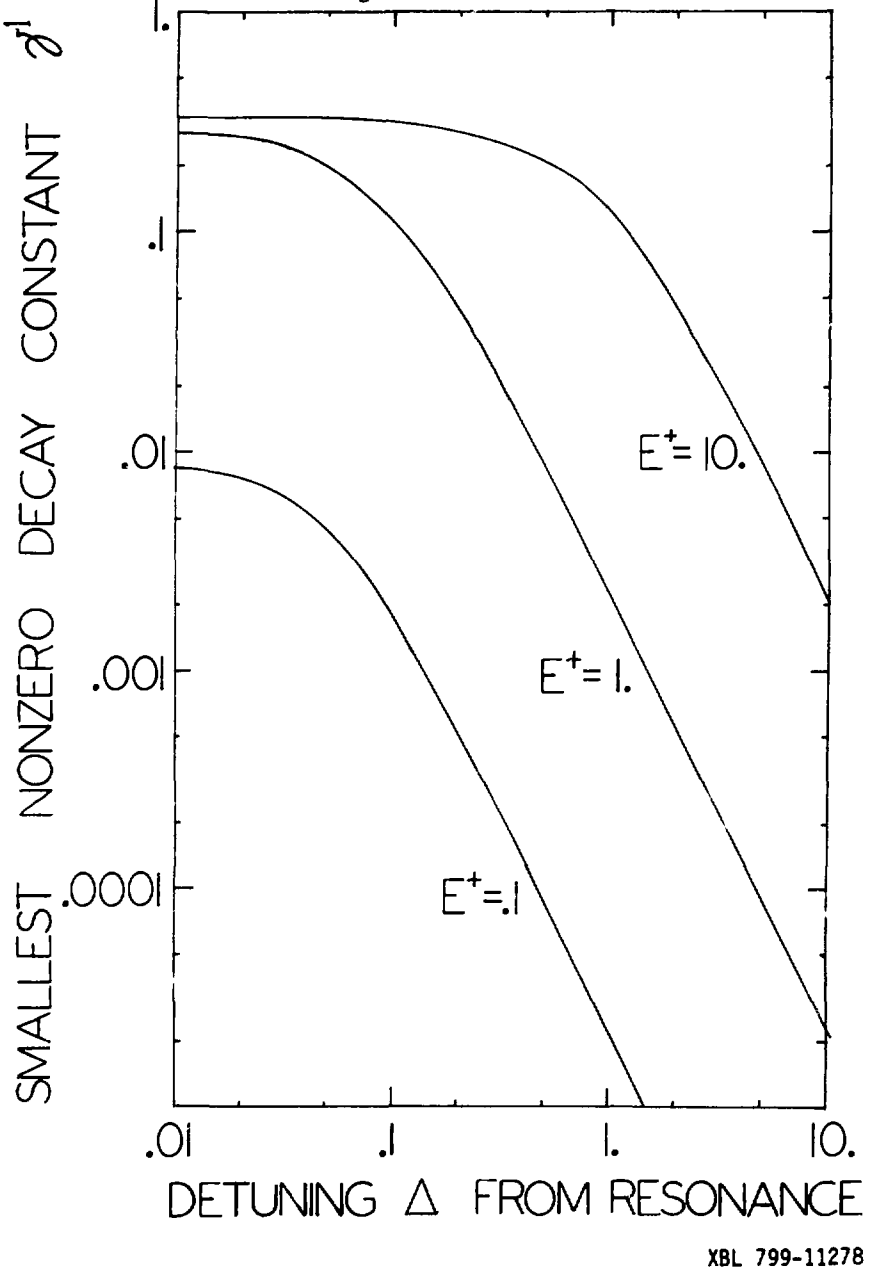

XBL 799-11278

CHAPTER 2 MULTIPHOTON DISSOCIATION OF MOLECULES

2.1 Introduction

This chapter is an account of experimental work on the process of infrared laser-induced multiphoton dissociation (MPD). We emphasize here the general understanding of the process. More detailed accounts of some of the experiments discussed in this chapter can be found in Appendices E and F, which are reprints of papers published previously.

As we shall see later, the MPD process is dominated by incoherent excitation of molecules. The coherent transitions discussed in the previous chapter can be important for initial excitation between low-lying discrete states. This part of the process represents a so-called "bottleneck" /2.1-3/ for the multiphoton excitation, in the sense that it may be difficult for some molecules to be excited out of these low-lying levels. However, this seems to be of little importance for the overall results of MPD. The experiments to be discussed here do not reveal very much about the nature of such initial excitation. We will see that our results can to a great extent be described independently from what is discussed in Chapter 1. Central to the understanding of the MPD process however, is the RRKM theory of unimolecular reactions. A brief outline of this theory is given in Appendix D, and a thorough discussion of it can be found in Ref. D.1.

Laser-induced multiphoton dissociation (MPD) of molecules is a collisionless unimolecular process. In the early studies, the collisionless nature of the process was inferred by the observation of instantaneous luminescence from the dissociation products following laser excitation and by the observation of linear pressure dependence of the disso-

ciation yield at sufficiently low gas pressures /2.4-7/. The experiments were done in gas cells in which excitation may be assumed collisionless if the laser pulse is much shorter than the mean free time between collisions of the molecules. Even so, after the laser pulse is over, molecular collisions in the gas cell are still unavoidable, leading to possible collisional dissociation of excited molecules and chemical reactions among dissociation products and excited parent molecules. Thus, it is generally recognized that the primary dissociation fragments cannot be unambiguously identified in the gas cell experiments.

The best way to study a collisionless process is of course in a collisionless experiment. A molecular beam method is therefore most appropriate for the study of MPD. Indeed, observation of infrared MPD in a molecular beam provides the most direct evidence that the process is collisionless /2.8/. The use of a mass spectrometer to detect the dissociation fragments from the beam allows us to identify the primary dissociation products in a straightforward way /2.8,9/. The latter information is in fact of great fundamental importance for the understanding of MPD, because it reveals whether there is any correlation between the pattern of molecular dissociation and the vibrational mode through which the initial excitation is attained.

With a molecular beam apparatus which will be described later in the chapter, the angular and velocity distributions of the fragments can also be measured. From the measurements, much additional information about the dynamics of MPD can be deduced. Once the major dissociation fragments have been identified, there are a number of important questions that need to be answered before a reasonable physical understanding of MPD can be achieved.

(1) What is the excitation mechanism? How is it possible for a molecule to be excited over the low-lying discrete rovibrational states, up into and through the so-called quasi-continuum /2.10/ where the molecular density of states is very high, and into the dissociative continuum states? Does the excitation remain as an orderly vibration characteristic of the normal mode being excited, or does the excitation become more random as the level of excitation increases? How many photons does each molecule absorb before dissociation, or equivalently, what is the average excitation level from which a molecule will dissociate? What eventually limits the level of excitation?

(2) Through which channel (or channels) does the molecule dissociate, and how does this depend on the laser excitation? More specifically, how do observed dissociation products, average dissociation rates, translational and internal energy in the products depend on parameters of the laser excitation pulse: intensity, duration and frequency? Is the major dissociation channel in MPD different from that in thermal decomposition? What is the dissociation rate of molecules and how does it depend on the level of excitation?

(3) What is the dynamics of dissociation? How does the energy available to the fragments distribute itself among the various degrees of freedom (translation, rotation, and vibration) of the fragments? What happens to the fragments after they are produced; can they absorb more laser energy and undergo a secondary MPD?

Most of these questions are usually difficult to answer from the analysis of final products in the gas cell experiments. However, as we shall see in this chapter, they can be and have been answered by measur-

ing angular and velocity distributions of the fragments in the molecular beam experiment. In addition to the molecular beam experiments, the newly developed laser induced fluorescence technique for detecting a small number of molecules has been used to detect dissociation fragments from collisionless MPD in a low-pressure gas cell /2.11-16/. Because of the good spatial and temporal resolution of the probing pulse, this technique can also yield information on the dissociation dynamics of the fragments. In principle, this detection method sometimes is even superior to the usual mass spectrometric detection method used in most molecular beam experiments, in the sense that it can also measure the rotational and vibrational energy distributions in the fragments. In practice, however, this technique is limited to some small fragments by the fact that the optical transitions of many larger dissociation fragments are either not known, too complicated, or cannot be reached by the available probe laser.

With the far reaching consequences such a possibility opens up in synthetic chemistry, it has been a hope that MPD might be mode-selective, that is, the excitation energy should remain to a large extent in the vibrational mode being excited. If this were true, the dissociation products could be different from those expected in thermal decomposition, and application of MPD to chemical synthesis could lead to a revolutionary change in the field. So far, however, aside from some erroneous conclusions, no concrete evidence of mode-selective MPD has been reported. The molecular beam experiments on many molecules described here have shown that in the infrared MPD process the rate of intramolecular energy transfer of dissociating molecules is faster than the rate of dissociation, such that the statistical theory of unimolecular decomposition /D.1/ can be used to describe the dissociation of excited molecules sat-

isfactorily. This is not really surprising, as discussed in Appendix D, in view of the fact that the energy deposition rate as well as the rate of dissociation is rather slow compared with intramolecular energy transfer rates. Indeed, the statistical theory, used convincingly to explain our molecular beam experiments, is the key to answering most of the questions concerning the dynamics of MPD. It can also be used to establish a simple and reliable phenomenological model /2.17-19/ which has been successful in describing the MPD process more quantitatively.

The subject of this chapter is the study of MPD in a molecular beam with high-power infrared lasers. We shall first describe the experimental apparatus and the experimental results, followed by a thorough discussion of the results, the interpretation, the various aspects of the problem, and our present understanding of the MPD process.

2.2 Experimental Arrangement

In order to understand the dynamics of infrared multiphoton dissociation of polyatomic molecules, it is necessary to carry out experiments under collision free conditions and obtain some information which is directly related to the dissociation dynamics. The positive identification of primary dissociation products, the measurement of the energy distribution of the fragments and the determination of the lifetime of the excited molecules are important data that need to be obtained in order to make an assessment of the extent of energy randomization and the level of excitation prior to the dissociation of excited molecules.

The crossed laser-molecular beam arrangement is very well suited for this purpose and is used in our experimental investigations. The molecular beam apparatus used is shown schematically in Fig. 2.1. It is a

modification of an apparatus originally designed for crossed molecular beam studies of cross sections for elastic and reactive scattering /2.8, 2.20/. The molecular beam was formed by expansion of the pure gas or a gaseous mixture using a rare gas as carrier at ~ 75-200 Torr stagnation pressure from a 0.1 mm-diameter quartz nozzle. Three stages of differential pumping were used along with two conical skimmers and a final collimating slit to produce a well defined beam ~ 2 mm in diameter in the laser irradiation region. The molecular beam had a very sharply delineated angular distribution of 1.2° full width at half-maximum (FWHM). Three stages of differential pumping were found to be necessary for this type of experiment in order to allow detection of the dissociation products near the molecular beam, since the fragmentation of beam molecules in the ionizer of a mass spectrometer produces the same mass peaks as those from the dissociation products. The velocity distribution of the molecular beam typically had a FWHM spread of 25% of the average velocity, or better. The density of molecules in the beam in the irradiation region was $\sim 3 \times 10^{11}/cm^3$. The velocity spread and the number density of the molecular beam are both limited by the stagnation pressure which had to be kept low to avoid the formation of Van der Waals dimers and polymers during the expansion. A Tachisto TAC II grating tuned CO_2 TEA laser (~ 1.0 J/pulse) was used in our experiments as the excitation source. The laser beam was admitted into the vacuum chamber via a ZnSe lens with a 25.4-cm focal length. The power and the energy fluence of the laser at the molecular beam was adjusted by varying the distance between the focal region of the lens and the molecular beam. The fragments produced by multiphoton dissociation of polyatomic molecules at the small intersection region were detected by a triply differentially pumped quadrupole mass spec-

trometer utilizing electron bombardment ionization and ion counting. The pressures in the three regions of the detector were maintained at $\sim 10^{-9}$, $\sim 10^{-10}$, and $\sim 10^{-11}$ Torr by a combination of ion pumps, a sublimation pump, a liquid nitrogen trap and a liquid helium cryopump. The partial pressure of the beam molecule in the third region where the ionizer is located was usually kept below 10^{-13} Torr. The angular position of the mass spectrometer around the beam intersection point could be varied so that the angular distribution of the fragments could be measured. The mass filter was usually adjusted to provide better than unit mass resolution. As shown schematically in Fig. 2.2, external triggering at 0.5 Hz was used to fire the laser and to enable a dual-channel scaler for recording counts of fragments from the mass spectrometer. Separate adjustments of delay and gate times were made to ensure that one scaler channel recorded only background (i.e., with the laser pulse off) while the other recorded both background and signal. Typically, 100-1000 laser shots were used to measure the fragments produced at each laboratory angle for the measurements of angular distributions. The angular resolution of the detector was 1°. In order to positively identify the dissociation products and to check for possible secondary dissociation of a primary product by the same laser pulse, the angular and velocity distributions were scanned at several mass peaks in the mass spectra of the dissociation products of a molecule under investigation. The fragment velocity distributions at various laboratory scattering angles were obtained by determining the arrival time of each fragment, after a flight path of 21 cm, at the detector, relative to the time origin defined by the laser pulse. This was done by multiscaling the mass spectrometer output signal. Typically, a 10 μs channel width was used in a scan over 2.5 ms, and the

time of flight spectra obtained were averaged over 100-5000 laser pulses.

The dissociation products and their angular and velocity distributions were extensively measured while varying the laser frequency, power, and energy fluence and the vibrational and rotational temperatures of the molecules.

2.3 Experimental Results

The major MPD products identified in our molecular beam experiments are listed in the first column of Table 2.1, which summarizes our results. The dissociation products observed are typically those from the channel with the lowest activation energy. According to the measurements by several other groups /2.11-16/ using laser induced fluorescence detection, they appear in their ground electronic states, or in some cases /2.21-22/, in low-lying electronic states.

For C_2F_5Cl and $CHClCF_2$, two dissociation channels corresponding to the two lowest activation energies have been observed. For CH_3CF_2Cl the HF and HCl molecular eliminations were suggested to have, within experimental uncertainty, the same activation energies in earlier thermal dissociation studies /2.23/, but the HCl elimination is the only channel observed in our experiments. For SF_6 and $CFCl_3$, secondary dissociation of the primary products is observed at high energy fluence ($SF_5 \rightarrow SF_4 + F$, $CFCl_2 \rightarrow CFCl + Cl$).

In the cases where two competitive dissociation channels are observed, the intensity of the laser pulse was found to influence the branching ratio. Figure 2.3 shows the relative dissociation yield of C_2F_5Cl into $CF_3 + CF_2Cl$ and $C_2F_5 + Cl$ as a function of laser energy. The chlorine atom elimination has a threshold at 0.5 J/cm^2 and saturates at

1 J/cm^2. The channel producing CF_3 + $CF_2C\ell$ has approximately the same threshold, but as the intensity is increased, the fraction dissociating by C-C bond rupture continues to increase.

The laboratory angular and velocity distributions for SF_5 in the fluorine atom elimination from SF_6 are shown in Figs. 2.4 and 2.5. The angular distribution of the SF_5 peaks as close to the SF_6 beam as can be measured (5°) and falls off monotonically with increasing angle. The velocity distributions of SF_5 shown in Fig. 2.5 were obtained from the time of flight measurements at three angles. Also shown is the SF_5 beam velocity distribution. The angular and velocity distributions for SF_6 are typical of the other halogen atom elimination reactions. For example, Figs. 2.6-8 show the laboratory angular and velocity distributions of CF_3 and I from MPD of CF_3I. Further examples can be found in Appendix E.

Translational energy distributions of dissociation products are derived from the measured laboratory angular and velocity distributions. First, an assumed center-of-mass translational energy distribution of the fragments is transformed to the laboratory coordinates, including the convolution over the beam velocity distribution and the length of the ionizer in the mass spectrometer. Then, the angular and velocity distributions in the laboratory coordinates can be calculated and fit to the experimental curves. A detailed description of this procedure is given in Appendix F. Center-of-mass angular distributions of products are found to be isotropic for all systems studied. This can be concluded from the agreement between experiments and theoretical curves deduced using this assumption, and from the observation that our results were independent of laser polarization. Figure D.2 shows the translational energy distribution of SF_5 + F derived from the experimental results /2.18/. The curves drawn

in Figs. 2.4 and 2.5 are the angular and velocity distributions calculated from the translational energy distributions shown in Fig. D.2. Similar results were obtained for a variety of molecules (see Appendix E).

Columns 4 and 5 of Table 2.1 give information on the average translational energy and the peak of the translational energy distribution. It is clearly seen that except for some 3- and 4-center eliminations, which are known to have additional potential energy barriers for dissociation, the translational energy distributions all peak at zero kinetic energy and the average translational energies of the products are generally very low.

The systems with an additional potential energy barrier in the exit channel have characteristically different translational energy distributions, which are reflected in laboratory angular and velocity distributions. Three-center elimination of HCℓ from $CHF_2C\ell$ is one of the examples. The velocity distributions of the HCℓ in this case is shown in Fig. 2.9. The center-of-mass translational energy distribution peaks at 5 kcal/mole, as shown in Fig. 2.10. Four-center elimination of HCℓ from $CH_3CC\ell_3$ and $CH_3CF_2C\ell$ and C-C bond rupture in $C_2F_5C\ell$ all have similar characteristic translational energy distributions. The three- and four-center elimination reactions are discussed extensively in Appendix F.

2.4 Discussion

Let us start by looking at some of our typical experimental results on the translational energy distribution of the dissociation fragments. Shown in Fig. 2.5 are the velocity distributions of SF_5 fragments from MPD of SF_6 at various angles with respect to the SF_6 beam /2.18,24/. We see that they are only slightly broader than that of the primary SF_6 beam

because the average translational energy imparted to the fragments in the dissociation is quite small. The same conclusion can be drawn from the angular distribution of SF_5 fragments shown in Fig. 2.4 It falls off rapidly as the angle from the SF_6 beam increases, again indicating that very little translational energy is released to the fragments. More quantitatively, this can be seen from the translational energy distribution of the fragments as shown in Fig. D.2, where the distribution curves actually yield velocity and angular distributions which fit the measured ones in Figs. 2.4 and 2.5 very well.

This form of translational energy distribution of the fragments is actually predicted by the RRKM theory. As explained in Appendix D, it predicts that as the excitation in a molecule increases above the dissociation energy, the dissociation rate constant increases. This will tend to favor dissociation through the lowest-energy dissociation channel. Experiments, in particular those using the molecular beam, show that the MPD of most molecules proceeds through the lowest-energy channel (see Ref. 2.9 and Appendices E and F). The RRKM theory also predicts how the excess energy (excitation energy minus dissociation energy) is distributed among the various vibrational modes of the molecule in the critical configuration, including the relative motion of the dissociating fragments. Figure D.2 shows the translational energy distributions that were used to fit the experimental results, calculated from the RRKM theory for excess energies of 5, 8, and 12 CO_2 laser photons. In Appendix E further examples can be found. The good fit indicates that the RRKM theory describes MPD quite well.

Based on the fit to the experimental results of the translational energy distribution calculated from RRKM theory, we conclude that the MPD

results on halogenated methanes show (see Table 2.1) that most of the molecules dissociate with excess energies of 1-3 CO_2 laser photons, as compared to around 8 photons for SF_6. On the other hand, C_2F_5Cl dissociates with around 13 photons of excess energy. How can the average excess energy depend so much on molecular structure?

To understand the above result we need to consider the excitation scheme presented in Fig. 2.11. The laser excites the molecule up a ladder of energy levels. As the excitation increases above the dissociation level, the dissociation rate increases rapidly, and dissociation soon starts to compete with the upexcitation. The average level of excitation from which most of the molecules will dissociate is then determined by a balance between upexcitation and dissociation.

The picture above is the idea behind a simple phenomenological model /2.17,18/ that has been quite successful in describing the experimental results on MPD of SF_6. The model can be written as a rate equation

$$\frac{dn_m}{dt} = \frac{I(t)}{h\sigma}\left[\sigma_{m-1}n_{n-1} + \frac{N_m}{N_{m-1}}\sigma_m n_{m+1} - \left(\frac{N_{m-1}}{N_m}\sigma_{m-1} + \sigma_m\right)N_m\right] - k_m n_m \qquad 2.1$$

where n_m is the normalized population in level m (with energy $E^* = mh\nu$), I(t) is the laser intensity, σ_m is the cross section for absorption from level m to level m + 1, N_m is the density of states at level m and k_m is the RRKM rate constant for dissociation from level m (see Eqs. D.4-5)

$$k_m = (hN_m)^{-1}\int_o^{mh\nu - E_o} dE_t N^{\dagger}(mh\nu - E_o - E_t) \qquad 2.2$$

However, just by using the simple qualitative picture of competition between upexcitation and dissociation (which is the essential content of

Eq. 2.1), we can already draw a number of important conclusions.

1) If we look at the expression for the rate constant k_m (Eq. 2.2), how it depends on the molecular density of states N_m, we see that in a heavier, more complex molecule that has more degrees of freedom and more low frequency vibrations, (e.g., SF_6 or C_2F_5Cl), the dissociation rate constant should increase more slowly with increase in energy. This is quite dramatically displayed in Fig. D.1, where the dissociation rate constants for SF_6 and CF_3I are compared. Consequently, the heavier molecules tend to reach higher levels of excitation before they dissociate. This explains why the C_2F_5Cl molecule has a higher excess energy than SF_6, which in turn has more excess energy than the halogenated methanes.

2) If the laser pulse is very short, none of the molecules dissociate before the laser pulse is over. Then the population distribution and the level of excitation from which dissociation occurs is completely determined by the total pulse energy fluence. (This follows directly from the form of Eq. 2.1.) However, if the laser pulse is sufficiently long, the excitation level reached is limited by the dissociation, and at this level the upexcitation rate and the dissociation rates are about equal. Thus the level of excitation in this case should be higher with higher intensity, or at laser frequencies where the transition rates are higher.

When the dissociation yield is near saturation, the time it takes for a molecule to be pumped up above the dissociation energy is about equal to the pulse duration. The time it takes to make a transition above the dissociation energy is a reasonable fraction of this time (say 1/10-1/50, since it takes some 10-50 transitions to get above the dissociation energy). Thus, in the case of dissociation rate limited excitation near saturation, the lifetime corresponding to the average level of excitation,

being about equal to the time it takes to make a transition, is of the order of 1/10 of the laser pulse duration. Our molecular beam experiments were done with a laser pulse of about 60 ns FWHM. From Table 2.1 we see that the dissociation lifetimes corresponding to the level of excitation calculated from the RRKM theory to fit the observed translational energy distributions are indeed in the 1-100 ns range (mostly around 10 ns).

3) Because the density of states N_m (Eq. 2.2) is a rapidly increasing function of energy $E^* = mh\nu$, the RRKM dissociation rate constant k_m should increase more rapidly with excess energy if the dissociation energy is lowered. CF_3I has a dissociation energy slightly more than half of that of SF_6, and this accounts in part for the difference in their dissociation rate constants shown in Fig. D.1. An even clearer example is N_2F_4, which has a dissociation energy of only about half that of CF_3I. Even though it has one atom more than CF_3I, and thus a higher density of states at a given excitation energy $E^* = mh\nu$, its dissociation rate grows so rapidly with excess energy that dissociation already dominates over up-excitation at a level one CO_2 laser photon above the dissociation energy. This is shown quite clearly by the translational energy distribution of NF_2 fragments in Fig. 2.12, as there are no fragments with more than one photon or 3 kcal/mole of translational energy.

4) Since only a small fraction of the excess energy is released as translational energy (see Appendix D), most of the excess energy remains as internal energy in the fragments. For heavy, complex molecules which reach high levels of excitation before dissociating, the fragments emerging from dissociation are already excited to their quasi-continuum and can readily absorb more energy from the laser field to go through another MPD process. This process of secondary dissociation is of course more

likely to occur if the fragments have a strong absorption band coinciding with the laser frequency. In our experiments, we have observed secondary dissociation in SF_6 and $CFCl_3$, with the fragments SF_5 and $CFCl_2$ dissociating further to form SF_4 and CFCl, respectively. The various products were identified through their different electron impact ionization spectra in the mass spectrometer. The laser frequency used was not in near resonance with any known strong IR absorption lines of $CFCl_2$ or SF_5, so the observed secondary dissociation must result from excitation of SF_5 and $CFCl_2$ already in the quasi ontinuum. Of course, for this to make sense, the primary dissociation must take place before the laser pulse is over. This is certainly the case — the translational energy distributions of SF_5 and $CFCl_2$ indicate that they are produced from parent molecules with lifetimes shorter than 10 ns, compared to the laser pulse duration of more than 60 ns.

In MPD of CF_3Cl, CF_3Br, and CF_3I, the CF_3 fragment produced has little internal energy (1-2 CO_2 laser photons), but CF_3 in the ground state is known to absorb /2.25/ close to the laser frequency used. Although the molecular beam experiments were not sensitive enough to detect dissociation of CF_3, in gas cell experiments on the same three molecules /2.26/ CF_2 radicals and F atoms have been observed, indicating that a secondary dissociation of CF_3 may have taken place.

Many of the products observed by the extremely sensitive laser induced fluorescence detection method are probably also produced from sequential dissociations of intermediate products. For example, C_2, CN, and CH have been observed /2.14-16,22/ in the dissociation of molecules with six or more atoms. Unfortunately, the laser induced fluorescence detection methods is not able to reveal anything about the intermediate

steps leading to these small final products. It seems that the secondary or sequential dissociation is an unavoidable effect in the MPD at high energy fluence of all but the lightest, simplest molecules. This is a factor which often complicates the studies of the MPD process, regardless of the method used for detection and analysis of the dissociation products.

5) For the heavier, more complex molecules, competing dissociation channels may also open up, provided their dissociation energies are not too far above that of the lowest energy channel. If the laser intensity is sufficiently high, the molecule can be excited well above the dissociation energies of several channels before dissociation dominates over up-excitation. Then several dissociation channels may start to compete with the lowest one. We should stress here that this effect is actually expected from the statistical theory of unimolecular dissociation. A system in which such an effect has been observed is C_2F_5Cl /2.27/. The energetics of the various dissociation pathways are not well known, except for the lowest one, which is the Cl atom elimination, with a dissociation energy of about 83 kcal/mole /2.28/. The next lowest channel is probably C-C bond rupture, with a dissociation energy of around 100 kcal/mole, judging from the C-C bond strength in similar ethane derivatives /2.29/. The RRKM calculations /2.27/ indicate that the rate constant for the C-C bond rupture grows more rapidly with excess energy than that for the Cl atom elimination. As already pointed out (Table 2.1), the average level of excitation in C_2F_5Cl pumped by a 1-J TEA laser can be around 13 CO_2 laser photons (40 kcal/mole) above the C-Cl bond energy, well above the dissociation energy of the C-C bond rupture. Thus the C-C dissociation rate can be comparable to the C-Cl dissociation rate. In the experi-

ments, a competition between the two channels has actually been observed. If we look at low laser intensities, the Cℓ atom elimination dominates over the C-C bond rupture. As the laser intensity is increased, thus pumping the molecules to higher levels of excitation, the Cℓ elimination channel very rapidly saturates, whereas the C-C bond rupture becomes increasingly important. This effect is not peculiar to MPD experiments. In pyrolysis of ethane compounds it has long been observed /2.30/ that at low temperature, elimination of atoms or diatomics dominate the dissociation, but as the temperature is increased, C-C bond rupture becomes progressively more important, making the analysis of such reactions exceedingly complicated.

Now, many of the results discussed under 1) - 5) above have also been obtained in an explicit model calculation on SF_6 /2.17,18/, using a simple set of rate equations (Eq. 2.1 with minor modifications). By fitting the free parameters in the model to experimental results on energy absorbed as a function of input laser energy fluence and laser pulse duration, the dissociation yield as a function of energy fluences, the onset of secondary dissociation, the level of excitation from which dissociation occurs, and thus, the translational energy distribution in the fragments, all can be calculated. All the results agree with the experiments, and illustrate quite clearly in a more quantitative way what we have discussed above in qualitative terms.

How will these results be modified if we cannot neglect molecular collisions? Depending on the collision partners, we can have a number of complications:

1) Collisions between excited molecules will lead to a thermalization of the energy deposited by the laser in the molecules via

intermolecular vibrational energy transfer. Thus any differences between thermal heating and multiphoton excitation will be washed out. The isotopic selectivity of the process will decrease, due to energy transfer between different isotopic species. Rotational and vibrational intermolecular energy transfer during the laser pulse can increase the number of molecules interacting resonantly with the laser field, thus reducing the bottleneck for excitation out of the discrete levels into the quasi-continuum. Collisionally induced dissociation can also occur, even in the absence of multiphoton dissociation.

2) Collisions between excited molecules and cold molecules will lead to a deactivation of the excited molecules. The cold collision partners may be buffer gasses, if present, or reaction products from the dissociation. Their presence will increase the energy absorption necessary for a given dissociation yield, and lower the level of excitation. Thus, in cases with competing dissociation channels, the lowest energy channel will be favored. Since the excited products from the dissociation can also be deactivated via collisions, secondary dissociation of the products will be inhibited.

3) Collisions between dissociation products, and between products and other atoms or molecules present usually lead to chemical reactions. The products from MPD are mostly highly reactive free radicals. Thus recombination or disproportionation of the dissociation products may occur, and complicated chemical reaction chains may follow the primary dissociation. Analysis of the process is complicated, and dependent upon detailed informa-

tion on the chemical kinetics of the reactions involved. Little information about the dynamics of the primary dissociation can be deduced from the final products.

In the preceding discussion on the translational energy distribution of fragments, we have actually only considered the simple cases where the observed distributions are in agreement with prediction of the RRKM theory. This is usually true for simple bond rupture reactions (see Appendix E). There is negligible interaction between the fragments once the critical configuration is passed, so that the energy distribution in the fragments remains the same as calculated in the RRKM theory for the critical configuration. However, in cases where such interaction cannot be neglected, the simple RRKM theory we have used cannot take into account this interaction, and translational energy distributions very different from the ones we have discussed so far may result. For a number of molecular elimination reactions, such as three-center elimination reactions from halogenated methanes, and four-center elimination from halogenated ethanes and ethenes, there is a considereable potential energy barrier between reactant and products. This potential energy will have to be distributed between the various vibrational, rotational and translational degrees of freedom in the fragments as they move away from the critical configuration on the top of the barrier. The RRKM theory cannot predict anything about how the energy will be distributed. It will depend on the nature of the potential energy surface for the fragments.

As an example, we will discuss the dissociation of CHF_2Cl into CF_2 + HCl, which has been studied in a molecular beam (see Appendix F) as well as with laser induced fluorescence detection of the CF_2 fragment /2.12/. Thus, translational, as well as rotational and vibrational energy distri-

butions in the CF_2 fragment have been measured. The conclusions that can be drawn from the results on $CHF_2C\ell$ are representative for molecules with this kind of dissociation dynamics.

The velocity distribution of HCℓ fragments at 10° from the $CHF_2C\ell$ beam is shown in Fig. 2.10, compared to the distribution calculated from the translational energy distribution in Fig. 2.11. We see that the products are quite a bit faster than the $CHF_2C\ell$ beam, due to the considerable amount of energy gained from the dissociation. Most CF_2 fragments have a translational energy of more than 2 kcal/mole while only a small percentage have less than 1 kcal/mole. Stephenson and King /2.12/ found the population distribution in the vibrational modes of CF_2 to be well represented by a thermal distribution of temperature 1160 K. The average rotational energy was also estimated in the experiments, although its value was too high for a detailed measurement of the distribution to be made. However, assuming a thermal distribution, a rotational temperature of about twice the vibrational temperature was obtained. The high translational energy content in the fragments means that there is a strong repulsive interaction between the departing fragments after they pass through the critical configuration. This repulsive interaction is quite asymmetric, giving the fragments considerable rotational energy.

However, we want to emphasize that although RRKM theory alone may be inadequate for predicting the final energy partitioning in the fragments, it still predicts the dissociation rates. If we add up all the energies in the fragments in the HCℓ elimination from $CHF_2C\ell$, using the results of King and Stephenson, we get to a level of excitation corresponding to an RRKM lifetime around 1 ns. This is what we should expect from the statistical theory of MPD as in the cases of the other halomethanes. In

fact, there exists no evidence in all the cases we have studied that the general statistical picture of the multiphoton excitation and dissociation process does not apply.

2.6 Concluding Remarks

There are still a number of assumptions and theoretical predictions about the dissociation that need to be checked experimentally. The partition of energy between all degrees of freedom in at least one of the two fragments from the dissociation should be measured in a case where the RRKM theory predicts the distributions. The dissociation lifetimes should be measured directly and independently, together with their dependence on laser intensity, under well characterized conditions. The processes of secondary dissociation and competing dissociation channels need better characterization. The methods that so far have revealed the most about the dissociation process are the molecular beam method and the laser induced fluorescence method. A natural extension would be to use laser induced fluorescence as a detection method in a molecular beam experiment. Studies of this kind are already being prepared in several laboratories. The work is hampered by the low particle densities involved in molecular beam experiments, insufficient knowledge of the spectroscopy of many of the radicals produced in the dissociation, and lack of tunable lasers in the UV frequency ranges of interest for many compounds.

Although there are some detailed questions which still need to be further investigated, the general physical picture constructed from various experimental and theoretical investigations is quite adequate for understanding and predicting many important features of the MPD process under various conditions. But since MPD is a rather complex process, it is

not possible to draw reliable conclusions unless all the experimental results are carefully analyzed. The dependence of the dissociation yield and the dynamics of dissociation on both the laser intensity and energy fluence is an important example.

For a given chemical species, the laser intensity required for a certain fraction of the molecules to overcome the discrete state bottleneck not only depends on the frequency, but also on the vibrational and rotational temperature of the molecules. Once the molecules are excited to the quasi-continuum, the energy fluence, not the power of the laser, was shown to be responsible for driving the molecules through the quasi-continuum and beyond the dissociation level /2.3,10/. But in most of the gas cell experiments, the dissociation yield of the molecules in the quasi-continuum is not simply related to the energy fluence alone. For molecules lying above the dissociation level, there is a complicated competition between unimolecular dissociation, collisional deactivation and laser upexcitation. Consequently, for a given gas pressure and a given laser energy fluence, a higher laser intensity should result in a higher level of excitation and an increased rate of dissociation. This in turn reduces the effect of collisional deactivation and thus increases the dissociation yield. In general, for smaller molecules, the laser intensity influences the yield by limiting the fraction of the molecules which can be excited to the quasi-continuum, but since the lifetime of small molecules becomes very short after only a couple of excess photons are deposited beyond the dissociation threshold, collisional deactivation could be overcome with a rather moderate intensity at low pressure. On the other hand, for larger molecules with many vibrational degrees of freedom, if an appropriate frequency is chosen, a large fraction of the

molecules will reach the quasi-continuum at a very moderate laser intensity. But since many more excess photons are required before the dissociation lifetime becomes comparable to the mean collision time, the laser intensity is expected to strongly influence both the dissociation yield and the ratio of competitive dissociation channels by controlling the level of excitation beyond the dissociation energy.

In most of the experiments carried out with a CO_2 TEA laser, one often adjusts the laser intensity or energy fluence by either adjusting the focusing condition or attenuating the laser output. Consequently both the laser intensity and energy fluence are varied simultaneously. If the energy fluence requirement for dissociation is met, the intensity of the laser is already high enough to pump some of the molecules to the quasi-continuum and dissociation is observed. However, it is important to keep in mind that both the intensity and energy fluence of the laser can separately affect the experimental results. Once the complicated dependence of the excitation and dissociation dynamics on the initial distribution of molecules over vibrational and rotational states, and on the frequency, intensity, and energy fluence of the laser is properly taken into account, we are indeed in a very good position to understand and predict the general behavior of MPD of the systems of interest.

References

2.1 R. V. Ambartzumian, Yu. A. Gorokhov, V. S. Letokhov, G. N. Makarov, and A. A. Puretzki, JETP Lett. 23, 22 (1976), Sov. Phys. JETP 44, 231 (1979); V. S. Letokhov and A. A. Makarov, Opt. Commun. 17, 250 (1976).

2.2 R. V. Ambartzumian, N. P. Furzikov, Yu. A. Gorokhov, V. S. Letokhov, G. N. Makarov, and A. A. Puretzki, JETP Lett. 23, 194 (1976); Opt. Commun. 18, 517 (1976).

2.3. J. G. Black, E. Yablonovitch, N. Bloembergen, and S. Mukamel, Phys. Rev. Lett. 38, 1131 (1977).

2.4 N. R. Isenor, V. Merchant, R. S. Hallsworth, and M. C. Richardson, Can. J. Phys. 51, 1281 (1973).

2.5 V. S. Letokhov, E. A. Ryabov, and O. A. Tumanov, Opt. Commun. 5, 168 (1972).

2.6 V. S. Letokhov, E. A. Ryabov, and O. A. Tumanov, Sov. Phys. JETP 36, 1069 (1973).

2.7 R. V. Ambartzumian, V. S. Dolzhikov, V. S. Letokhov, E. A. Ryabov, and N. V. Chekalin, Sov. Phys. JETP 42, 36 (1976).

2.8 M. J. Coggiola, P. A. Schulz, T. Y. Lee, and Y. R. Shen, Phys. Rev. Lett. 38, 17 (1977).

2.9 Aa. S. Sudbø, P. A. Schulz, E. R. Grant, Y. R. Shen, and Y. T. Lee, J. Chem. Phys. 68, 1306 (1978).

2.10 N. Bloembergen and E. Yablonovitch, Physics Today 35(5), 23 (1978).

2.11 D. S. King and J. C. Stephenson, Chem. Phys. Lett. 51, 48 (1977).

2.12 J. C. Stephenson and D. S. King, J. Chem. Phys. 69, 1485 (1978).

2.13 J. D. Campbell, G. Hancock, J. B. Halpern, and K. H. Welge, Opt. Commun. 17, 38 (1976); Chem. Phys. Lett. 44, 404 (1976).

2.14 J. D. Campbell, M. H. Yu, M. Mangir, and C. Wittig, J. Chem. Phys. 69, 3854 (1978).

2.15 S. E. Bialkowski and W. A. Guillory, J. Chem. Phys. 68, 3339 (1978).

2.16 M. L. Lesiecki and W. A. Guillory, J. Chem. Phys. 69, 4572 (1978).

2.17 E. R. Grant, P. A. Schulz, Aa. S. Sudbø, Y. R. Shen, and Y. T. Lee, Phys. Rev. Lett. 40, 115 (1978).

2.18 P. A. Schulz, Aa. S. Sudbø, E. R. Grant, Y. R. Shen, and Y. T. Lee, submitted to J. Chem. Phys.

2.19 J. L. Lyman, J. Chem. Phys. 67, 1868 (1977).

2.20 Y. T. Lee, J. D. McDonald, P. R. LeBreton and D. R. Herschbach, Rev. Sci. Instr. 40, 1402 (1969).

2.21 J. Danon, S. V. Filseth, D. Feldmann, H. Zacharias, C. H. Dugan, and K. H. Welge, Chem. Phys. 29, 345 (1978).

2.22 J. D. Campbell, M. H. Yu, and C. Wittig, Appl. Phys. Lett. 32, 413 (1978).

2.23 T. Ichimura, A. W. Kirk, and E. Tschuikow-Roux, Int. J. Chem. Kinet. IX, 697 (1977).

2.24 E. R. Grant, M. J. Coggiola, Y. T. Lee, P. A. Schulz, Aa. S. Sudbø, and Y. R. Shen, Chem. Phys. Lett. 52, 595 (1977).

2.25 D. E. Milligan and M. E. Jacox, J. Chem. Phys. 48, 2265 (1968).

2.26 E. Wurzberg, L. J. Kovalenko, and P. Houston, Chem. Phys. 35, 317 (1978).

2.27 D. J. Krajnovich, A. Giardini-Guidoni, Aa. S. Sudbø, P. A. Schulz, Y. R. Shen, and Y. T. Lee, Proceedings of the European Physical Society Conference, Heriot-Watt University, Edinburgh, Scotland, Sept. 20-22, 1978.

2.28 J. W. Coomber and E. Whittle, Trans. Far. Soc. 63, 2656 (1967).

2.29 Handbook of Chemistry and Physics, 58th edition (Chemical Rubber Co., Cleveland, 1977).

2.30 M. V. C. Sekhar and E. Tschuikow-Roux, J. Phys. Chem. 78, 472 (1974).

Table 2.1. Dynamics of multiphoton dissociation.

Molecule	Endoergicity (kcal/mole)	Potential energy barrier (kcal/mole)	Average translational energy (kcal/mole)	Peak of translational energy distribution (kcal/mole)	Estimated average energy available to products (kcal/mole)	Estimated lifetime (ns)
$SF_5 \rightarrow SF_5 + F$	93	0	3	0	25	20
$\quad\quad \rightarrow SF_4 + F$	51	0	1	0	7	20
$CF_3Cl \rightarrow CF_3 + Cl$	86	0	1.1	0	4	5
$CF_3Br \rightarrow CF_3 + Br$	71	0	1.2	0	5	2
$CF_3I \rightarrow CF_3 + I$	53	0	1.1	0	4	1
$CF_2Cl_2 \rightarrow CF_2Cl + Cl$	82	0	2	0	10	5
$CF_2Br_2 \rightarrow CF_2Br + Br$	61	0	1.6	0	7	5
$CFCl_3 \rightarrow CFCl_2 + Cl$	75	0	1.2	0	5	12
$\quad\quad \rightarrow CFCl + Cl$	~70	~0	-	0	-	-
$C_2F_5Cl \rightarrow C_2F_5 + Cl$	83	0	4	0	35	60
$C_2F_5Cl \rightarrow CF_3 + CF_2Cl$	≥97	0	3.3	0.4	21	200
$N_2F_4 \rightarrow 2NF_2$	22	0	0.4	0	2	1
$(NH_3)_2 \rightarrow 2NH_3$	4	0	0.3	0	1.5	-
$CHClCF_2 \rightarrow C_2HF_2 + Cl$	~80	0	1	0	-	-
$CHClCF_2 \rightarrow C_2F_2 + HCl$	58	>0	1	0	-	-
$CHF_2Cl \rightarrow HCl + CF_2$	50	6	8	5	-	-
$CH_3CCl_3 \rightarrow HCl + CH_2CCl_2$	12	42	8	?	-	-
$CH_3CF_2Cl \rightarrow HCl + CH_2CFCl$	14	55	12	6	-	-

Figure Captions

Fig. 2.1 Schematic of the apparatus used for the measurement of angular and velocity distributions of fragments from multiphoton dissociation of polyatomic molecules.

Fig. 2.2 Experimental arrangement. The "SF_6 beam source" is the molecular beam source. The pulse generator triggers the laser (which partly dissociates a section of the molecular beam) and the multichannel scaler, opens a gate to scaler 1 a few hundred microseconds later (to count dissociation product signal and background signal) and a gate to scaler 2 a few milliseconds later (to count background signal only).

Fig. 2.3 Dissociation yields for the products from MPD of C_2F_5Cl

$C_2F_5Cl \rightarrow C_2F_5 + Cl$ ($C_2F_4^+$ detected)

$C_2F_5Cl \rightarrow CF_3 + CF_2Cl$ (CF_2Cl^+ detected)

Fig. 2.4 Angular distribution of SF_5 fragments from MPD of SF_6 (see also Fig. D.2)

. experimental distribution

- - - RRKM theory, 5 kcal/mole excess energy

- · - RRKM theory, 8 kcal/mole excess energy

——— RRKM theory, 12 kcal/mole excess energy

Fig. 2.5 Speed distribution of SF_5 fragments from MPD of SF_6 at 5°, 10°, and 15° from the SF_6 beam. Symbols as in Fig. 2.4. Bottom: SF_6 beam speed distribution.

Fig. 2.6 Angular distribution of CF_3 fragment from MPD of CF_3I.

° experimental distribution

- - - RRKM theory, 3 kcal/mole excess energy

——— RRKM theory, 4.5 kcal/mole excess energy

· · · RRKM theory, 6 kcal/mole excess energy

Fig. 2.7 Angular distribution of I atoms from MPD of CF_3I. Symbols as in Fig. 2.6.

Fig. 2.8 Speed distribution of I atoms from MPD of CF_3I at 10°, 15°, 20°, and 25° from the CF_3I beam. Symbols as in Fig. 2.6. Bottom: Speed distribution of CF_3I beam.

Fig. 2.9 Speed distribution of HCℓ fragments from the MPD of $CHF_2Cℓ$

° experiment

- - - calculated from Fig. 2.10

Fig. 2.10 Center-of-mass translational energy distribution in the fragments from MPD of $CHF_2Cℓ$.

Fig. 2.11 Schematic representation of the excitation-dissociation process around the dissociation energy.

Fig. 2.12 Center-of-mass translational energy of a pair of NF_2 fragments from the MPD of N_2F_4.

Figure 2.1

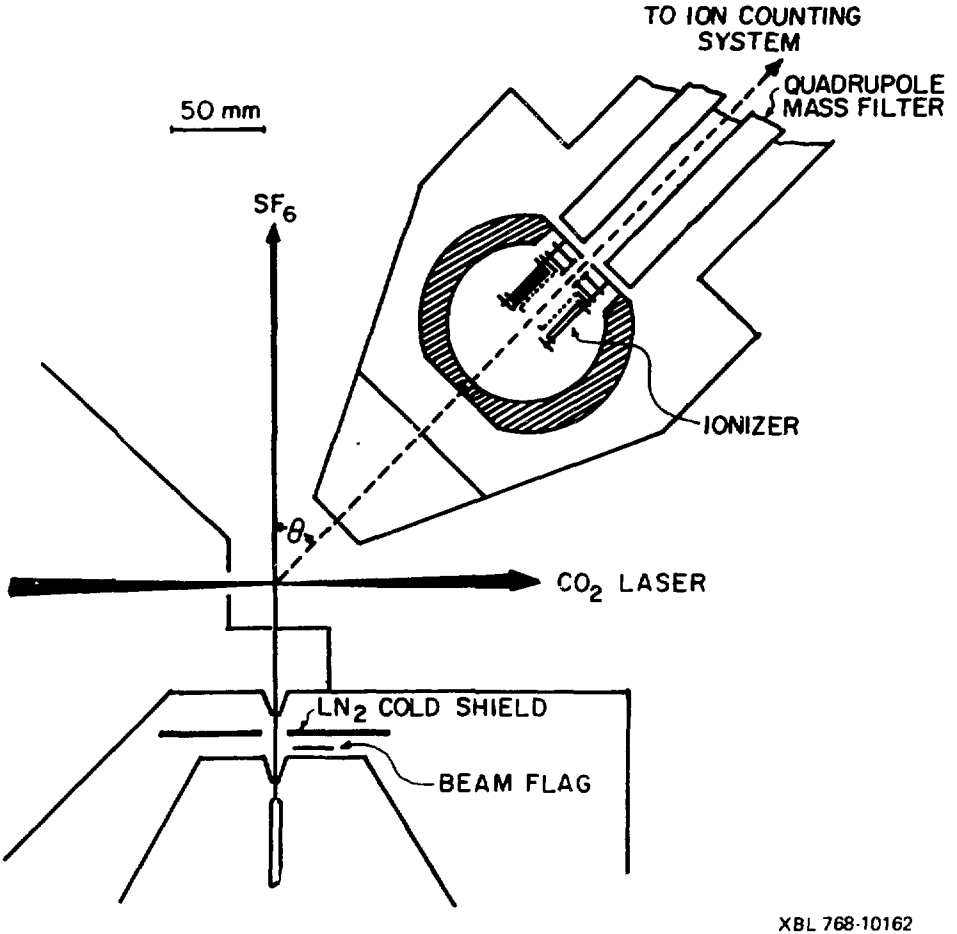
TO ION COUNTING SYSTEM
QUADRUPOLE MASS FILTER
50 mm
SF6
IONIZER
θ1
CO2 LASER
LN2 COLD SHIELD
BEAM FLAG
XBL 768-10162

Figure 2.2

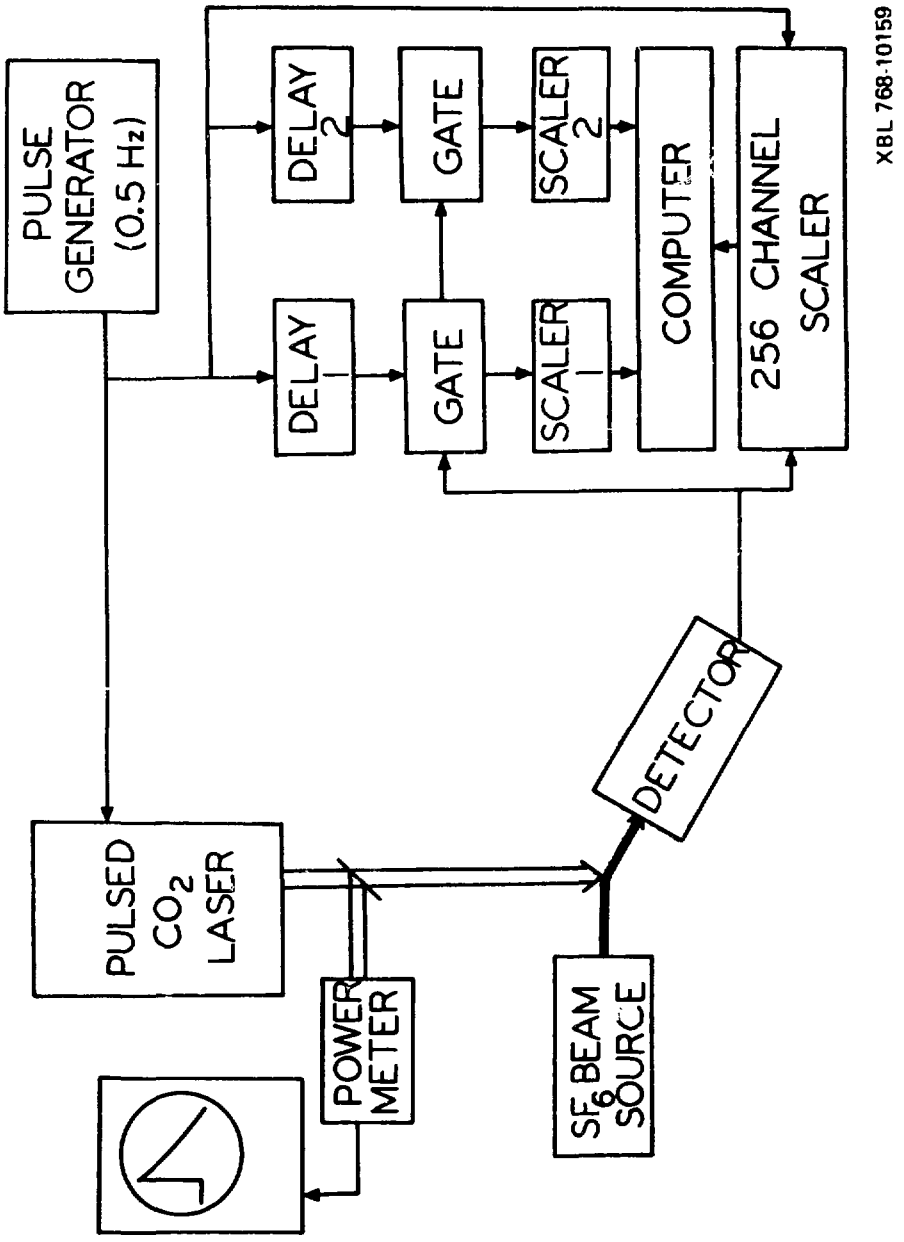
PULSE GENERATOR (0.5 Hz)
DELAY 2
GATE
SCALER 2
COMPUTER
256 CHANNEL SCALER
DELAY 1
GATE
SCALER 1
PULSED CO_2 LASER
DETECTOR
POWER METER
SF_6 BEAM SOURCE
XBL 768-10159

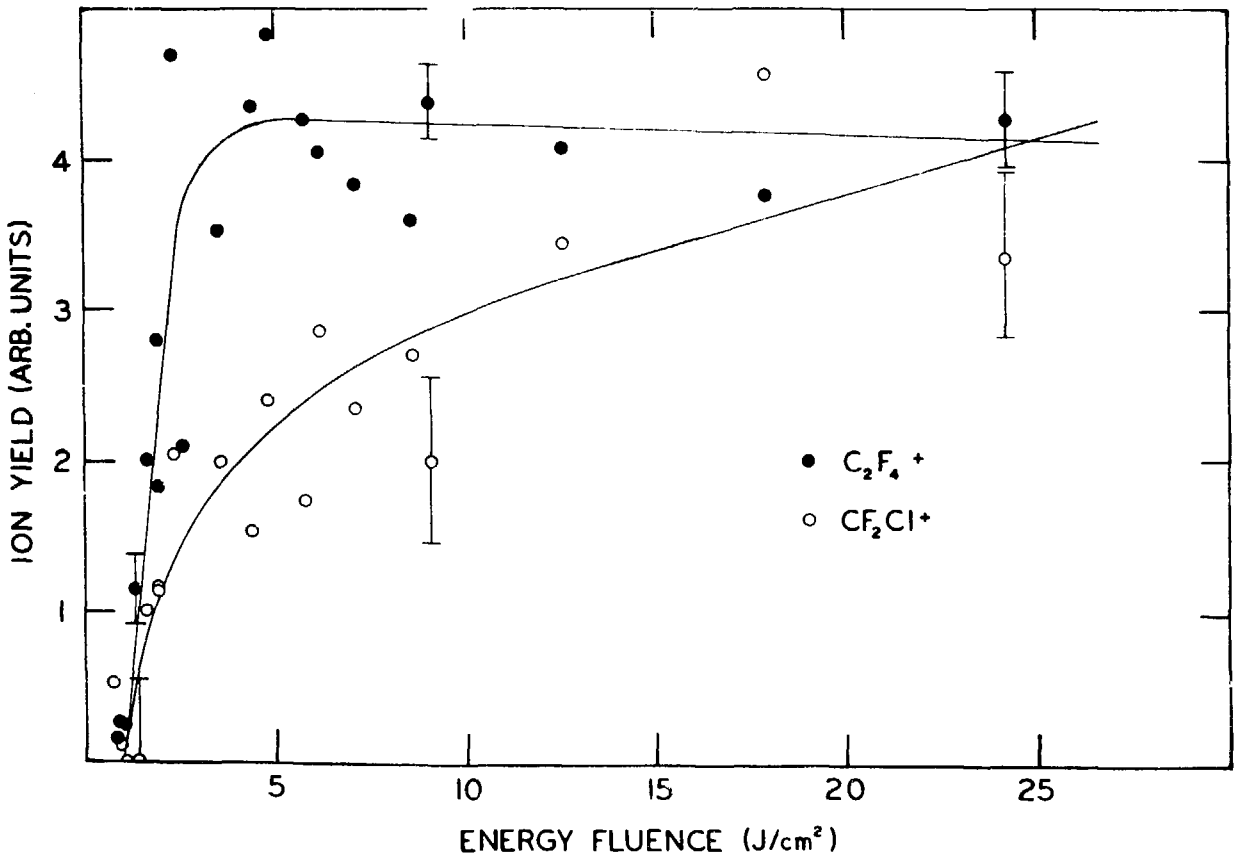

XBL 791-7900

Figure 2.3

Figure 2.4

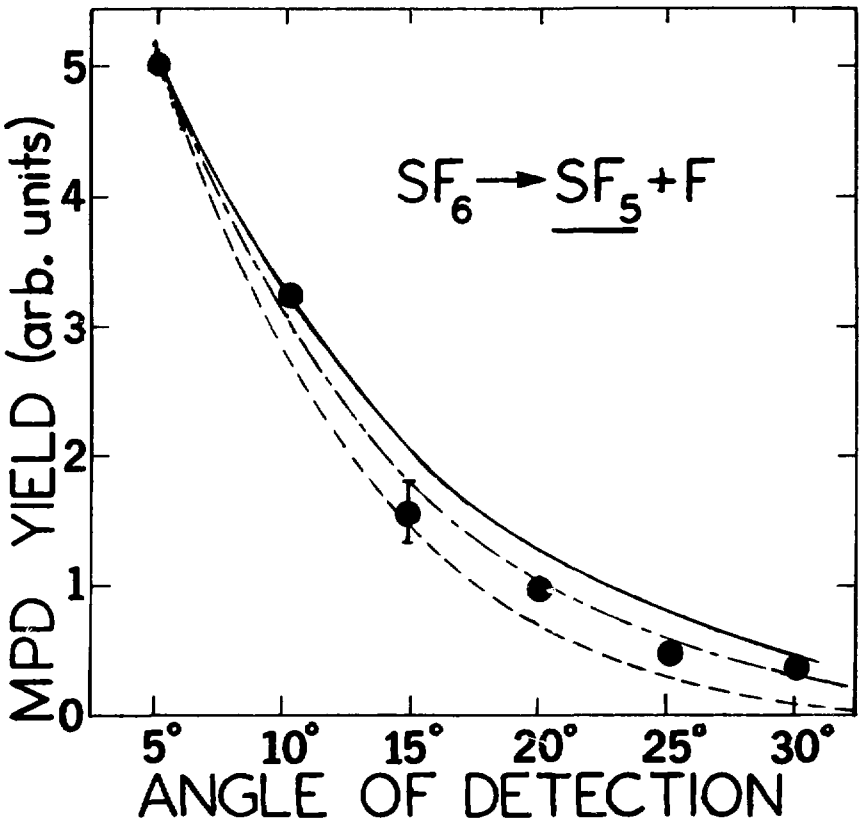
MPD YIELD (arb. units)
0
1
2
3
4
5
$SF_6 \rightarrow SF_5 + F$
5°
10°
15°
20°
25°
30°
ANGLE OF DETECTION
XBL 785-8834A

Figure 2.5

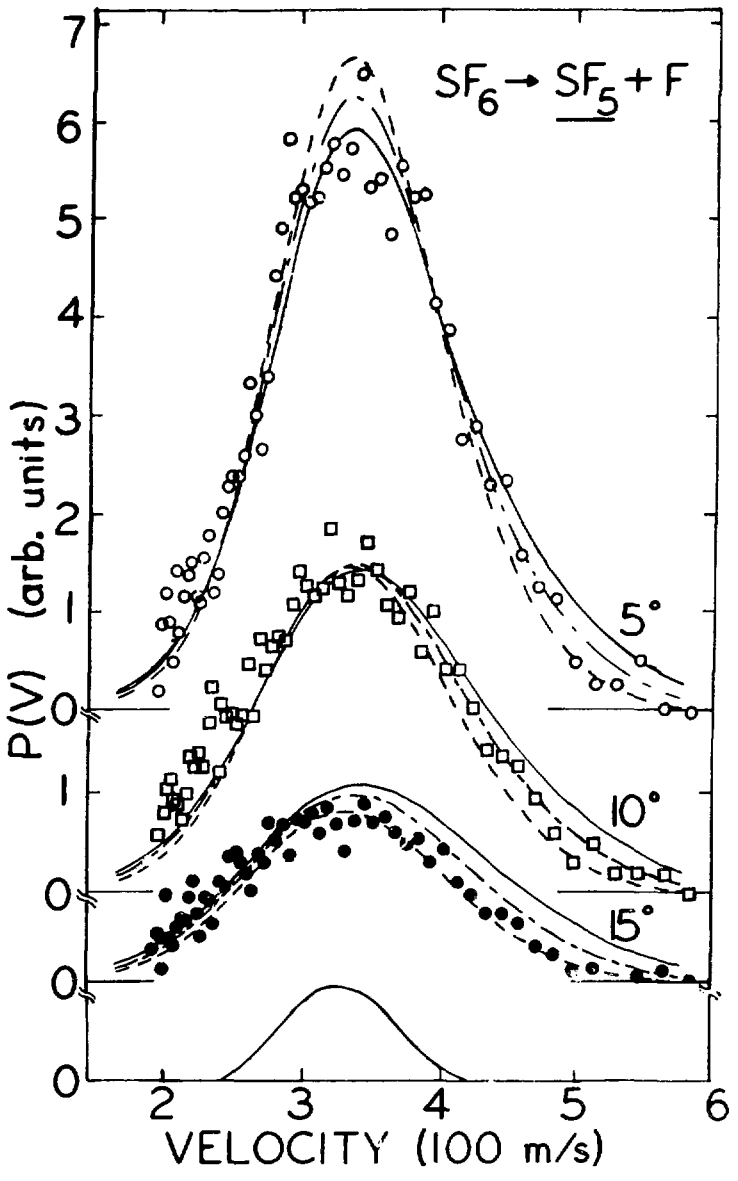

XBL 792-8359

Figure 2.6

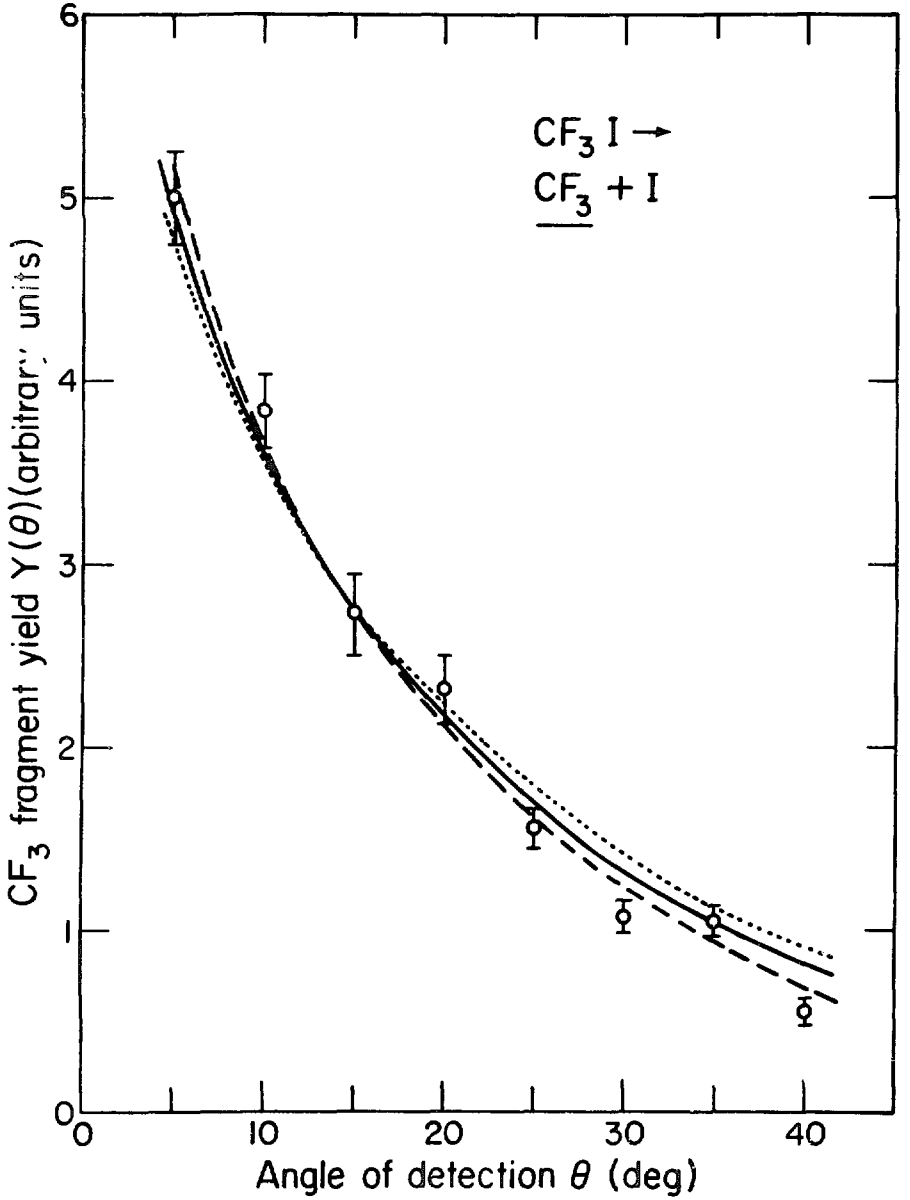

XBL 783-444

Figure 2.7

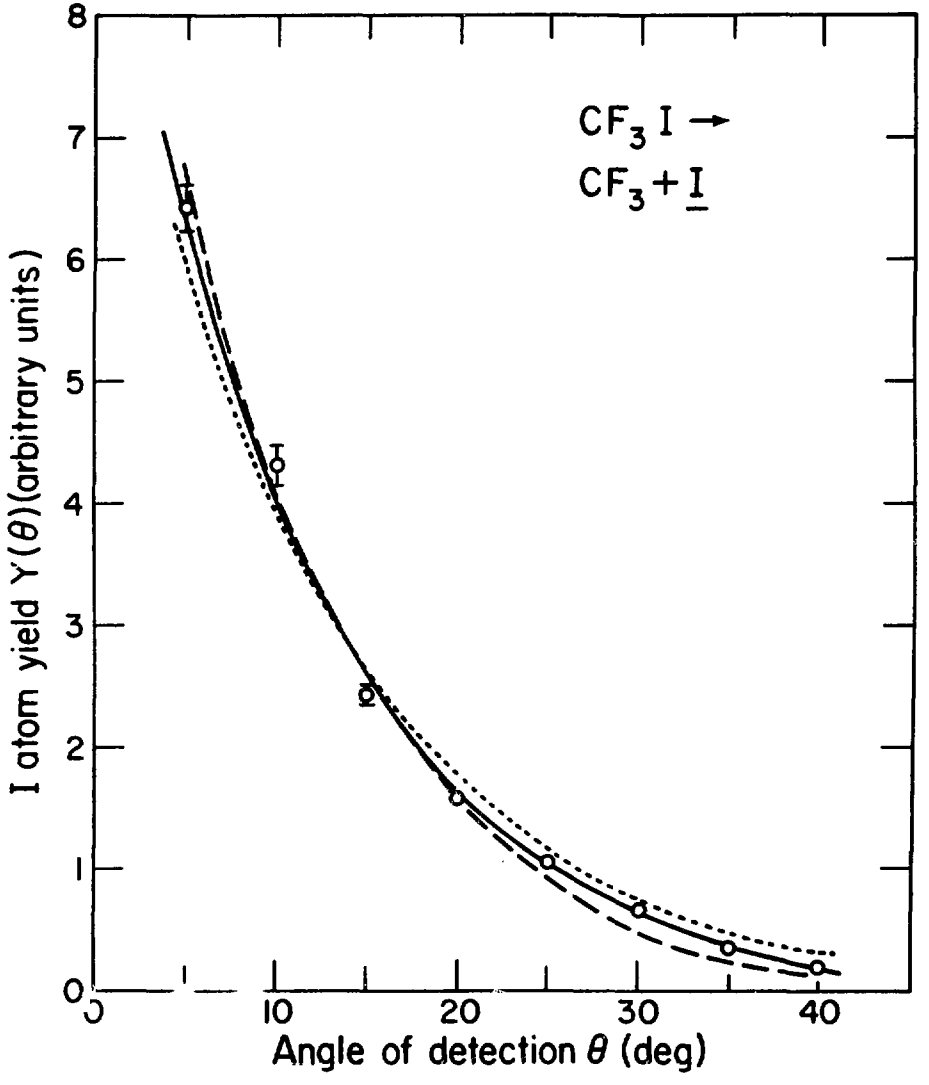
$CF_3I \rightarrow$
$CF_3 + \underline{I}$
I atom yield $Y(\theta)$(arbitrary units)
Angle of detection θ (deg)
0
1
2
3
4
5
6
7
8
10
20
30
40
XBL783-442

Figure 2.8

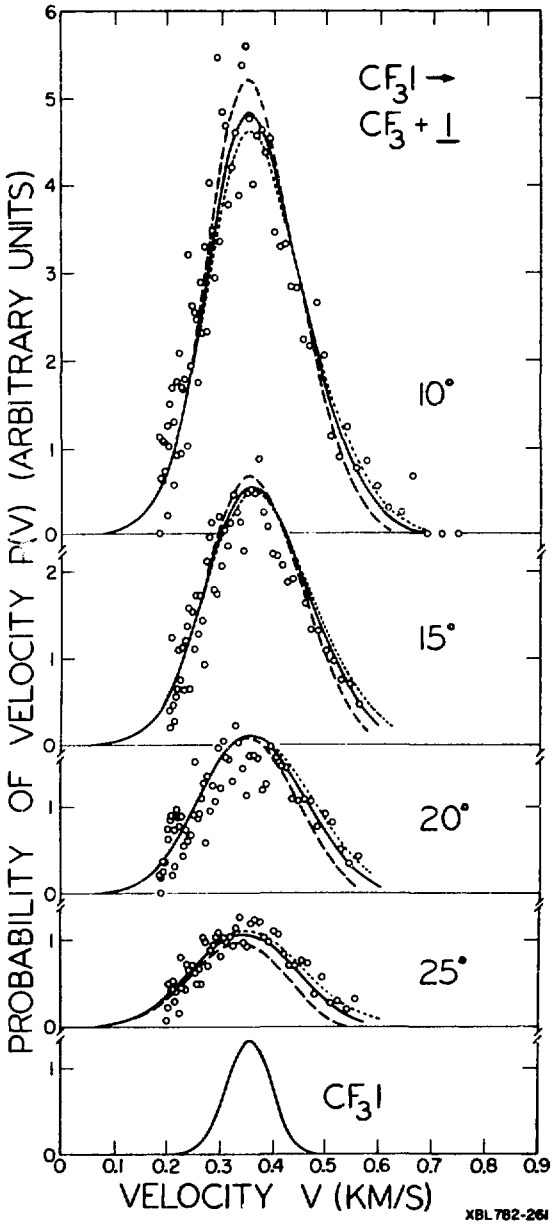
CF3I →
CF3 + I
10°
15°
20°
25°
CF3I
PROBABILITY OF VELOCITY P(V) (ARBITRARY UNITS)
VELOCITY V (KM/S)
0 0.1 0.2 0.3 0.4 0.5 0.6 0.7 0.8 0.9
XBL762-261

Figure 2.9

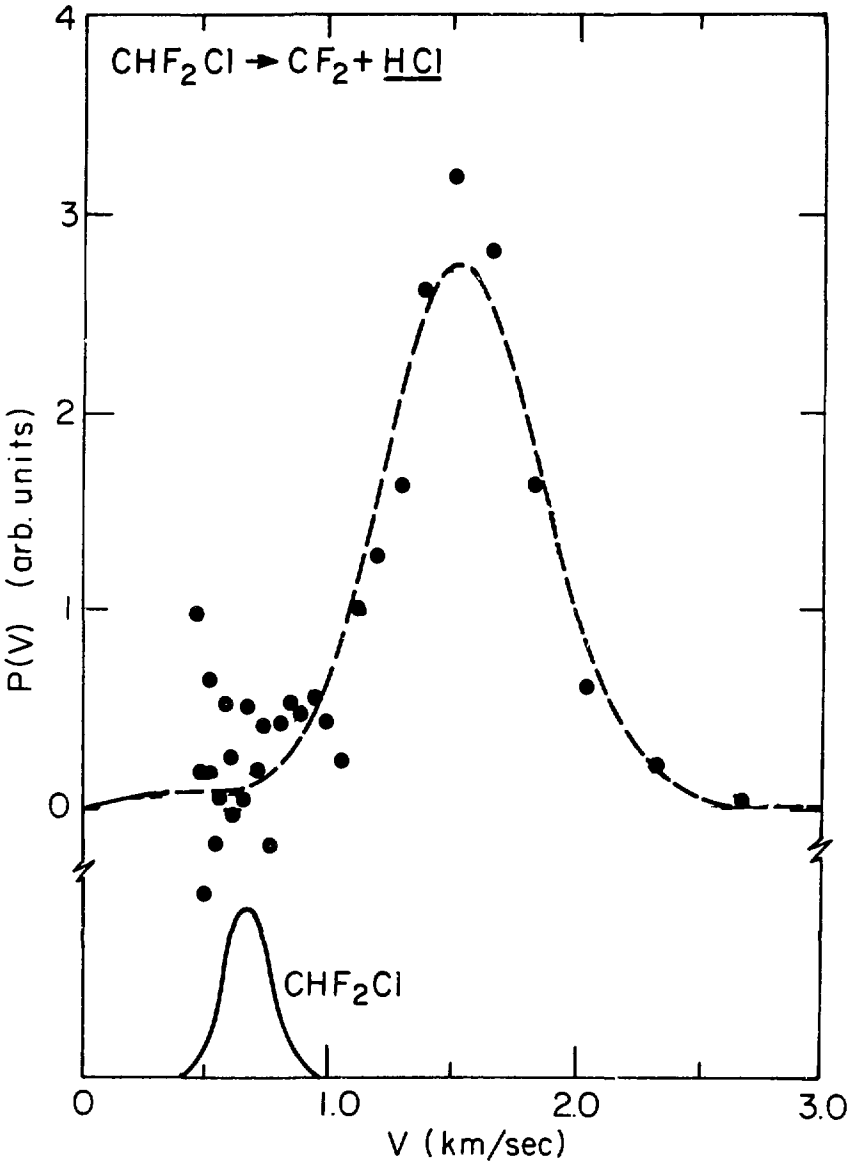

XBL 781-4439A

Figure 2.10

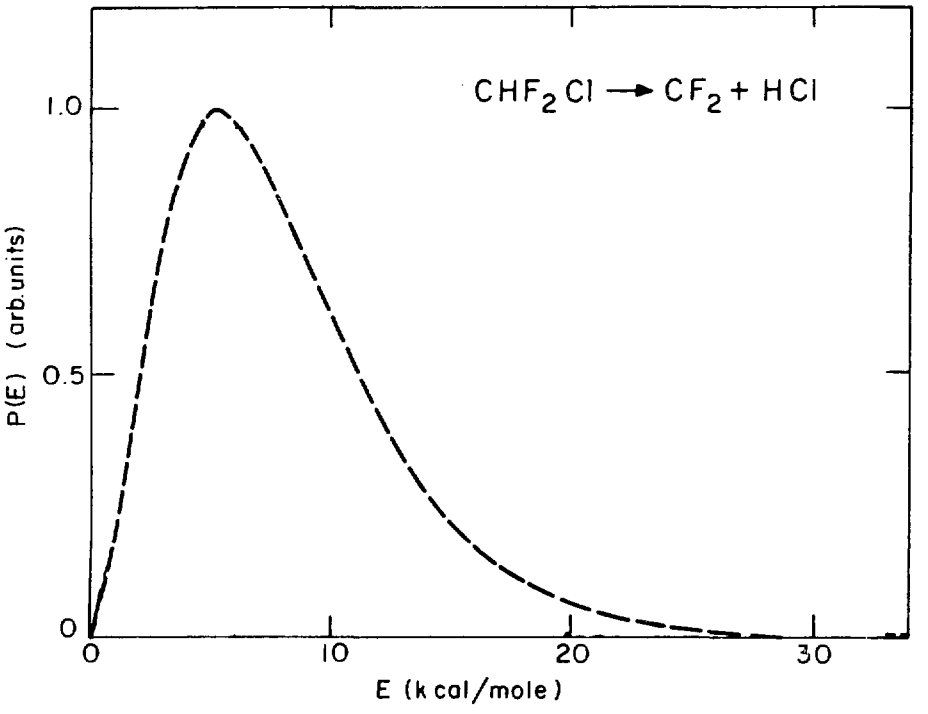

XBL 781-4438A

Figure 2.11

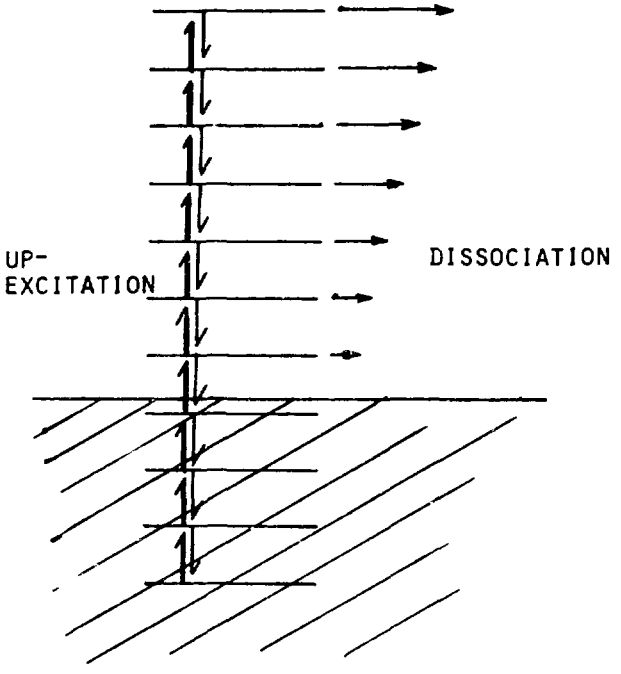

XBL 795-9878

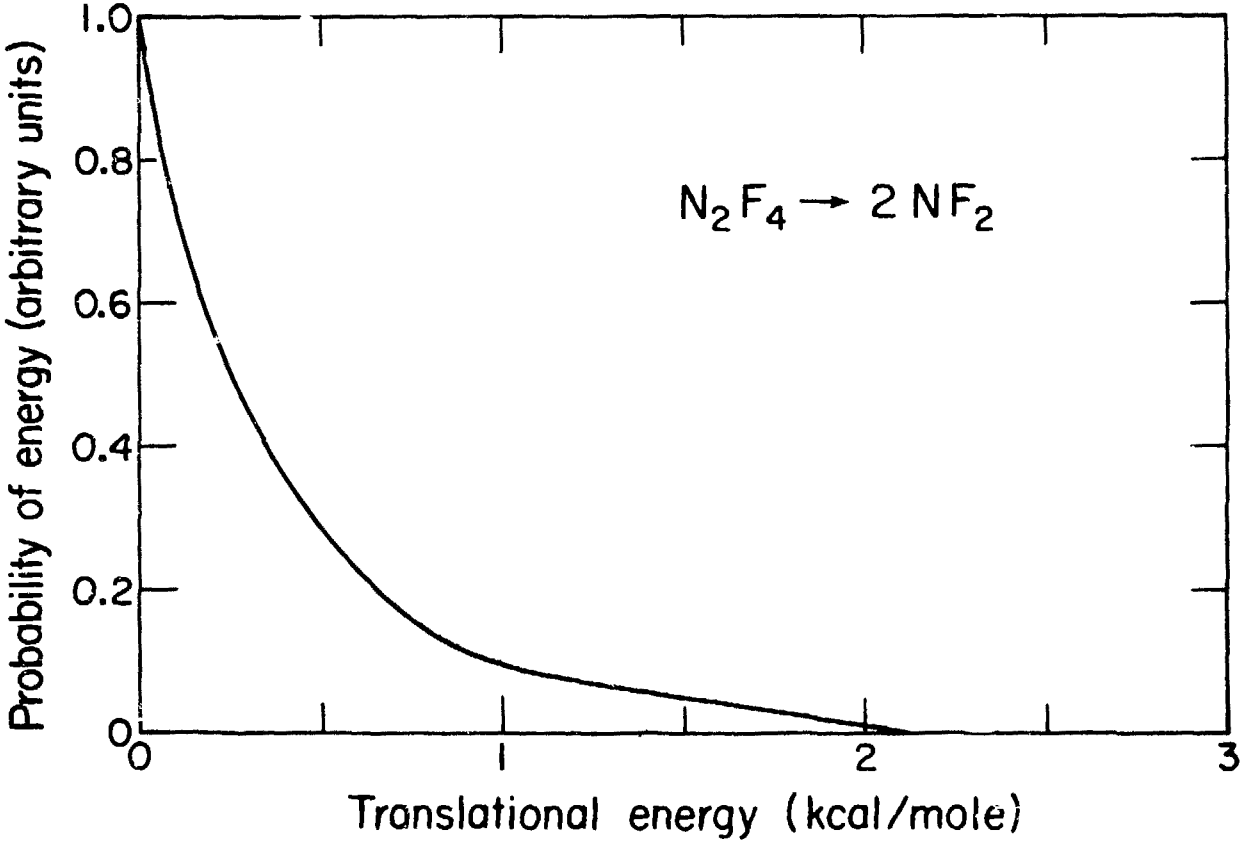

XBL783-446A

Figure 2.12

Appendix A: SCHRODINGER AND LIOUVILLE EQUATIONS WITH OSCILLATING EXTERNAL FIELDS

This appendix deals with the mathemathics of solving the initial value problem associated with the equation

$$i\dot{\rho}_k = \Sigma_\ell L_{k\ell}(t)\rho_\ell \qquad \text{A.1a}$$

where $L_{k\ell}(t)$ oscillates in time. The functions $\rho_k(t)$ describe a system of interest, and the oscillating part of $L_{k\ell}(t)$ is due to an external field. The physics of the solution to this problem is discussed in detail in chapter 1, and in this appendix, the only physics lies in justifying the various approximations chosen.

A.1. Basic Equations

Consider the equation

$$i\dot{\rho}_k = \Sigma_\ell L_{k\ell}(t)\rho_\ell = \Sigma_\ell (L^o_{k\ell} + L^1_{k\ell}\exp(i\omega t))\rho_\ell \qquad \text{A.1b}$$

where $L^o_{k\ell}$ and $L^1_{k\ell}$ are time independent, and $L^1_{k\ell}$ is a matrix with elements that all are small compared to ω. The generalization to

$$L_{k\ell}(t) = \Sigma_m L^m_{k\ell}\exp(im\omega t) \qquad \text{A.2}$$

is straightforward, as we shall see later.

The assumption of small $L^1_{k\ell}$ compared to ω is well justified in

the situation when Eq. A.1 descibes a quantum mechanical system excited by an optical field of practical strength. This permits a series expansion of the solution $\rho_k(t)$ in powers of $1/\omega$, the lowest order terms of which we shall make use of.

Floquet's theorem /A.1/ states that there exists solutions of Eq. A.1 of the form

$$\rho_k^a(t) = \exp(-i\Omega^a t)\Sigma_n \rho_{k;n}^a \exp(-in\omega t) \qquad A.3$$

with values of $\mathrm{Re}(\Omega^a)$ in the range between 0 and ω. Provided the various $\rho_k^a(0)$, a = 1, 2, 3, ... span the space of ρ_k's, an arbitrary solution of Eq. A.1 can be constructed as a linear combination of $\rho_k^a(t)$'s. Let us assume this to be true for all $L_{k\ell}$ of interest to us. This is like assuming that the eigenvectors of any hamiltonian of interest in physics span the space of physical state vectors.

Inserting Eq. A.3 in Eq. A.1, we get a set of eigenvalue equations for Ω^a:

$$\Omega^a \rho_{k;n}^a = \Sigma_\ell((L_{k\ell}^o - n\omega\delta_{k\ell})\rho_{\ell;n}^a + L_{k\ell}^1 \rho_{\ell;n-1}^a) \qquad A.4$$

If ρ_k has N components, this system has, using the completeness assumption mentioned above, N linearly independent solutions. In the literature, $\hbar\Omega^a$ is usually called the quasienergy of the system /A.2/, when Eq. A.1 represents the corresponding Schrödinger equation.

We will limit our treatment to systems excited close to resonance by a monochromatic field - i.e., we consider only one photon transitions, or resonantly enhanced (in every step) multiphoton transitions.

Mathematically, this amounts to the following: For each component ρ_k that we include in the treatment, we can find an integer n_k such that the matrix element L^o_{kk} satisfies the relation $|L^o_{kk} - n_k\omega| << \omega$. We note that in this appendix, L is just mathematical operator and ρ the eigenvector. Thus, L may represent the hamiltonian and ρ the wavefunction. In this case L^o_{kk} is the eige frequency ω_k of level k. If the ground state is chosen to have zero energy, n_k will take values 0, 1, 2, ... up to some maximum value n_{max}. We can also let L represent the liouvillian operator of a system. Th n L^o_{kk} is the oscillation frequency of the k'th component of the density matrix (in the absence of damping and external fields), and n_k will take values between $-n_{max}$ and n_{max}. In particular, if ρ_k is a diagonal component of the density matrix, we have $n_k = 0$, since the diagonal components of the density matrix do not oscillate. With these assumptions we can apply standard Rayleigh-Schrödinger time independent perturbation theory to Eq. A.4. The first order solution is obtained by including all terms $\rho^a_{k;n_k}$ for which $|L^o_{kk} - n_k\omega| << \omega$. All other $\rho^a_{k;n}$, $n \neq n_k$, are negligible, because by assumption $L^o_{kk} - n\omega \simeq (n_k - n)\omega$, far removed from $L^o_{kk} - n_k\omega$ when $n \neq n_k$. This neglect of all but one Fourier component $\rho^a_{k;n}$ is the so-called rotating wave approximation, widely used in quantum optics. Being consistent, we can also in this approximation neglect all ρ_k that are not excited on resonance, i.e., all ρ_k for which $(L^o_{kk} - n\omega)$ is roughly of the same order of magnitude as ω, regardless of choice of n. We shall return later to the problem of estimating what errors we make in applying this approximation. At this point let us just say that it is essential for the approximation to be

valid that all the $L^{o}_{k\ell}$ and $L^{1}_{k\ell}$, $k \neq \ell$, are small compared to ω (or, to be more exact, compared to the $(L^{o}_{kk} - n\omega)$ for which $\rho^{a}_{k;n}$'s are neglected). In the applications of Eq. A.4 in chapter 1, the $L^{o}_{k\ell}$, $k \neq \ell$, are either zero or equal to damping rates in the system, and the $L^{1}_{k\ell}$ are the field-dipole interaction matrix elements. All of these are usually very small compared to the frequency of the field exciting the system. Furthermore, in the applications in chapter 1 the form of $L^{o}_{k\ell}$ is such that $L^{o}_{k\ell} = 0$ whenever $n_k \neq n_\ell$. This allows Eq. A.4 in the rotating wave approximation to take the form

$$\omega^{a}\rho^{a}_{k;n_k} = \Delta_k \rho^{a}_{k;n_k} + \Sigma_{\ell \neq k} L'_{k\ell}\rho^{a}_{\ell;n_\ell} \qquad \text{A.5a}$$

where

$$\Delta_k = L^{o}_{kk} - n_k\omega \qquad \text{A.5b}$$

and

$$L'_{k\ell} = \begin{cases} L^{o}_{k\ell} \text{ if } n_\ell = n_k \\ L^{1}_{k\ell} \text{ if } n_\ell - n_k = 1 \\ 0 \quad \text{otherwize} \end{cases} \qquad \text{A.5c}$$

We are now in the position to make the generalization to $L_{k\ell}(t)$ of the form in Eq. A.2. From the derivation of Eq. A.5 the only modification necessary is to redefine $L'_{k\ell}$:

$$L'_{k\ell} = \begin{cases} L^{n}_{k\ell} & \text{if } n_k = n_\ell - n \\ 0 & \text{otherwize} \end{cases} \qquad \text{A.5d}$$

Combining Eqs. A.5 and A.3 we then get that the expression for $\rho^a_k(t)$ takes the simple form

$$\rho^a_k(t) = \rho^a_k \exp[-i(\Omega^a + n_k\omega)t] \qquad \text{A.6a}$$

where we have introduced the short form notation

$$\rho^a_k \equiv \rho^a_{k;n_k} \qquad \text{A.6b}$$

If $L'_{k\ell}$ is hermitean, the eigenvalues Ω^a are all real, and the corresponding eigenvectors ρ^a_k are orthogonal. If $L_{k\ell}$ is not hermitean, the eigenvalues Ω^a may be real or complex, and the eigenvectors ρ^a_k are not necessarily orthogonal.

We mentioned before that we shall assume the set of $\rho^a_k(0)$ (Eq. A.3), a = 1, 2, 3, ... to be complete in the vector space of ρ_k's. Looking at Eq. A.6 this means that the ρ^a_k form a complete set. Then (see, e.g., Ref. A.4 for details) there exists a unique set of vectors r^a_k satisfying

$$\Sigma_k \; r^a_k \rho^b_k = \delta_{ab} \text{ for all a and b} \qquad \text{A.7a}$$

$$\Sigma_a \; r^a_k \rho^a_\ell = \delta_{k\ell} \text{ for all k and } \ell \qquad \text{A.7b}$$

The r_k^a are related to the eigenvalue Eq. A.5a, since they also satisfy

$$r_k^a \Omega^a = r_k^a \Delta_k + \Sigma_{\ell \neq k} r_\ell^a L'_{\ell k} \qquad \text{A.7c}$$

If L'_k is hermitean, $r_k^a = \rho_k^{a*}$.

The solution of the initial value problem associated with Eq. A.1 can thus be written

$$\rho_k(t) = \Sigma_a b^a \rho_k^a \exp[-i(\Omega^a + n_k \omega)t] \qquad \text{A.8}$$

where

$$b^a = \Sigma_k r_k^a \rho_k(0) \qquad \text{A.9}$$

The time development operator U defined by

$$\rho_k(t) = \Sigma_\ell U_{k\ell}(t,t')\rho_\ell(t') \qquad \text{A.10a}$$

can be verified by substitution to be

$$U_{k\ell}(t,t') = \Sigma_{abm} \rho_k^a r_m^a \rho_m^b r_\ell^b \exp[-i(\Omega^a t - \Omega^b t') - i n_m \omega(t-t')] \qquad \text{A.10b}$$

A.2. Perturbation theory.

Just like in the standard treatment of the time independent Schrödinger equation, where one is interested in what effect a small change in the hamiltonian has on the energy eigenvalues and eigenvectors of the system, we are interested in what effect a small change in the operator $L_{k\ell}(t)$ in Eq. A.1 may have on the solution $\rho_k(t)$. Consider the equation

$$i\dot{\rho}_k = \Sigma_\ell \, (L_{k\ell}(t) + \ell_{k\ell}(t)) \qquad \text{A.11}$$

where the solutions of the equation $i\dot{\rho}_k = \Sigma_\ell \, L_{k\ell}\rho_\ell$ are now assumed to be known, given by Eq. A.6, and where $\ell_{k\ell}$ is "small" compared to $L_{k\ell}$. Since the ρ_k^a are assumed to form a complete set of vectors, we may expand $\rho_k(t)$:

$$\rho_k(t) = \Sigma_a \, a^a(t)\rho_k^a \exp(-in_k\omega t) \qquad \text{A.12}$$

Inserted in Eq. A.11 this yields, with the help of Eq. A.7:

$$i\dot{a}^a = \Omega^a a^a + \Sigma_b \, \ell^{ab} a^b \qquad \text{A.13a}$$

where

$$\ell^{ab} = \Sigma_{k\ell} \, r_k^a \ell_{k\ell} \rho_\ell^b \exp[i(n_k - n_\ell)\omega t] \qquad \text{A.13b}$$

From Eq. A.13 we see that the operator $\ell_{k\ell}$ of Eq. A.11 can be considered "small" when the ℓ^{ab} are small compared to the spacings between the various Ω^a.

For transparency it is useful to write Eq. A.13 in integral form:

$$a^a(t) = a^a(t_o) - i\int_{t_o}^{t} dt' \exp[-i\Omega^a(t-t')]\Sigma_b \ell^{ab}(t')a^b(t') \qquad \text{A.13c}$$

From this we see that only the terms $\ell^{ab}a^b$ that oscillate close to the frequency Ω^a will contribute significantly to the integral for $t >> t_o$. Thus of all the terms in ℓ^{ab} (see Eq. A.13b), only a few need to be taken into account.

Let us consider four different forms of the perturbation $\ell_{k\ell}(t)$. In chapter 1 the relevance of the various forms to physical problems is demonstrated.

A.2a. Time independent perturbation.

This case is relevant, e.g., when our system is perturbed by weak time independent damping terms, weak external D.C. fields, etc. With a time independent perturbation, the terms in Eq. A.13b that have $n_k \neq n_\ell$ all oscillate at nonzero integer multiples of the external field frequency. Since the rotating wave approximation we use presupposes $|\Omega^a| << \omega$ for all a, all terms in ℓ^{ab} (Eq. A.13b) with $n_k \neq n_\ell$ can be disregarded, to give

$$\ell_o^{ab} = \Sigma'_{k\ell}\, r_k^a \ell_{k\ell} \rho_\ell^b \qquad \text{A.14}$$

where the sum extends only over k and ℓ such that $n_k = n_\ell$. Furthermore, since the ℓ^{ab} are small compared to the spacings between the various Ω^a, we can simplify even more. If all the Ω^a are nondegenerate, in the lowest order approximation the effect of ℓ_o^{ab} with $a \neq b$ can be neglected in comparison with the effect of ℓ_o^{aa} in Eq. A.13a, which then takes the form

$$i\dot{a}^a = (\Omega^a + \ell_o^{aa})a^a \qquad \text{A.15a}$$

or

$$a^a(t) \propto \exp[-i(\Omega^a + \ell_o^{aa})t] \qquad \text{A.15b}$$

I.e., the only effect the perturbation $\ell_{k\ell}$ has on ρ_k^a for nondegenerate Ω^a is to replace Ω^a in Eq. A.6 by $\Omega^a + \ell_o^{aa}$.

A.2b. Oscillatory perturbation at the same frequency ω as $L_{k\ell}(t)$.

This case corresponds, e.g., to the system being excited by an external field of a definite polarization, and being perturbed by a small admixture of the opposite polarization. This case proceeds exactly like case A.2a, except that the expression for ℓ_o^{ab} changes. Let $\ell_{k\ell} = \ell_{k\ell}^o \exp(i\omega t) + \ell_{\ell k}^{o*} \exp(-i\omega t)$. Now, the only terms of ℓ^{ab} (Eq. A.13b) that do not oscillate very rapidly are those with $n_k - n_\ell = \pm 1$. Thus $\ell_o^{ab} = \Sigma_{k\ell}^{+} r_k^a \ell_{k\ell}^o \rho_\ell^b + \Sigma_{k\ell}^{-} r_k^a \ell_{\ell k}^{o*} \rho_\ell^b$, where $\Sigma_k^{\pm}$ means sum over k and ℓ such that $n_k - n_\ell \pm 1 = 0$.

A.2c. Response of a damped system to a weak oscillatory perturbation.

This is relevant, e.g., for estimating the response of the system (absorption, dispersion) to a weak probing field at frequency ω' (not necessarily equal to the frequency ω of the strong external field driving the system). Without loss of generality, since we are interested in the steady state response, we write $\ell_{k\ell}$ as

$$\ell_{k\ell}(t) = \ell^{o}_{k\ell}[\exp(i\omega' t) + \exp(-i\omega' t)] \qquad A.16$$

where $\ell^{o}_{k\ell} = \ell^{o*}_{\ell k}$. As discussed in chapter 1, the typical systems described by Eq. A.1 ($\ell^{o}_{k\ell} = 0$), in the presence of damping have one and only one stable solution

$$\rho_k(t\to\infty) = \rho^{o}_{k}\exp(-in_k\omega t) \qquad A.17$$

corresponding to the eigenvalue $\Omega^{o} = 0$ in Eq. A.5a. All other Ω^{a} have negative imaginary parts. The solution A.17 is the zeroth order solution to Eq. A.11. Using the first Born approximation with $\ell_{k\ell}(t)$ as the perturbation in Eq. A.13c, we obtain for $a \neq 0$:

$$a^{a}(t) = -i\int_{-\infty}^{t}dt'\,\Sigma_{\ell m}\, r^{a}_{\ell}\ell^{o}_{\ell m}\rho^{o}_{m}\{\exp[-i\Omega^{a}t + i(\Omega^{a} + (n_\ell - n_m)\omega + \omega')t'] + \exp[-i\Omega^{a}t + i(\Omega^{a} + (n_\ell - n_m)\omega - \omega')t']\} \qquad A.18a$$

$$a^{a}(t) \simeq -\Sigma_{\ell m} r^{a}_{\ell}\ell^{o}_{\ell m}\rho^{o}_{m}\exp[i(n_\ell - n_m)\omega t]\ X \qquad A.18b$$

$$X\{\exp(i\omega' t)/[\Omega^{a} + (n_\ell - n_m)\omega + \omega'] + \exp(-i\omega' t)/[\Omega^{a} + (n_\ell - n_m)\omega - \omega']\}$$

or with Eq. A.18b inserted in Eq. A.12

$$\rho_k(t) = \rho_k^o \exp(-in_k\omega t) -$$
$$- \Sigma_{a\neq 0}\Sigma_{\ell m} \rho_k^a r_\ell^a \ell_{\ell m}^o \rho_m^o \exp[-i(n_k - n_\ell + n_m)\omega t] \times$$
$$\times \{\exp(i\omega' t)/[\Omega^a + (n_\ell - n_m)\omega + \omega'] +$$
$$+ \exp(-i\omega' t)/[\Omega^a + (n_\ell - n_m)\omega - \omega']\} \qquad \text{A.18c}$$

From this we see that there is a resonance with a halfwidth $\mathrm{Im}(\Omega^a)$ at $\omega' = \mathrm{Re}(\Omega^a) + (n_\ell - n_m)\omega$.

The case when ω' is close to a multiple $(n_\ell - n_m)\omega$ of the external field frequency ω is interesting and worth further discussion, since the above treatment is not valid in this case.

We refer back to Eq. A.13. When $\ell_{k\ell}$ oscillates at a frequency ω' which is near an integer multiple of ω, the only important terms in ℓ^{ab} (Eq.A.13b) are those for which $|(n_k - n_\ell)\omega \pm \omega'| << \omega$. Then, if we define $f = n\omega - \omega'$, where $n\omega$ is the integer multiple of ω closest to ω', ℓ^{ab} takes the form

$$\ell^{ab} = \Sigma_{m=\pm 1} \ell_m^{ab} \exp(imft) \qquad \text{A.19}$$

where $\ell_{\pm 1}^{ab}$ is the sum of all terms in Eq. A.13b that oscillate at the frequency $\pm f$. Then we see that Eqs. A.13a and A.1b have the same form, and that in analogy with Eq. A.3 we may write the solutions of Eq. A.13a as

$$a_p^a(t) = \Sigma_n a_p^{a;n} \exp[-i(F_p + nf)t] \qquad \text{A.20a}$$

The correspondence between Eqs. A.1 and A.3 and Eqs. A.13 and A.20a relies on the following identifications:

Eq. A.13	Eq. A.1
a^k	ρ_k
$a^{k;n}_a$	$\rho^a_{k;n}$
Ω^k	L^o_{kk}
$\Omega^k - nf$	$L^o_{kk} - n\omega$
$\ell^{k\ell}_m$	$L^m_{k\ell}$
f	ω
F_a	Ω^a

Thus F_p and $a^{a;n}_p$ satisfy the eigenvalue equation (analogous to Eq. A.4)

$$F_p a^{a;n}_p = (\Omega^a - nf)a^{a;n}_p + \Sigma_{bm}\, \ell^{ab}_m a^{b;n-m}_p \qquad \text{A.20b}$$

For $\ell^{ab}_m = 0$ the solutions are $F_p = \Omega^p$ and $a^{a;n}_p = \delta_{ap}\delta_{n0}$. Since an equivalent solution is $F_p = \Omega^p - mf$, $a^{a;n}_p = \delta_{ap}\delta_{mn}$, where m is any integer, we seek the eigenvalues F_p of Eq. A.20b that approach Ω^p as ℓ^{ab}_m tends to zero.

The trace of the density matrix is conserved. As discussed in chapter 1, usually the system described by Eq. A.1 is such that $\mathrm{Tr}\ \rho^a = \delta_{a0}$. Using Eq. A.12 we then get that the trace of the density matrix is equal to $a^o(t)$. Thus, using Eq. A.20a, we have

$$0 = \dot{a}^o(t) = (d/dt)\{\Sigma_{pn}\, b_p a^{0;n}_p \exp[-i(F_p + nf)t]\} \qquad \text{A.21}$$

for all possible choices of b_p's. This implies that for all times t

$$\Sigma_n (F_p - nf) a_p^{0;n} \exp(inft) \equiv 0 \qquad \text{A.22}$$

for all p. Since F_p only is determined modulo f, let us consider, for a moment, $f/2 \geq F_p > -f/2$. If $F_p \neq 0$, Eq. A.22 implies that $a_p^{0;n} = 0$. Only if $F_p = 0$ can we have $a_p^{0;n} \neq 0$, and then only if $n = 0$. As we shall se below, this only occurs if $p = 0$. Thus the result of the requirement that the trace of the density matrix is conserved is that

$$F_0 = 0 \text{ and } a_p^{0;n} = \delta_{n0}\delta_{p0} \qquad \text{A.23}$$

Now, let us remind ourselves of the properties of the Ω^a and the ℓ_m^{ab}:

(1) The separation between the various Ω^a is large compared to the ℓ_m^{ab}'s, since in Eq. A.11 $\ell_{k\ell}$ is assumed to be a weak perturbation on $L_{k\ell}$.

(2) From the definition of ℓ_m^{ab} following Eq. A.19 we have $\ell_m^{ab} = 0$ unless $m = \pm 1$.

(3) Typically one, and only one, Ω^a, $a = 0$, is exactly zero.

In Eq. A.20b we have one case when $a_p^{a;n}$ deviates significantly from $\delta_{ap}\delta_{n0}$: when $|f|$ is close to any of the Ω^a's. The steady state response for f close to a nonzero Ω^a is already given by Eq. A.18.

Since $|\Omega^p - \Omega^a| >> |\ell_m^{ap}|$ for $a \neq p$, F_p is close to Ω^p (see Eq. A.20b), and $a_p^{a;n}$ is only considerably different from zero if $a = p$.

Thus F_p and $a_p^{p;n}$ can be obtained from Eq. A.20b by the approximation of including only elements $a_p^{p;n}$:

$$(F_p - \Omega^p)a_p^{p;n} = -nfa_p^{p;n} + \Sigma_m \ell_{n-m}^{pp} a_p^{p;m} \qquad A.24$$

We see that only when f is so small as to be comparable to ℓ_n^{pp} are the $a_p^{p;n}$'s significantly different from zero for $n \neq 0$.

Using the fact that $a_p^{a;n}$ is small compared to $a_p^{p;n}$ when $a \neq p$, we get in this case, using Eq. A.20b

$$\begin{aligned} a_p^{a;n} &\simeq \Sigma_m \ell_{n-m}^{ap} a_p^{p;m}/(F_p - \Omega^a + nf) \\ &\simeq \Sigma_m \ell_{n-m}^{ap} a_p^{p;m}/(\Omega^p - \Omega^a + nf) \end{aligned} \qquad A.25$$

Thus we get, combining Eqs. A.12, A.20a, A.23, and A.25

$$\begin{aligned} \rho_k(t) = \Sigma_a\, a^a(t)\rho_k^a \exp(-in_k\omega t) = \\ = \rho_k^o \exp(-in_k\omega t) + \\ + \Sigma_{p\neq 0,n}\, b_p a_p^{p;n} \rho_k^p \exp[-i(F_p + n_k\omega + nf)t] + \\ + \Sigma_{p\neq a, a\neq 0, m, n}\, b_p \ell_{n-m}^{ap} a_p^{p;m} \rho_k^a \times \\ \times \exp[-i(F_p + n_k\omega + nf)t]/(\Omega^p - \Omega^a + nf) \end{aligned} \qquad A.26$$

The constants b_p are determined from initial value conditions. If $a_0^{0;0}$ is chosen to be unity, $b_0 = 1$. Eq. A.26 should be compared to Eq. A.18c. Taking the limit $|f| >> |\ell_n^{pp}|$ (so that $a_p^{p;n} \simeq \delta_{n0}$) and $t \to \infty$ (so that the terms with $p \neq 0$ will decay away, because $\mathrm{Im}(F_p) \simeq \mathrm{Im}(\Omega^p) < 0$ if $p \neq 0$), we see that Eq. A.26 reduces to Eq. A.18c.

However, Eq. A.26 in addition describes the transient response ($p \neq 0$) and the modifications necessary to introduce in Eq. A.18c when the condition $|f| >> |\varepsilon_n^{pp}|$ is not met.

A.2d. Errors introduced by the rotating wave approximation.

In this section we will try to establish what criteria to use, to test wether Eq. A.5a is a reasonable approximation in the description of a given system. Consider the following case: Suppose we have chosen to neglect a term ρ_{N+1} in Eq. A.5. This term corresponds in zeroth order to an eigenvalue $\Omega^{N+1} = \Delta_{N+1}$ (where, following the notation of Eq. A.5, Δ_{N+1} has the form $\Delta_{N+1} = L^o_{N+1,N+1} - n_{N+1}\omega$) and an eigenvector $\rho_k^{N+1} = \delta_{k,N+1}$. Calling the perturbed eigenvalues of Eq. A.5a Ω'^a, and expanding in terms of ρ_k^a the corresponding eigenvectors $\rho_k'^a = \Sigma_b\, a^{ab}\rho_k^b$, we get

$$\Omega'^a\rho_k'^a = \Sigma_{\ell=1}^N L_{k\ell}\rho_\ell + \delta_{k,N+1}\Sigma_{\ell=1}^N L'_{N+1,\ell}\rho_\ell'^a + L'_{k,N+1}\rho_{N+1}'^a \qquad \text{A.27a}$$

or by using Eq. A.5a and $\Sigma_k r_k^a\rho_k^b = \delta_{ab}$

$$\Omega'^a a^{ab} = \Omega^b a^{ab} + \delta_{b,N+1}\Sigma_c L_\rho^c a^{ac} + L_r^b a^{a,N+1} \qquad \text{A.27b}$$

where

$$L_\rho^a = \Sigma_{\ell=1}^N L'_{N+1,\ell}\rho_\ell^a \qquad \text{A.27c}$$

$$L_r^a = \Sigma_{\ell=1}^{N+1} r_\ell^a L'_{\ell,N+1} \qquad \text{A.27d}$$

Being neglected in the unperturbed ρ_k^a, $|\Delta_{N+1}| \gg |\Omega^a|$ for all a. Also, $\Omega'^a \approx \Omega^a$, and $a^{ac} \approx \delta_{ac}$, in Eq. A.27. Then for $a \neq b$, we get from Eq. A.27b

$$a^{ab} = (\delta_{b,N+1}L_\rho^a + \delta_{a,N+1}L_r^b)/(\Omega^a - \Omega^b). \qquad \text{A.28}$$

If we reinsert this in Eq. A.27b we get (using $a^{aa} \approx 1$) for $a \neq N + 1$

$$\Omega'^a - \Omega^a = L_r^a L_\rho^a/(\Omega^a - \Delta_{N+1}) \qquad \text{A.29a}$$

and for $a = N + 1$

$$\Omega'^{N+1} - \Delta_{N+1} = L_\rho^{N+1} + L_r^{N+1} + \Sigma_{c\neq N+1} L_\rho^c L_r^c/(\Delta_{N+1} - \Omega^c). \qquad \text{A.29b}$$

This can straightforwardly be generalized to include the effect of neglecting not one, but several terms ρ_{N+1}^a, ρ_{N+2}^a ... in Eq. A.5. The qualitative results are still the same. To the extent that Δ_{N+1}, Δ_{N+2} ... are of order of magnitude like ω and not Ω^a, the corrections to ρ_k^a are terms of order $L_{k\ell}/\omega$ (see Eq. A.28) whereas the Ω^a have corrections of order $|L_{k\ell}|^2/\omega$ (see Eq. A.29). Strictly speaking, this holds only if the various ρ_k^a are orthonormal or close to being orthonormal. If two ρ_k^a, ρ_k^a and ρ_k^b are nearly parallel and normalized, $\Sigma_k|\rho_k^a|^2 = 1 = \Sigma_k|\rho_k^b|^2$, then, since $\Sigma_k r_k^a \rho_k^b = 0$ and $\Sigma_k r_k^a \rho_k^a = 1$, the norm $\Sigma_k|r_k^a|^2$ of r_k^a is much greater than one. This implies that the corresponding L_r^a (see Eq. A.27d) may be much greater than the various $L'_{k,N+1}$. Thus after Eq. A.5 (with terms ρ_ℓ^a neglected on the basis that $L_{\ell k}/\Delta_\ell$ and $L_{k\ell}/\Delta_\ell$ are small) has been solved, the various r_k^a corresponding to normalized ρ_k^a must be

checked to make sure they do not have a norm too different from one, before the solution can be trusted. Also, since the solutions for the eigenvalues Ω^a have correction of the order of $\tau^{-1} \approx |L^a_{r,\rho}|^2/\omega$, the time τ defines a time duration within which the corresponding $\rho_\kappa(t)$ (see Eq. A.6) can be trusted.

References

A.1 Floquet's theorem can be found in standard texts on different equations, e.g. A. F. Forsyth, "Theory of Differential Equations," Vol. III, Ch, IX, p. 411 (University Press, Cambridge, 1902). In solid-state physics it is called "Block's Theorem," see C. Kittel, "Quantum Theory of Solids."

A.2 For a review of the quasienergy concept, see, e.g., Ya. B. Zel'dovich, Sov. Phys. Ushpekhîi 16, 427 (1973).

A.3 D. Grischkowsky and M. M. T. Loy, Phys. Rev. A12, 2514 (1975).

A.4 J. H. Wilkinson, "The Algebraic Eigenvalue Problem," Ch. 2 (Clarendon Press, Oxford, 1965).

APPENDIX B: Two-level System

The two-level system with a lower state 1 of zero energy and an upper state 2 of energy $\hbar\mathcal{E}$ is the simplest nontrivial q.m. system. Its interaction with a strong e.m. field has been treated extensively /B.1/. We review here a few results of the problem relevant to the formalism of Chapter 1, as a simple illustration. The Hamiltonain of the system in a field $E = E_o \cos \omega t$ can be written as

$$H = \begin{pmatrix} 0 & 0 \\ 0 & \mathcal{E} \end{pmatrix} + V \begin{pmatrix} 0 & e^{i\omega t} + e^{-i\omega t} \\ e^{i\omega t} + e^{-i\omega t} & 0 \end{pmatrix} \qquad B.1$$

where $V = \mu E_o/2\hbar$, and μ is the dipole matrix element for transitions from 1 to 2. In the rotating wave approximation when $\mathcal{E} \approx \omega$, this reduces to the eigenvalue problem (cf. Eq. A.5)

$$\Omega^a \begin{pmatrix} \Psi_1 \\ \Phi_2 \end{pmatrix} = \begin{pmatrix} 0 & V \\ V & \Delta \end{pmatrix} \begin{pmatrix} \Phi_1 \\ \Phi_2 \end{pmatrix} \qquad B.2$$

with $\Delta = \mathcal{E} - \omega$, which has solutions

$$\Omega^{\pm} = \tfrac{1}{2}[\Delta \pm (\Delta^2 + 4V^2)^{\frac{1}{2}}] \qquad B.3a$$

or $\Omega^+ = V \tan\phi \quad \Omega^- = -V \cot\phi$

$$\begin{pmatrix} \Phi_1^+ & \Phi_1^- \\ \Phi_2^+ & \Phi_2^- \end{pmatrix} = \begin{pmatrix} \cos\phi & -\sin\phi \\ \sin\phi & \cos\phi \end{pmatrix} \qquad B.3b$$

where $\tan\phi = [\Delta + (\Delta^2 + 4V^2)^{\frac{1}{2}}]/2V$. Thus $\Phi_1(t)$ will have components os-

cillating at Ω^+ and Ω^-, whereas $\Phi_2(t)$ will have components oscillating at $\Omega^+ + \omega$ and $\Omega^- + \omega$. This is what is referred to as AC Stark splitting of levels 1 and 2. The splitting is

$$\Omega_{ac} = \Omega^+ - \Omega^- = (\Delta^2 + 4V^2)^{\frac{1}{2}}. \qquad \text{B.4}$$

Thus the fluorescence spectrum from the system due to the oscillating polarization $\langle\Phi|\mu|\Phi\rangle$ will have components at the combination frequencies ω and $\omega \pm \Omega_{ac}$.

The widths of the components in the spectrum can be obtained from the density matrix formulation. For weak damping (e.g., weak collisions, spontaneous emission) there are two decay constants A_1 and A_2 in the problem, and Eq. A.5 takes the form

$$\Omega^a \begin{pmatrix} \rho^a_{11} \\ \rho^a_{22} \\ \rho^a_{12} \\ \rho^a_{21} \end{pmatrix} = \begin{pmatrix} 0 & iA_1 & -V & V \\ 0 & -iA_1 & V & -V \\ -V & V & -iA_2 - \Delta & 0 \\ V & -V & 0 & -iA_2 + \Delta \end{pmatrix} \begin{pmatrix} \rho^a_{11} \\ \rho^a_{22} \\ \rho^a_{12} \\ \rho^a_{21} \end{pmatrix} \qquad \text{B.5}$$

or, using the real, symmetrized form of Eq. 1.17b, with $\gamma^a = i\Omega^a$

$$\gamma^a \begin{pmatrix} \rho_1 \\ \rho_2 \\ \rho_3 \\ \rho_4 \end{pmatrix} = \begin{pmatrix} 0 & -A_1 & 0 & -2V \\ 0 & A_1 & 0 & 2V \\ 0 & 0 & A_2 & -\Delta \\ V & -V & \Delta & A_2 \end{pmatrix} \begin{pmatrix} \rho_1 \\ \rho_2 \\ \rho_3 \\ \rho_4 \end{pmatrix} \qquad \text{B.6}$$

By using $\rho_- = \rho_2 - \rho_1$ and $\rho_+ = \rho_1 + \rho_2 = 1$, one can easily recognize Eq.

B.6 as the optical Block equations:

$$\gamma^a \begin{pmatrix} \rho_+ \\ \rho_- \\ \rho_3 \\ \rho_4 \end{pmatrix} = \begin{pmatrix} 0 & 0 & 0 & 0 \\ A_1 & A_1 & 0 & 4V \\ 0 & 0 & A_2 & -\Delta \\ 0 & -V & \Delta & A_2 \end{pmatrix} \begin{pmatrix} \rho_+ \\ \rho_- \\ \rho_3 \\ \rho_4 \end{pmatrix} . \qquad \text{B.7}$$

For completeness, we also remind ourselves that in the case of spontaneous emission being the only damping mechanism, $A_1 = A$ and $A_2 = \frac{1}{2}A$, where A is the Einstein A-coefficient of the transition.

Equation B.7 has one solution $\gamma^a = 0$ corresponding to

$$\begin{pmatrix} \rho_+^o \\ \rho_-^o \\ \rho_3^o \\ \rho_4^o \end{pmatrix} = \begin{pmatrix} 1 \\ -(\Delta^2 + A_2^2)/N \\ -\Delta V/N \\ -A_2 V/N \end{pmatrix} \qquad \text{B.8a}$$

where

$$N = \Delta^2 + A_2^2 + 4V^2 A_2/A_1 . \qquad \text{B.8b}$$

As we can see, the in-phase component (relative to the external field) of the density matrix, ρ_3^o, gives the dispersive response of the system, whereas the out-of-phase component ρ_4^o gives the absorption, which has a halfwidth $A_2 + 4V^2 A_2/A_1$. The term $4V^2 A_2/A_1$ is the power broadening of the absorption.

For $a \neq 0, \rho_+^a = 0$, and the eigenvalue γ^a satisfies the cubic equation

$$(\gamma^a - A_1)[(\gamma^a - A_2)^2 + \Delta^2] + 4V^2(\gamma^a - A_2) = 0 \qquad \text{B.9}$$

whereas ρ_k^a is given by

$$\begin{pmatrix} \rho_-^a \\ \rho_3^a \\ \rho_4^a \end{pmatrix} = N_a \begin{pmatrix} 4V(\gamma^a - A_2) \\ -\Delta(\gamma^a - A_1) \\ (\gamma^a - A_1)(\gamma^a - A_2) \end{pmatrix} \qquad \text{B.10}$$

and the normalization constant N_a is determined by initial conditions.

If 2V and Δ are small compared to A_1 and A_2, there are two roots γ^a of Eq. B.9 near A_2 and one near A_1. If $|d| \gg 2V$, where $d = \frac{1}{2}(A_1 - A_2)$, we get simple expressions for these roots:

$$\gamma^{\pm} = A_2 + V^2/d \pm i[\Delta^2 - (V^2/d)^2]^{\frac{1}{2}} \qquad \text{B.11a}$$

$$\gamma^1 = A_1 - 8V^2 d/(4d^2 + \Delta^2). \qquad \text{B.11b}$$

Thus, with the introduction of a weak oscillatory external field, the decay constants for the nonstationary components ρ_k^a (with $a \neq 0$) change slightly. If $V^2/d > \Delta$, the off-diagonal elements of ρ will oscillate at the field frequency ω (all the γ^a are real) and have no components oscillating at the system eigenfrequency $\mathcal{E} = \omega + \Delta$.

If A_1 and A_2 are small compared to V, we can use Eq. 1.15 and Eq. B.3 to find

$$\gamma^{\pm} = \pm i\,\Omega_{ac} + \gamma \ , \ \gamma^{1} = \gamma' \qquad \text{B.12}$$

where

$$\gamma = 2A_1 \sin^2\phi \cos^2\phi + A_2(\cos^4\phi + \sin^4\phi) \qquad \text{B.13a}$$

$$\gamma' = A_1(\cos^2\phi - \sin^2\phi)^2 + 4A_2 \sin^2\phi \cos^2\phi. \qquad \text{3.13b}$$

For zero detuning ($\Delta = 0 \Rightarrow \phi = \pi/4$) this reduces to $\gamma = \frac{1}{2}(A_1 + A_2)$, $\gamma' = A_2$, whereas for large detuning ($\tan\phi \approx \Delta/V \gg 1$) we obtain $\gamma = A_2$, $\gamma' = A_1$. Thus a two-level system relaxes to its steady-state response $\rho_k(t \to \infty) = \rho_k^o(t)$ on the time scale given by A_1 and A_2, regardless of detuning.

In the semiclassical picture, the resonance fluorescence scattering is proportional to the oscillating polarization, which in a two-level system is proportional to $\rho_3(t)$. Thus we have four components of scattered light: one elastically scattered component, corresponding to $\rho_3^o(t)$, one of halfwidth γ' centered at the driving frequency ω, corresponding to $\rho_3^1(t)$, and two components of halfwidth γ, centered at $\omega \pm \Omega_{ac}$, corresponding to $\rho_3^{\pm}(t)$. If A_1, A_2 and V are of comparable magnitude, then Eq. B.6 **has to** be solved. **This** amounts to solving the cubic Eq. B.9 for γ^a. Only on resonance ($\Delta = 0$) do we get simple expressions for the nonzero eigenvalues γ^a:

$$\gamma^{\pm} = \bar{A} \pm i(4V^2 - \bar{A}^2)^{\frac{1}{2}} \qquad \text{B.14a}$$

$$\gamma^{1} = A_2 \qquad \text{B.14b}$$

where $\bar{A} = \frac{1}{2}(A_1 + A_2)$. Thus, on resonance, the triplet structure of the fluorescence spectrum is retained for external fields such that $2V > d$.

References

B.1 C. Cohen-Tannoudji and S. Reynaud, in Ref. 1.1, pp. 103-118; H. Walther, in Ref. 1.1, pp. 129-144; M. Sargent, M.O. Scully, and W. E. Lamb, Laser Physics (Addison-Wesley, Reading 1974); L. Allen and J. H. Eberly, Optical Resonance and Twolevel Atoms (Wiley, New York 1975).

APPENDIX C: External Fields of Arbitrary Time Dependence

In Appendices A and B we have treated the equation $i\dot{\rho} = L\rho$, where $L = L^0 + L^1\exp(i\omega t) + L^{1\dagger}\exp(-i\omega t)$, and L_o and L^1 are time independent operators. This can easily be formally extended to the case where ω, L^0 and L^1 vary in time. Let L^0 and L^1 depend on a set of real parameters $\{E_m\}$, which vary in time. The parameters may, e.g., be external field amplitudes, frequencies, and phases, in which case the treatment applies to excitation of a quantum mechanical system by a train of picosecond pulses, by a frequency chirped pulse, by a phase and/or amplitude modulated single longitudinal mode laser field, or by a laser pulse of Fourier transform limited bandwith.

Now let the solutions of

$$i\dot{\rho}_k = \Sigma_\ell[L^0_{k\ell}(\{E_m\}) + L^1_{k\ell}(\{E_m\})\exp(i\omega t) + L^{1*}_{\ell k}(\{E_m\})\exp(-i\omega t)]\rho_\ell \qquad C.1$$

be

$$\rho^a_k(t) = \rho^a_k\exp[-i(\Omega^a + \omega_k)t] \qquad C.2$$

when the E_m's are constant. The Ω_a, ρ^a_k and ω_k are then functions of the E_m's. If the E_m's depend on time, we seek a solution of the form

$$\rho_k = \Sigma_a\, \alpha^a(t)\rho^a_k\exp(-i\omega_k t) \qquad C.3$$

Using C.1 and the rotating wave approximation (see Sect.A.1 of Appendix A), we obtain the following equation of motion for α^a (using $\Sigma_k r^a_k \rho^b_k =$

δ_{ab}, see Eq. A.7)

$$i\dot{\alpha}^a = \Omega^a \alpha^a - \Sigma_b A^{ab} \alpha^b \qquad \text{C.4a}$$

with

$$A^{ab} = i\Sigma_{km}\left(r_k^a \frac{\partial \rho_k^b}{\partial E_m} \dot{E}_m - i\dot{\omega} n_k r_k^a \rho_k^b\right) =$$

$$= - i\Sigma_{km}\left(\frac{\partial r_k^a}{\partial E_m} \rho_k \dot{E}_m + i\dot{\omega} n_k r_k^a \rho_k^b\right). \qquad \text{C.4b}$$

This is, of course, only useful if the Ω^a, ρ_k^a, r_k^a and $\partial \rho_k^a / \partial E_m$ are known for the values of E_m of interest. This limits the usefulness of Eq. C.4 to problems with only a few levels involved, or other systems where simple analytical solutions for Ω^a, ρ_k^a and r_k^a can be found. However, we have transformed Eq. C.1, which has terms oscillating rapidly at a frequency ω, into Eq. C.4, which has terms varying with the slower parameters E_m. This is of great importance for numerical integration of the problem. Note that Eq. C.4 is valid even if E_m is rapidly varying - the only approximation used is the rotating wave approximation.

If E_m is varying sufficiently slowly, and in addition the Ω^a are nondegenerate, we can neglect A^{ab} compared to Ω^a, and get the so-called adiabatic /C.1/ approximation $i\dot{\alpha}^a = \Omega^a \alpha^a$, or

$$\alpha^a(t) = \alpha^a(t_o) \exp\left[- i \int_{t_o}^{t} dt' \Omega^a(\{E_m(t')\})\right]. \qquad \text{C.5}$$

For a two-level system excited at resonance with no damping, this reduces to the familiar result, related to the pulse area theorem /C.1/,

that the state of the system at time t only depends on the integrated field amplitude $\int_{-\infty}^{t} dt' E_o(t')$, and not on the detailed time dependence of the field. Analogous, although not as simple and transparent, statements can be made about any multilevel system, with basis in Eq. C.5.

Now let us assume that [illegible] typical system with damping. As discussed in Chapter 1, one and only one stationary state $\rho_k(t \to \infty) = \rho_k^o(t)$ exists. If the system initially is in this state, then $\alpha^a(t_o) = \delta_{ao}$ in Eq. C.5, and $\Omega^a = \Omega^0 = 0$, implying $\alpha^a(t) = \delta_{ao}$ for all t. Thus the adiabatic approximation of Eq. C.5 only works rigorously, in the presence of damping, when the field varies so slowly that the system is left in its initial state after the field is turned off.

References

C.1 See, e.g., Allen and Eberly of Ref. B.1, or A.Yariv, Quantum Electronics, 2nd edition (Wiley, New York, 1975) p. 392.

APPENDIX D: RRKM (Rice-Ramsperger-Kassel-Marcus) Theory of Unimolecular Reactions

The RRKM theory /D.1/ is designed to describe unimolecular reactions in the gas phase, where molecules are constantly being energized and de-energized by collisions. This way, some of the molecules may be supplied with enough energy to dissociate. In the theory one assumes that, on average, the molecules with internal energy within a small range about any given energy are randomly distributed over the available energy states in that range. One further assumes that the dissociation proceeds so slowly that this holds even for molecules excited above the dissociation energy, i.e., that the dissociating states are being rapidly replenished as molecules dissociate.

Even though the multiphoton excitation is in several respects very different from thermal, collisional excitation, the above picture can be directly transferred to describe multiphoton dissociation. Based on our experimental results, we can say that the process can be understood as composed of two stages: the multiphoton excitation, and the unimolecular dissociation competing with the excitation, when the molecules have internal energy above the dissociation energy. Multiphoton excited molecules, prior to dissociation, are likely to have energies distributed randomly in all available degrees of freedom. This experimental result is not surprising, in view of the following: The excitation and dissociation rates typically observed are in the range of 10^{-9} sec^{-1} or smaller (see Chapter 2). Intramolecular relaxation rates for highly excited molecules, as deduced from a series of chemical activation experiments

/D.2/, are $10^{11} - 10^{12}$ sec^{-1}. Thus a statistical theory should be perfectly applicable in describing the dissociation of multiphoton excited molecules.

In this appendix, the basic ideas in the RRKM theory will be presented, and in the simplest possible form, expressions will be deduced for the dissociation rate constants and the translational energy distribution of fragments from a given energy above the dissociation energy. For more extensive discussions, see Ref. D.1.

In a statistical approach, the important concept is that of the available phase space, i.e., the collection of states available to the system. Consider a bound molecule. For a molecule with energy above the dissociation energy E_o, a somewhat arbitrary but intuitively acceptable boundary between "bound" and "dissociated" system is defined. The coordinate in the molecule corresponding to movement of the two dissociation fragments relative to one another, normal to this boundary, is called the "reaction coordinate." Then consider any configuration of atoms in the molecule where the distance along the reaction coordinate of the dissociation fragments from this boundary is smaller than a distance Δ. This region of phase space is called the "critical configuration." (The size of Δ is immaterial, since it is an auxiliary parameter that cancels out in the final mathematical expressions.)

The number of states available to a bound molecule with energy between E^* and $E^* + \Delta E$ is

$$N(E^*)\Delta E \ , \qquad \text{D.1}$$

where $N(E^*)$ is the density of states in the molecule at energy E^*. At a

given energy, the possible configurations of the molecule is limited by the molecular potential energy surface and (for $E^* > E_o$, the dissociation energy) by the arbitrary boundaries defined as a division between the bound and dissociated molecule. For calculation of the density of states $N(E^*)$, this complicated surface is usually approximated by that of harmonic oscillators with frequencies equal to the low-energy vibrational frequencies of the molecule.

The number of states available in the critical configuration is calculated in the same manner, but here one essentially has to guess what this region of phase space looks like. The common assumption is one of a "particle in a box" for one coordinate (corresponding to the region of thickness 2Δ along the reaction coordinate) and harmonic oscillators for the remaining coordinates. One then has to make guesses or estimates of the oscillation frequencies for motion orthogonal to the reaction coordinate. The number of states with energy between E^* and $E^* + \Delta E$ available for a molecule where the fragments are separating with a relative kinetic energy between E_t and $E_t + \Delta E_t$ ($E_t = \frac{1}{2}\mu u^2$, where μ is the reduced mass of the two dissociation fragments, and u is their relative speed along the reaction coordinate) is then

$$(2\Delta/h)(2\mu/E_t)^{\frac{1}{2}}\Delta E_t \cdot N^\dagger(E^* - E_o - E_t)\Delta E. \qquad \text{D.2}$$

$N^\dagger(E)$ is now the density of states in the critical configuration, restricted to coordinates orthogonal to the reaction coordinate, approximated by a harmonic oscillator density of states. Thus the probability of finding a molecule in the critical configuration, with relative kinetic energy of the dissociation fragments between E_t and $E_t + \Delta E_t$, is

$$p(E^*,E_t) = \frac{(2\Delta/h\omega)N^\dagger(E^* - E_o - E_t)}{N(E^*)}\Delta E_t. \qquad D.3$$

The rate at which dissociation takes place, is half of this probability (since only the fragments moving away from each other can dissociate), divided by the time $2\Delta/u$ a molecule spends in the critical configuration before it dissociates:

$$k(E^*,E_t)\Delta E_t = \frac{N^\dagger(E^* - E_o - E_t)}{hN(E^*)}\Delta E_t. \qquad D.4$$

The total dissociation rate is found by integrating over all values of E_t:

$$k(E^*) = \int_o^{E^*-E_o} k(E^*,E_t)dE_t. \qquad D.5$$

The corresponding average dissociation lifetime is

$$\tau_{E^*} = (k(E^*))^{-1}. \qquad D.6$$

In Fig. D.1 are shown dissociation rates as a function of excess energy $E^* - E_o$, for the molecules CF_3I and SF_6. The normalized distribution of relative translational energy in the dissociation fragments is

$$p_{E^*}(E_t) = \tau_{E^*}k(E^*,E_t). \qquad D.7$$

Examples of typical center-of-mass translational energy distributions can be found in Fig. 2.9. The distribution in the fragments from SF_6 for three different excess energies are shown. Further examples can be found

in Appendix F. Expression D.7 can be used to describe correctly the energy distribution of the dissociation fragments in the center-of-mass coordinates only if there are no interactions between the fragments after the critical configuration is passed. As seen in Chapter 2, this is true for a number of atomic elimination cases. However, if there is a potential energy barrier (Appendix F) between reactant and products, or if there is appreciable angular momentum in the molecule before dissociation /D.3/, the above expressions have to be modified.

The translational energy distributions, Eq. D.7, look very much like exponentials, especially for high energies E^*, and in heavy molecules. It is easy to understand why this is so, in a statistical picture of the dissociation. To any single degree of freedom in a molecule with many degrees of freedom, the rest of the molecule looks like a heat bath, even though the molecule as a whole has a well-defined energy. Thus, any single degree of freedom, including the one corresponding to the reaction coordinate, will have a close to theremal, i.e., exponential, energy distribution. The energy is shared between all degreees of freedom, and only a small fraction resides on average in any one degree of freedom. Translated, this means that only a small fraction of the excess energy $E^* - E_o$ will end up as translational energy in the fragments, especially if the dissociating molecule has many atoms. Most of the energy thus remains as internal energy in the fragments.

References

D.1 P. J. Robinson and K. A. Holbrook, Unimolecular Reactions (Wiley, London, 1972); W. Forst, Theory of Unimolecular Reactions (Academic, New York, 1973).

D.2 I. Oref and B. F. Rabinovitch, Acct. Chem. Res. 12, 166 (1979).

D.3 S. A. Safron, N. D. Weinstein, D. R. Herschbach, and J. C. Tully, Chem. Phys. Lett. 12, 564 (1972).

Figure Captions

Fig. D.1 RRKM dissociation rates as functions of excess energy for CF_3I and SF_6.

Fig. D.2 Center-of-mass translational energy distribution of the fragments from the MPD of SF_6, calculated from RRKM theory.

- - - 5 kcal/mole excess energy

- · - 8 kcal/mole excess energy

——— 12 kcal/mole excess energy

Figure D.1

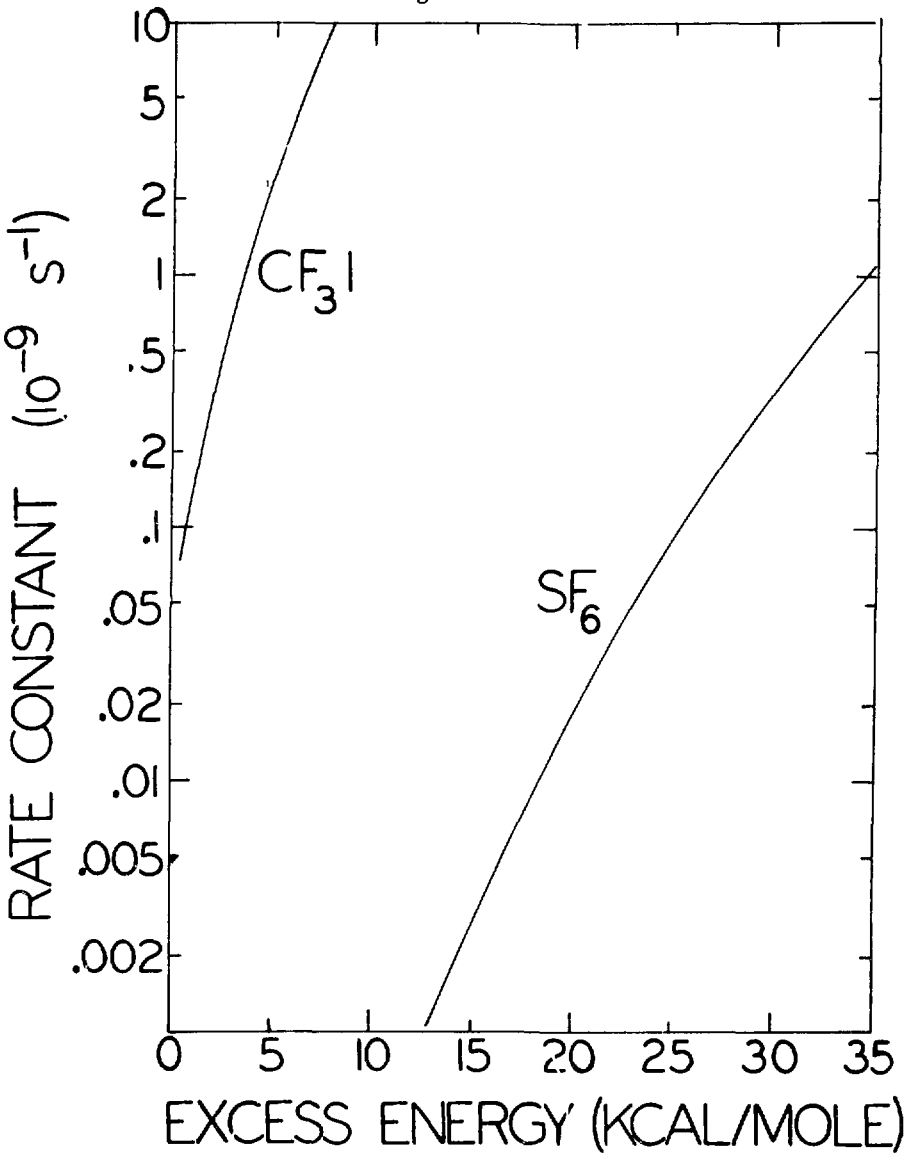

XBL 785-8835

Figure D.2

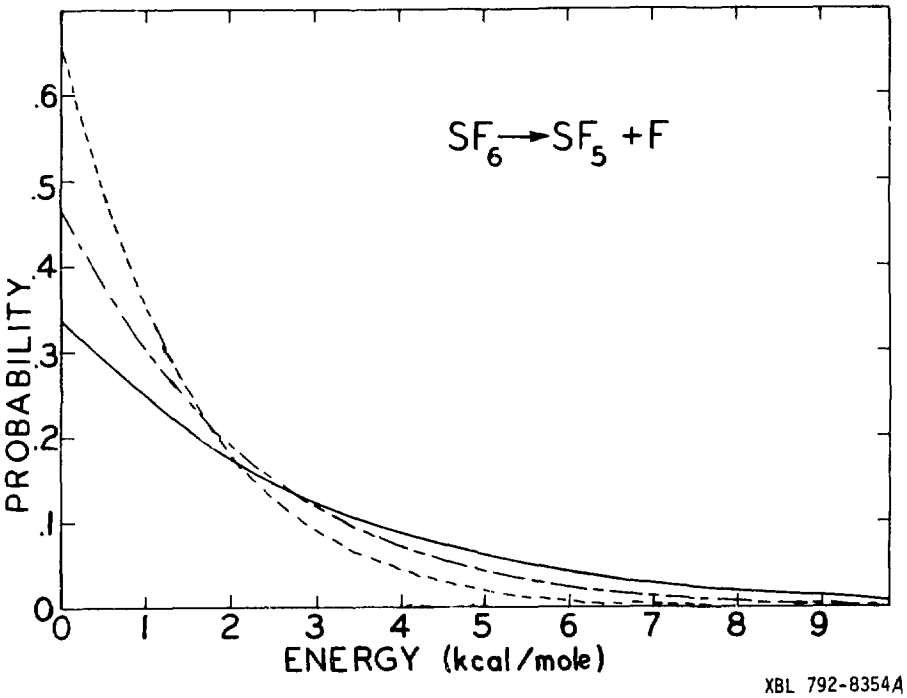
SF6→SF5 +F
PROBABILITY
.6
.5
.4
.3
.2
.1
0
0
1
2
3
4
5
6
7
8
9
ENERGY (kcal/mole)
XBL 792-8354A

LBL-9796
Appendix E
See Journal of Chemical Physics, Vol. 70, No. 2, January 15, 1979

Appendix F
See Journal of Chemical Physics, Vol. 69, No. 6, September 15, 1978